BLAST RESPONSE AND VULNERABILITY ASSESSMENT OF PILED FOUNDATIONS

By

Laddu Bhagya Jayasinghe

BSc Eng (Hons)

A THESIS SUBMITTED TO

SCIENCE AND ENGINEERING FACULTY

QUEENSLAND UNIVERSITY OF TECHNOLOGY

IN PARTIAL

FULFILMENT OF THE REQUIREMENTS FOR THE DEGREE OF

DOCTOR OF PHILOSOPHY

April 2014

Dedicated to my parents

Acknowledgements

TABLE OF CONTENTS

LIST OF FIGURES

LIST OF TABLES

Abstract

Due to increased number of terrorist attacks in recent years, loads induced by surface explosions need to be incorporated in building designs. Surface explosions may result with either total or partial collapse of the structure depending on the severity of blast and structural properties. When an explosion occurs near the ground surface, various types of waves are generated and propagated. In addition to air blast pressure, air-induced ground motions and directly transmitted ground shocks are possible. Air-induced ground shock is caused when the air-blast shock wave compresses the ground surface and sends a stress pulse into the underlying media. The air-induced ground motions are maximum at the ground surface and reduce with depth. Direct ground shock results from the explosive energy being transmitted directly through the ground.

Previous studies mainly investigated loads induced on structures by air propagated waves. No attempt has been made in studying the blast induced ground shock effects on foundations. For safer performance of any structure, the foundation should have sufficient strength and stability. Therefore, prior to any reconstruction or rehabilitation of a building that has been subjected to blast load, it is important to examine the adverse effects on the foundation caused by blast induced ground shocks. This research was proposed to address the above aspects through a comprehensive analysis of the pile structures subjected to both surface and underground explosions.

Due to various constraints, relevant experimental data are extremely scarce. Thus, adequately detailed numerical simulation becomes a desirable alternative.

This research presents a comprehensive study on the blast response of pile foundations. Computer modelling of the pile foundation system was developed using the finite element software LS DYNA. High strain rate effects were introduced for steel and concrete and taken into account in the analyses. Responses such as displacements and plastic effective strains were used to identify local damage in piles

and their potential failure under blast loading. The influence of soil type, the pile reinforcement and the spacing between piles in a pile group have been investigated. The modelling techniques developed and applied in this research and its outcomes can be useful in future studies on the blast response and failure analysis of pile foundations.

Key words

Blast analysis, Underground explosion, Surface explosion, Pile foundation, Reinforced concrete, Numerical simulation, Soil, Finite element method, Fully coupled analysis, Material models, Pile damage

Publications

International Journal Papers

- Jayasinghe L.B, Thambirtnam D.P, Perera N and Jayasooriya J.H.A.R, "Computer simulation of underground blast response of pile in saturated soil", **published** in Elsevier, *Computers and Structures*, 120 (2013), pp 86-95.

- Jayasinghe L.B, Thambirtnam D.P, Perera N and Jayasooriya J.H.A.R, "Blast induced ground shock effects on pile foundations", **published** in *World Academy of Science Engineering and Technology,* 76 (2013), pp 176-180.

- Jayasinghe L.B, Thambirtnam D.P, Perera N and Jayasooriya J.H.A.R, "Blast response of reinforced concrete pile using fully coupled computer simulation techniques", **published** in Elsevier, *Computers and Structures,* 135 (2014), pp 40-49.

- Jayasinghe L.B, Thambirtnam D.P, Perera N and Jayasooriya J.H.A.R, "Blast response and failure analysis of pile foundations subjected to surface explosion", **published** in Elsevier, *Engineering Failure Analysis*, 39 (2014), pp 41-54.

- Jayasinghe L.B, Thambirtnam D.P, Perera N and Jayasooriya J.H.A.R, "Effect of soil properties on the response of pile to underground explosion", **accepted** in IABSE, *Structural Engineering International journal,* 2014.

- Jayasinghe L.B, Thambirtnam D.P, Perera N and Jayasooriya J.H.A.R, "Numerical analysis of the performance of pile foundations to blast loads", **under review** in Taylor & Francis Online, *Structure & Infrastructure Journal.*

International Conference Papers

- Jayasinghe L.B, Thambirtnam D.P, Perera N and Jayasooriya J.H.A.R, "Numerical modelling of effects of blast loads on single pile", **published** in 38th International Conference on Our World in Concrete & Structures, Singapore, August 2013.

Statement of original authorship

The work included in this thesis has not been previously submitted for a degree or diploma at any other higher educational institution. To the best of my knowledge and belief, the thesis contains no material previously published or written by another person except where due reference is made.

QUT Verified Signature

Laddu Bhagya Jayasinghe

April 2014

Chapter 1: Introduction

1.1   BACKGROUND

Many countries across the world have encountered a significant increase in terrorist bomb attacks over the past two or three decades. Figure 1.1 illustrates the steep increase in terrorist bomb attacks on buildings. These bombs are mainly targeted at significant and iconic buildings either by indoor and outdoor explosions. Table 1.1 details confirmed terrorist bombings which occurred in close proximity to buildings. Events such as the truck bomb explosion in the World Trade Centre in New York on February 26, 1993 and the Alfred P. Murrah Federal Building bombing incident in Oklahoma City on April 19, 1995 have caused considerable interest among researchers to investigate the blast response and design of structures in order to protect the integrity of structures and their occupants from the adverse effects of bombings.
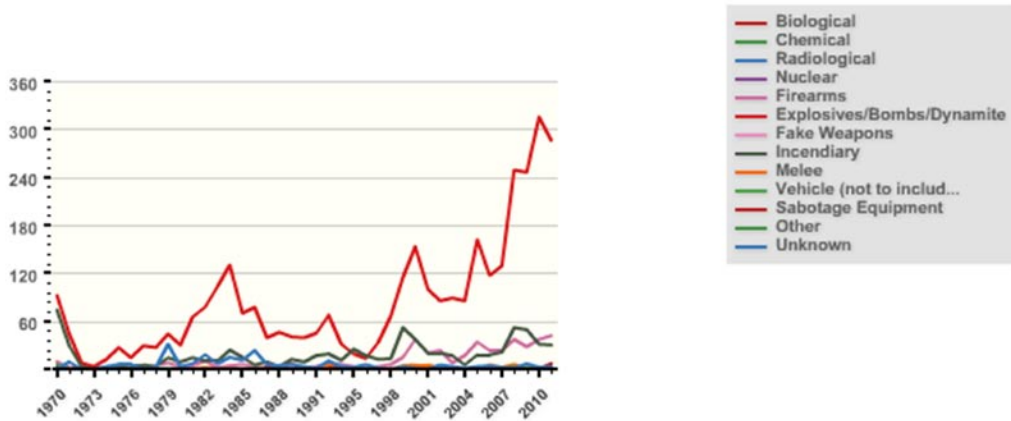
Figure 1.1- Comparison of types of terrorist attacks on buildings (GTD, 2013)

Table 1.1- Terrorist explosions targeting buildings

Date	Building Name	Location	Description
1993 (Feb)	World Trade Center	New York city, USA	Truck bomb in the underground car park 6 people killed
1994 (Jul)	AMIA Jewish Community Center	Buenos Aires, Argentina	Car bomb 85 people killed Partial collapse

1995 (Apr)	Alfred P.Murrah Federal Building	Oklahoma, USA	Truck bomb outside the building 168 people killed Partial collapse
1995 (Sep)	Middlesex Shopping Center	Essex, Maryland	Car bomb at shopping mall 5 people killed
1996 (Jan)	Central Bank	Colombo, Sri Lanka	Truck bomb at the main gate of the building 91 people killed
1996 (Feb)	Midland building and South Quay Plazza	Docklands, London	Truck bomb 2 people killed
1996 (Jun)	Khobar Towers	Khobar, Saudi Arabia	Truck bomb outside the building 19 people killed
1997 (Oct)	World Trade Center	Colombo, Sri Lanka	Truck bomb 15 people killed
1998 (Aug)	US embassy	Dar es Salaam, Tanzania and Nairobi, Kenya	Car bomb 224 people killed
2002 (Jun)	American Consulate	Karachi, Pakistan	Truck bomb 12 people killed
2002 (Oct)	2 Night clubs	Bali, Indonesia	Car bomb 240 people killed
2003 (Aug)	Marriott Hotel	Jakarta, Indonesia	Car bomb 12 people killed
2003 (Nov)	London Bank and British Consulate	Isanbul, Turkey	Truck bomb 26 people killed
2004 (Sep)	Australian embassy	Jakarta, Indonesia	Car bomb 9 people killed
2007 (Dec)	UN office and Algerian government building	Algiers, Algeria	2 Car bombs 60 people killed
2008 (Jun)	FIA building	Lahore, Pakistan	2 Car bombs 28 people killed
2008 (Jun)	Danish embassy	Islamabad, Pakistan	Car bomb 6 people killed
2008 (Sep)	US embassy	Sana'a, Yemen	Car bomb 19 people killed
2009 (Mar)	Shopping mall	Northern Baghdad, Iraq	Car bomb 16 people killed

2009 (Jun)	JW Marriott hotel and Ritz-Carlton hotels	Jakarta, Indonesia	9 people killed
2009 (Oct)	Ministry of Justice and the Baghdad Provincial Council building	Baghdad, Iraq	2 Car bombs 155 people killed
2010 (Feb)	German Bakery	Pune, India	17 people killed
2010 (Jul)	Ethiopian Village resturant	Kampala, Uganda	74 people killed
2010 (Nov)	CID building	Karachi, Pakistan	18 people killed
2011 (May)	Frontier Constabulary training center	Charsadda, Pakistan	98 people killed
2011 (Jul)	Municipal governement building	Taji, Iraq	Car bomb 35 people killed

Bomb explosions provide a sudden violent release of energy from a chemical reaction of an explosive material. In an explosion, part of energy is released as thermal energy, and part is released into the air (air blast) and into the ground (ground shock) as rapidly expanding shock waves (TM5-1300, 1900). Blast loads are short duration dynamic loads with a single phase loading profile. Their typical duration is about 1000 times shorter than that of earthquakes. Thus, structural response under blast loading could be significantly different from that under much longer duration loads such as seismic loads. Blast assessment of structures is complex as it involves an extensive range of parameters related to the blast loading and material behaviour under rapid strain rates. These parameters must be included in any evaluation of the blast response of building structures (Jayasooriya et al., 2011). When a structure subjected to normal loads such as superimposed dead, live, wind or snow loads, it can behave in the elastic range. However, yielding and plastic behaviour must be incorporated in to the blast analysis and design.

Currently, Australian and International standards have limited provisions for designing structures for blast loading (Remennikov, 2003). The Australian standards do not currently provide any guidance for RC pile foundations subjected to blast loading. The

most relevant standard, AS 2159 (2009) is limited and simply refers to the actions specified in AS/NZS 1170 (2002), as well as permanent actions of pile and pile cap, ground movement, handling, installation, and any additional loads. Blast loading is not a consideration within ground movement, and although allowance of additional loads is made, a process is not provided to design specially for blast loads. Even though the actions listed in AS/NZS 1170 (2002) include liquid and earth pressures, they refer to static loads rather than dynamic loads such as blast loads. Also, this standard does not consider settlement, sliding, subsidence, liquefaction or faulting, which are possible effects of blast loading. AS 3600 (2009) provides design guidelines to superstructure members of concrete structures and footings and pile caps, however piles are omitted and fire resistance is the only explosion related consideration in the standard. The content relating to blast loading in the Euro codes is similar to that of the Australian standards. However, EN 1991 Euro code 1 (2006) specially mentions accidental actions due to impact and explosions, but this is not inclusive of external explosions.

In order to design structures to withstand blast loading, it is necessary to ensure the design is suitable for the level of risk and adheres to the appropriate standards. It is then feasible to examine the possible blast effects before establishing a blast resistant design method. The understanding of blast effects on structures, combined with structural damage data from historical explosions, as well as information from research on the response of structures under blast loading enables the evaluation of the effectiveness of current design standards and practices.

Many research projects on blast resistant designs have been carried out by the military services, and the relevant documents are restricted to official use only. In open literature, much effort has been spent in investigating dynamic response and damage of structures to blast loading using different approaches such as analytical methods, experiments and numerical analyses. In analytical methods, the problem is solved using a theoretical model under appropriate assumed conditions. However, this method is only applicable to simple problems. Small scale or prototype experiments involving explosion are very expensive. They also require the use of large amount of explosives, involving risk and danger. Thus, they are typically not feasible in civilian research. These experiments were mainly carried out by military services. With recent development of computer hardware technology, increased research in numerical

simulation of partial differential equations, finite element (FE) modelling and simulations provide a viable and cost effective method for detailed investigation of blast response of the structures for different blast scenarios.

Historical records indicate that the majority of terrorist incidents occurred using a car or a small truck bomb (as can be seen in Table 1.1) where the height of detonation of the bomb from the ground surface is small. In such cases, the explosion occurs near the ground surface. An explosion on the ground surface generates both air-blast pressure and ground shock on structures which are close to the detonation point. However, wave propagation velocities are different for geo-materials and air, and this leads to the ground shock exciting the structure foundation before the air blast pressure arrives at the structure. It is also possible that in some cases both the ground shock and the air blast pressure act on the structure simultaneously. This depends on the distance between explosion centre and the structure and ground motion properties (Wu and Hao, 2005). But in most scenarios, the ground shock excites the structure before the air blast pressure.

Previous studies mainly investigated effect of the loads induced on structural components by air propagated blast shock waves. Relatively less attention has been paid towards the blast loading on and response of foundations. The performance of foundations of structures subjected to blast loads is a critical research area, as these provide an important role in the overall structure response. Pile foundations are the most common foundation systems for civil engineering structures such as high-rise buildings and bridges. Pile foundations transfer the large loads from the superstructure above into deeper, competent soil layers which have adequate capacity to carry these loads. It follows that if these foundations are structurally damaged due to blast loading, the superstructure becomes vulnerable to failure. Therefore, it is important to examine adverse effects on foundation caused by ground shocks prior to any reconstruction or rehabilitation procedures.

The FE method was adopted in this research to investigate the blast response of Reinforced Concreted (RC) pile structures under different blast scenarios. The FE method is an efficient tool for the analysis of soil-pile interaction problems. It can be used to obtain reliable results for the blast response of the single piles and pile groups

by considering the nonlinear behaviour of the materials, dynamic behaviours of the materials including strain-rate effects and separation at the soil-pile interface. However, verification of the FE techniques with experimental data or analytical solutions, whenever possible, is necessary.

1.2   RESEARCH PROBLEM

At present, the performance of the foundation is not normally considered, when evaluating the blast response of a building. Current literature mainly addresses the effect of the air propagated blast shock waves on the dynamic nonlinear responses of structural components such as beams, slabs, and columns (Lan et al., 2005; Ngo et al., 2007; Bao and Li, 2010; Jayasooriya et al, 2011). However, excessive dynamic movements from a blast load may result in unacceptable foundation damage, which can be difficult and expensive to repair because of inaccessibility. Also, the failure of foundation of a structure could result in subsequent damages, such as partial settlement and tilting of the superstructure, leading to cracking and weakening of those structures. Therefore, it is important to examine adverse effects on foundation caused by blast loads prior to any reconstruction or rehabilitation procedures.

A foundation system can fail even if the piles are not damaged by the blast simply due to the combination of secondary action effects such as reduction of effective capacity of the pile due to blast damage, amplification of moments induced by displacements, and amplification of buckling effects. The potential damage due to blast load has not received proper attention in the current practice of pile design. Thus, design of pile foundation under dynamic lateral loads induced by blast remains a challenging issue. This is due to the lack of knowledge on assessing the response of the pile to blast load. This emphasises the need for a study to determine the blast response and vulnerability of pile foundations.

Various parameters including the size, shape, type of the explosive and depth of burial of the explosive, soil properties, the standoff distance of the explosive charge from the pile and pile properties affect the response of pile foundation. It is therefore necessary to identify the influence of each parameter on the blast response of pile foundation system. This research develops and applies comprehensive FE technique to study the blast

response of pile foundation. It also evaluates the influence of important parameters on the response the reinforced concrete pile. Consequently, outcomes of this study will expand the current knowledge on the blast response of a pile foundation and will guide as a reference for future analysis and design.

1.3   AIMS AND OBJECTIVES

The main aim of this research is to develop and apply a comprehensive FE modelling technique to study the response/damage of RC pile foundations embedded in homogeneous single soil profile when subjected to both surface explosions and underground explosions, and assess their vulnerability. To achieve this main objective, the specific objectives are set as follow

- To develop the fully coupled FE models incorporating different material models and strain rate effect to predict the damage of pile foundations subjected to blast loads.
- To verify the developed FE models through available experimental data on blast response.
- To evaluate and compare the behaviour of pile response under different blast event scenarios.
- To conduct parametric studies to study the influence of soil type, pile reinforcement and distance between piles in a pile group on the blast response.

1.4   RESEARCH SCOPE

A surface explosion generates both air blast pressure and ground shock on nearby structures and is described in Figure 1.2(a). Therefore, it can be expected to cause deformations in building superstructure and its foundation due to blast pressures on the superstructure and its pile as shown in Figure 1.2(b). In this Figure, ΔS and ΔP are the superstructure and pile head displacement due to blast pressure on the superstructure and its pile, respectively. Figure 1.3 shows the forces acting on a typical pile. In this Figure, M_s is the vertical load acting on the pile due to the weight of the superstructure above, and F_s is the base shear induced at the top of the pile head by the superstructure due to blast pressures on the superstructure. However, to simplify the analysis, this investigation neglected the action effects induced by the superstructure response to blast

loads. In any case, the blast pressure reaches the pile foundation before it reaches the superstructure and hence considering the blast load effect on the superstructure may be redundant. This means that the scope of this research was limited to studying the response of piles subjected to blast loads neglecting the horizontal base shear force due to blast loads on the superstructure.

(a)

(b)
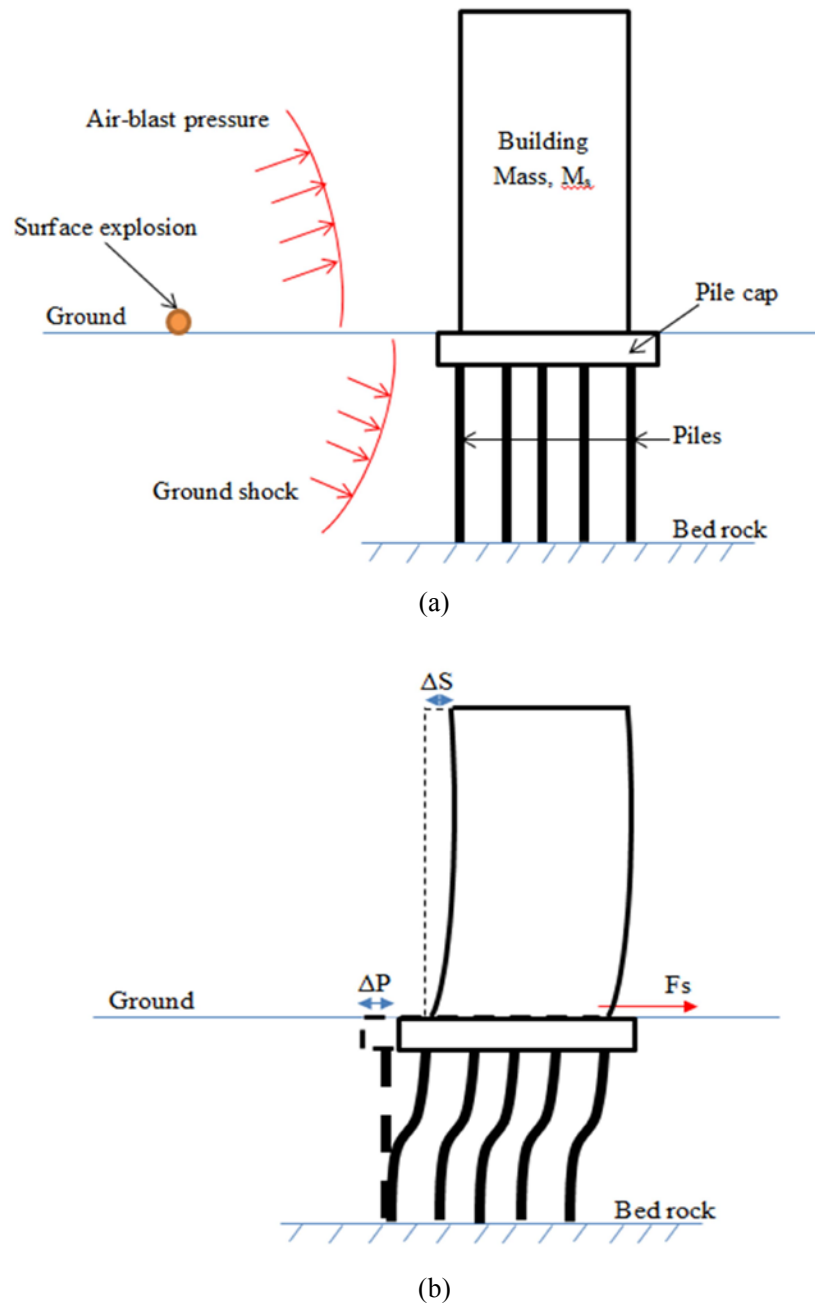
Figure 1.2- (a) Blast pressures on superstructure and its pile (b) Response of structure and foundation
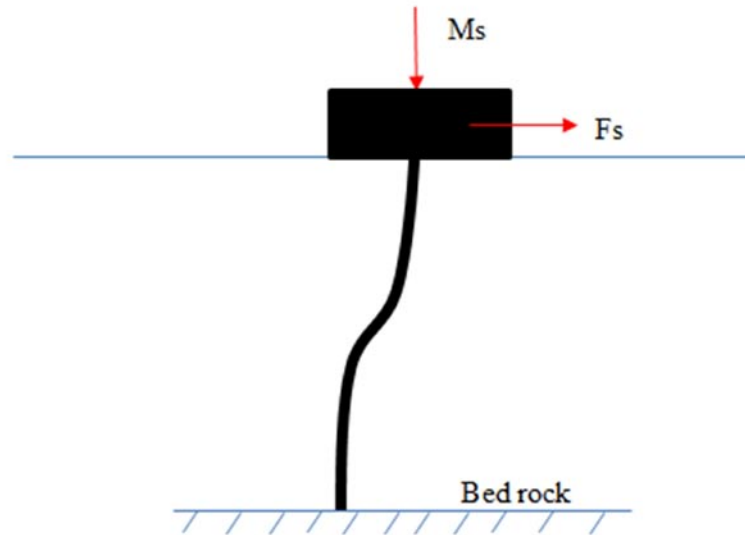
Figure 1.3- Simulation of blast action effect on a single pile – Actual scenario

This research has been carried out using finite element modelling (FEM) and the numerical models were validated using the available results from field experiments. The study was limited to piles (single piles and pile groups) embedded in homogeneous soil deposits. Pile was assumed as a reinforced concrete pile with a straight axis, circular cross section, and is placed vertically. A pile foundation response to the blast loads was investigated under three different soil conditions: saturated soil, partially saturated soil and loose dry soil.

1.5   SIGNIFICANCE AND INNOVATION OF THE RESEARCH

Increasing terrorist attacks have led to greater scrutiny of the design of structures to random and unexpected loads such as impacts and blasts. For safer performance of a structure, its foundation should have sufficient strength and stability. Foundation failure can initiate progressive and catastrophic collapse of the structure under blast load. Despite this, there is inadequate guidance available to assess the vulnerability of foundations to a potential blast load scenario. As a result, there is a need to develop appropriate guidance to design foundations of structures to provide safety to both occupants and structure. There is also a need for information on post event behaviour of the foundations under normal design loads in order to evaluate the required

rehabilitation measures. This research aims in generating the required information that will address these two concerns. The findings of this research provide valuable information on the effects of bomb explosions on pile foundation and will guide future development, validation and application of computer models.

1.6   THESIS OUTLINE

This thesis presents the analysis and outcomes obtained from a FE modelling based numerical investigation on the damage and vulnerability assessment of the RC pile foundations, subjected to different blast scenarios.

The thesis is organized as follows.

- In Chapter 2, a comprehensive literature review is presented.
- Chapter 3 describes the theory behind the numerical methods and material models which were used in this study.
- In Chapter 4, a detailed description on the three-dimensional (3D) FE models and material models to analyse the single pile response under blast loads is provided, and validation of the numerical model using past experimental data is presented and discussed.
- Chapter 5 describes developed FE models to investigate the response of RC pile foundation subjected to different blast scenarios. Various parameters including size and shape of the explosive, depth of burial of the explosive charge and pile reinforcement are considered in order to study their effects on the dynamic response of RC pile subjected to blast loads.
- The study of blast wave propagation in different soils and the evaluation of the effect of soil properties on the pile response under buried explosion are discussed in Chapter 6.
- Chapter 7 describes study on the blast response of RC single pile and pile groups subjected to surface explosion. Two types of boundary conditions at the pile head are considered for the purpose comparison.
- Chapter 8 gives overall conclusions with findings of the research and their significance. The recommendations for further studies are also proposed in this chapter.

Chapter 2: Literature Review

2.1 INTRODUCTION

This chapter reviews the current knowledge on bomb explosion and blasts related parameters, ground shock wave propagation phenomena, crater formation, foundation response under ground shocks and soil-pile interaction.

2.2 CHARACTERICSTICS OF BOMB EXPLOSION

Bomb is an explosive weapon of any range (long or short distance) which provides a sudden violent release of energy from an exothermic reaction of an explosive material. In an explosion, part of the energy is released as thermal energy, and part is released into the air (air blast) and into the soil (ground shock) as rapidly expanding shock waves.

The characteristics of blast loading are affected by the following factors:

- Type and size of explosives
- Location of the explosion centre relative to the structure (e.g. internal or external, confined or unconfined)
- Distance from the explosion centre to the structure

2.2.1 Classification of explosives

Explosions are different from one to another by their explosion characteristics such as detonation rate or velocity, effectiveness, amount of energy released, etc. There are three major groups of explosions.

- Physical explosions (e.g. over pressurized steam boiler)
- Atomic/ nuclear explosions
- Chemical explosions

The research basically focused on chemical explosions. Further, chemical explosives can be categorized into different groups according to their performance, uses and sensitivity as shown in Figure 2.1 (Akhwan, 2004).
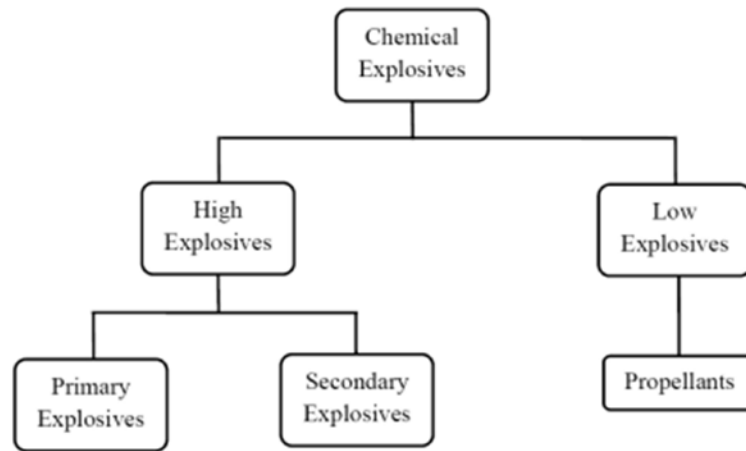
Figure 2.1 – Classification of explosives (Akhwan, 2004)

High explosives are the explosive materials that detonate. This means the explosive shock front occurs and passes through the explosive at a supersonic speed. Their detonation velocities are in the range of 3500-9000 m/s (Shekar, 2010). Low explosive are compounds where the rate of decomposition proceeds through the material at less than the speed of sound. High explosives are divided into two classes according to their sensitivity as primary explosive and secondary explosive.

Primary explosives are also called primary high explosives. When the primary explosives are subjected to heat or shock they are generally get in to detonate. They undergo a very rapid transition from burning to detonation and can transmit the detonation to less sensitive explosives. Because of their sensitivity, they are initiation to detonate by shock, friction, electric spark or high temperatures (Shekar, 2010).

Secondary explosives are generally less sensitive explosive substances and they cannot be detonated easily by heat or shock like primary explosives. They are only can be detonated by a shock produced from a primary explosive. Secondary explosives are generally used in most demolition, mining and military applications. Some examples for

secondary explosives are Trinitrotoluene (TNT), RDX, HMX and Pentaerythritoltetranitrate (PETN).

Propellants are a mixture of combustible materials and an oxidant that decomposes rapidly. Propellants are ready to burn easily but do not make any explosion. They burn more slowly than a high explosive. They can be initiated by a flame or spark and change from a solid to a gaseous state relatively slowly. Examples for propellants are black powder, smokeless propellant.

2.2.2   Chemistry of explosives

Complex chemical and physical processes are involved within the explosive in explosive detonations. The chemical reactions involved in a detonation are exothermic and oxidation reactions. Thus, the reactants are oxidized to give mixture of hot gaseous products.

There are two major types of oxidation reactions involved in a detonation.

- In the first type, there are two reactants, one is an oxidizer and other is a fuel. They react to form the products of the explosion.
- The second type is common in explosives. It involves a single reactant where the oxidizer and the fuel are contained in the same molecule, which decomposes during the reaction and is transformed into oxidized products.

The majority of the explosives are formed from Carbon (C), Hydrogen (H), Nitrogen (N) and Oxygen (O). These are called CHNO explosives and can be represented by the general formula $C_cH_hN_nO_o$, where c, h, n, o are the number of carbon, hydrogen, nitrogen and oxygen atoms, respectively, contained in one molecule of the explosive. During the decomposition reaction, the reactant molecule breaks down into its individual components as follows.

$$C_cH_hN_nO_o \rightarrow cC + hH + nN + oO$$

Then, these individual atoms recombine to form the final products as following;

$2N \rightarrow N_2$

$2H + O \rightarrow H_2O$

$C + O \rightarrow CO$

$CO + O \rightarrow CO_2$
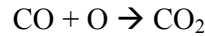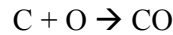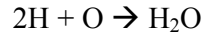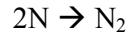
The compositions are formed as the above sequence according to the oxygen availability. If oxygen remains after the formation of carbon dioxide, then the explosive is called **over-oxidized** and forms O_2. If they do not have sufficient oxygen to convert all of the carbon to CO_2, these are called **under-oxidized** explosives. These explosives, the products of the reaction extract oxygen from the surrounding air as they expand freely. The heat generated by an under oxidized explosive is less than that generated by an explosive that oxidizes completely. Therefore, the relative amount of oxygen in an explosive is an important factor in determining the chemical reactivity of the detonation products. It is quantitatively expressed as oxygen balance.

2.2.3   Oxygen balance

Oxygen Balance (OB) is a method to indicate the degree to which an explosive can be oxidized (Zukas and Walters, 1998). If an explosive molecule contains just enough oxygen to convert all of its carbon and hydrogen to carbon dioxide and water, the molecule is said to have a zero oxygen balance. Generally, the oxygen balance is expressed in terms of the weight precent of excess oxygen compared to the weight of explosive.

The general formula to calculate the OB for an explosive is (Cooper, Kurowski, 1996);

$$OB = 100 \frac{AW_O}{MW_{exp}} \left[o - \left(2c + \frac{h}{2} \right) \right]$$ Equation (2.1)

Where,

AW_o – Atomic weight of oxygen

MW_{exp} – Molecular weight of explosive material

o – Number of oxygen atoms

c – Number of carbons atoms

h – Number of hydrogen atoms

Based upon the Eq.2.1, OB for trinitrotoluene or TNT ($C_7H_5N_3O_6$) is -74%. A negative sign indicates a deficiency of oxygen. Hence, the explosive TNT is highly under oxidized.

OB for explosive nitroglycol ($C_2H_4N_2O_6$) is 0%, which indicates that nitroglycol is a perfectly balanced explosive. Nitroglycerine ($C_3H_5N_3O_9$) is an example for over oxidized explosive. Its OB is 3.52%.

2.2.4   Explosives and TNT equivalent

Explosives are different from one to another by their explosion characteristics such as detonation rate, effectiveness, and amount of energy released. TNT equivalent is a datum of quantifying the energy released in explosions. The ton of TNT is a unit of energy equal to 4.184 gigajoules (GJ), which is the amount of energy released in the detonation of one ton of TNT. TNT equivalent is used to compare the blast effects of an explosive with that of TNT.   This is done for technical design reasons in scaling calculation such as for the predication of blast waves, craters and structural response. This is the mass of TNT that would give the same blast performance as the mass of the explosive compound. Some conversation factors for common explosive materials are shown in Table 2.1.

Table 2.1 – TNT equivalent of common explosives materials (Jayasooriya et al., 2011)

Explosive	TNT Equivalent
ANFO	0.82
Composition A-3	1.09
Composition B	1.1-1.2

Composition C-4	1.37
Cyclotol (70/30)	1.14
HBX-1	1.17
HBX-3	1.14
HMX	1.3
H-6	1.38
Minol II	1.2
Nitro-glycerine	1.5
Octol(70/30)	1.06
PBX-9010	1.29
PETN	1.27
Pentolite	1.42/1.38/1.5
Picratol	0.9
RDX	1.2
Tetryt1	1.07
TNETB	1.36
TNT	1
TRITONAL	1.07

2.2.5 Stand-off distance

As shown in Figure 2.2, stand-off distance is the distance between source of the blast and the target. It is very important in the evolution of the threat of an explosion because energy released from a blast decrease rapidly over the stand-off distance.
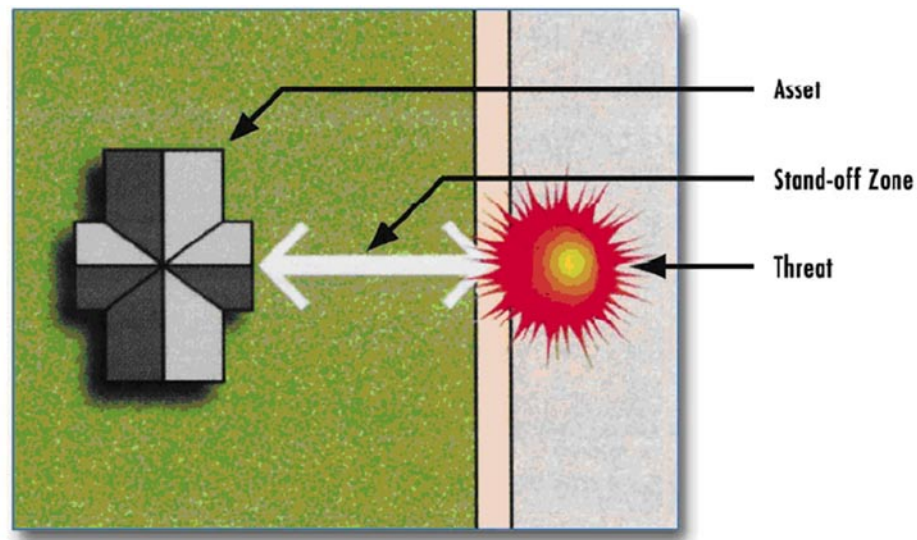
Figure 2.2 – Stand-off distance (FEMA-426, 2003)

2.2.6   Scaled distance

In blast analysis, scaling of the properties of blast waves from explosive is a common practice. Scaled distance, *Z*, is defined as a fundamental parameter to determine the blast-wave characteristic generally in practice. This is described as cube root scaling and it is illustrated as:

$$Z = \frac{R}{W^{1/3}}$$ Equation (2.2)

Where,

Z is the scaled distance in m/kg $^{-1/3}$

R is the range from the centre of the charge (Stand-off distance)

W is the mass of the spherical TNT charge equivalent.

2.3   EXPLOSIONS ON GROUND AND GROUND SHOCK PROPAGATION

When an explosion occurred on the ground, ground shock results from the energy imparted to the ground by the explosion. A part of this energy is directly transmitted through the ground as directly induced ground shock, while part is transmitted through the air as air-induced ground shock.

2.3.1   Air-blast induced ground shock

Air induced ground shock results when the air blast shock wave compresses the ground surface and sends a stress pulse into the underlying soil media. The air induced ground motions are typically downward, and the maximum is at the ground surface (TM5-1300, 1990).

Newmark (1963) used one dimensional wave propagation theory and experimental data to estimate the properties of air blast induced ground shock from nuclear explosion. The same approach has been adopted in TM5–1300 (1990) for conventional high explosives. In there, the maximum vertical displacement, velocity and acceleration at the ground surface are found in terms of overpressure, charge weight and density and seismic velocity of soil.

$$D_v = \frac{i_s}{1000 \rho C_p}$$
Equation (2.3)

$$V_v = \frac{P_{so}}{\rho C_p}$$
Equation (2.4)

$$A_v = \frac{100 P_{so}}{g \rho C_p}$$
Equation (2.5)

Where, D_v, V_v and A_v are the maximum vertical displacement, velocity and acceleration at the ground surface respectively. P_{so}, i_s, ρ and C_p are peak positive incident pressure, unit positive incident impulse, mass density of soil and the compression wave seismic velocity in the soil, respectively.

The maximum horizontal ground motions are expressed in terms of the maximum vertical motions, the seismic velocity of soil and the shock wave velocity (TM5-1300, 1990), so that:

$$D_H = D_v \tan\left[\sin^{-1}\left(\frac{C_p}{12000U}\right)\right]$$

Equation (2.6)

$$V_H = V_v \tan\left[\sin^{-1}\left(\frac{C_p}{12000U}\right)\right]$$

Equation (2.7)

$$A_H = A_v \tan\left[\sin^{-1}\left(\frac{C_p}{12000U}\right)\right]$$

Equation (2.8)

Where, D_H, V_H and A_H are the maximum horizontal displacement, velocity and acceleration at the ground surface, respectively; and U is the shock front velocity.

2.3.2 Direct- induced ground shock

Direct shock results from the explosive energy being transmitted directly through the ground. This motion includes both the true explosion-induced motion and cratering-induced motion (TM5-1300, 1990). Empirical equations have been developed to predict direct-induced ground motions. The equations apply for TNT detonations at or near the ground surface. The maximum vertical displacement, D_v, and horizontal displacement, D_H, of ground surface are given as (TM5-1300, 1990):

$$D_v = \frac{0.25R^{1/3}W^{1/3}}{Z^{1/3}}$$, for rock

Equation (2.9)

$$D_v = \frac{0.17R^{1/3}W^{1/3}}{Z^{2.3}}$$, for soil

Equation (2.10)

$$D_H = 0.5D_v$$, for rock

Equation (2.11)

$$D_H = D_v$$, for soil

Equation (2.12)

Where, *R, W* and *Z* are ground distance from the explosion, weight of TNT charge and scaled distance from the explosion, respectively.

The maximum vertical velocity, V_V and horizontal velocity, V_H, for all ground media are given by (TM5-1300, 1990),

$$V_v = \frac{150}{Z^{1/3}}$$
<div align="right">Equation (2.13)</div>

$$V_H = V_v$$
<div align="right">Equation (2.14)</div>

The maximum vertical acceleration, A_V and horizontal acceleration, A_H, of the ground surface are given by (TM5-1300, 1990),

$$A_v = \frac{10000}{W^{1/3}Z^2}$$
<div align="right">Equation (2.15)</div>

$$A_H = A_v$$
<div align="right">Equation (2.16)</div>

2.3.3 Ground shock wave propagation

The theory of propagating stress wave has been discussed in various text books and publications (Richart et al., 1970; Graff, 1975; Rinehert, 1975; Milklowitz, 1978). This section has briefly summarized some aspects of stress wave propagation applicable to explosions in soils.

The ground shock waves generated due to an explosion can be categorized into different wave types as shown in Figure 2.3. Both body waves and surface waves will be created by explosions on or under the ground surface. Body waves travel through the interior of the earth, and surface waves move along the ground surface. Primary waves, also known as P-waves, travel through the ground medium by causing particles in the medium are displaced in the same direction of wave propagation as shown in Figure 2.4(a). Secondary waves, known as S-waves, move through the ground medium by causing particles in the medium are displaced perpendicularly to the direction of the wave is propagating as can be seen in Figure 2.4(b). In other words, P-waves are

compressional waves that are longitudinal in nature and S-waves are shear waves that are transverse in nature. P-waves are propagated through the medium faster than the other wave types.

The first kind of surface wave is Love wave. It is the fastest surface wave and moves the ground from side to side as shown in Figure 2.4(c). Figure 2.4(d) shows the other kind of surface wave, is called Rayleigh wave (R-wave). On the ground surface, the particles adopt a circular motion in the same direction that the R-wave is moving. Their amplitude at the ground surface can be very large, but this amplitude decays exponentially with depth. As a general rule, body waves (P and S waves) dominate for underground explosions at a short range and also in the other hand, Rayleigh (R-wave) dominates for surface explosions.
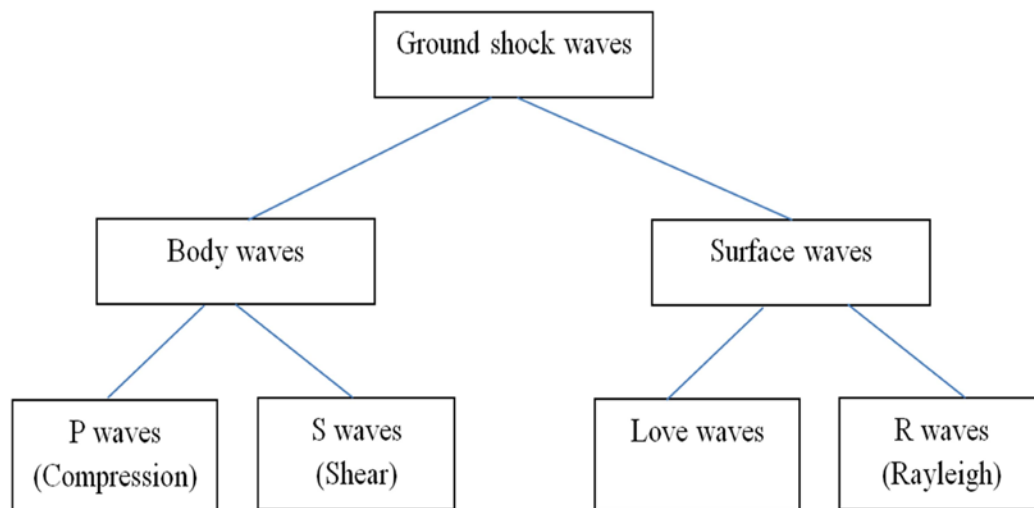
Figure 2.3 – Characterization of ground shock waves
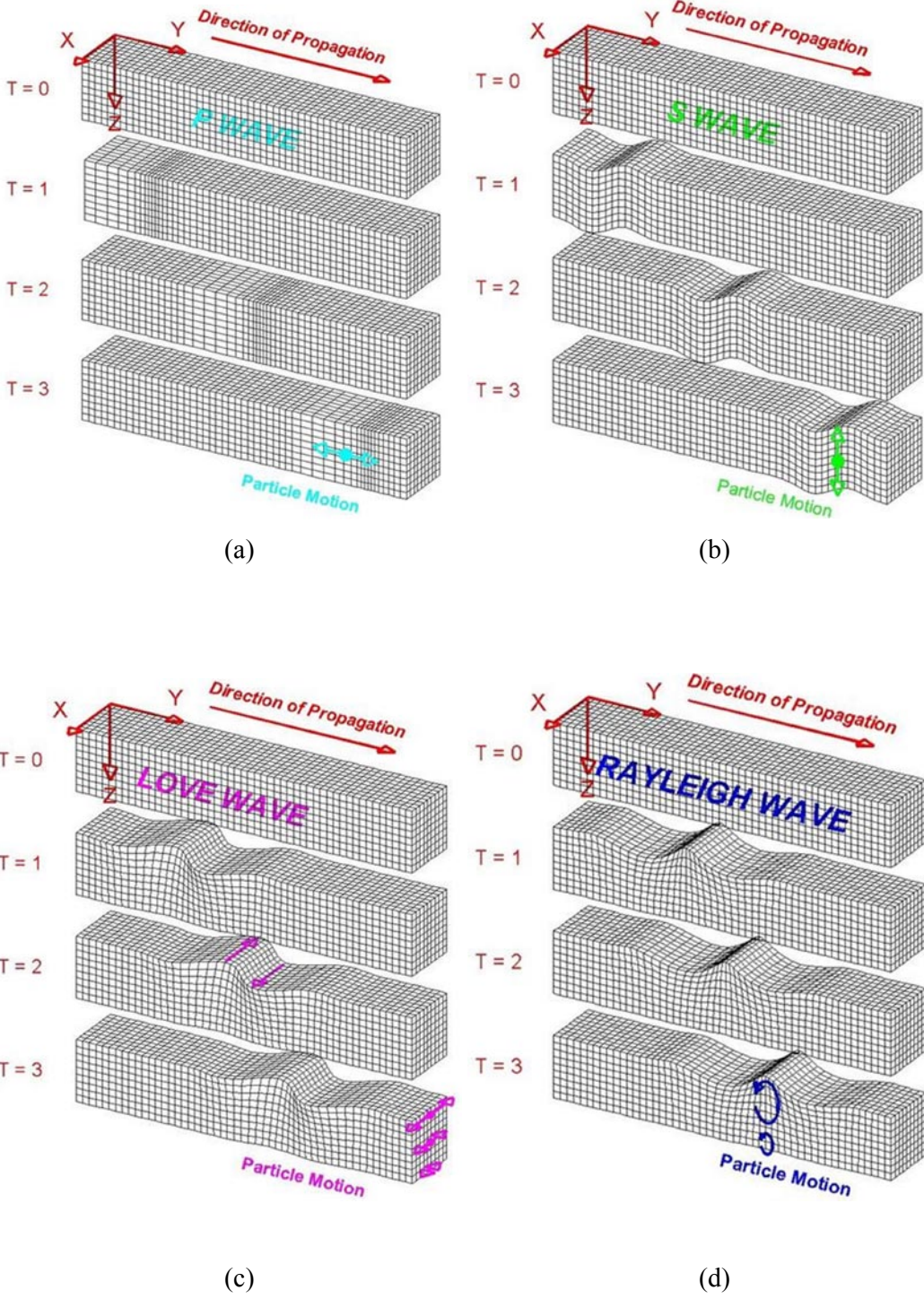
Figure 2.4 – Body waves and Surface waves (a) P wave (b) S wave (c) Love wave (d) Rayleigh wave (Michigan Tech, 2013)

Many studies have been done on the blast wave propagation in the soils and rocks (Drake and Little, 1983; Westine and Friensenhahn, 1983; Wu et al., 2004). Drake and

Little (1983) stated that there are three important variables affect the ground shock intensity induced by conventional weapons. These are weapon size and distance to the structure, the depth of the penetration of the weapons, and the properties of the surrounding soil or backfill. Ground shock intensity can be predicted by using empirical equations. Several past studies present the empirical equations for predicting peak stress caused by confined detonations of explosives in soils. All equations are of the same form for the peak stress, σ_{pk}, and are represented as

$$\sigma_{pk} = f \left(\frac{R}{W^{1/3}}\right)^{-n}$$

Equation (2.17)

Where, f and n are constants depending on site characteristics, and R and W are distance from the explosive charge and mass of the charge, respectively. Table 2.2 shows the values reported for f and n from past investigations.

Table 2.2 – Constants for empirical peak stress equations

f	n	Site characteristic	Reference
59	1.05	Saturated sand	Lyakhov (1961)
10	3	Wet soil	Crawford et al. (1971)
47	1.5	Saturated soil	Drake and Little (1983)
50	1.5	Saturated sand	Bretz (1989)

Note - σ_{pk} in Mpa, R in m, W in kg

2.4   CRATER FORMATION

In the case of explosions above or under the ground, the response and the mechanism of crater formation are still more complex due to the anisotropy and nonlinear nature of the material, to the variability of mechanical properties of the soil. A crater produced by an explosive charge situated on or above the ground level is illustrated in Figure 2.5. Kinney and Graham (1985) defined the crater dimensions produced by explosion on or

above the ground. *D* is the apparent crater diameter, D_r is the actual crater diameter and H_2 is the apparent depth of the crater. The depth of the crater created by an explosion normally is about one quarter its diameter, but this ratio depends on the type of soil involved. The diameter of the crater produced by an explosion also depends on the relative location of the explosive charge to the ground surface. Thus explosions above surface may not create any crater at all (Kinney and Graham, 1985; Ambrosini and Luccioni, 2007).
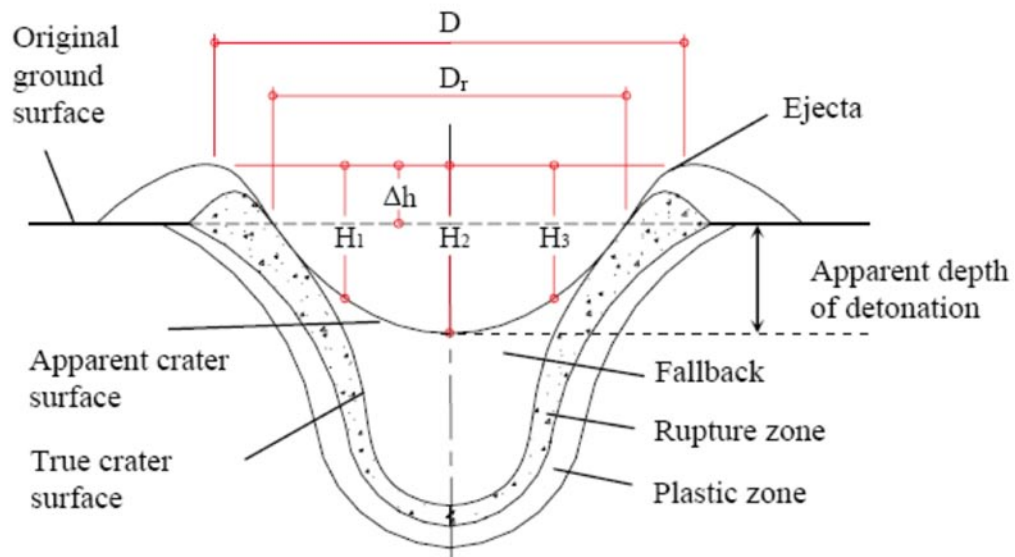
Figure 2.5 – Definitions of the crater dimensions (Ambrosini and Luccioni, 2007)

Most research is related to underground explosions and only few papers are concerned with explosions at ground. If the explosion is close to the surface, a crater is formed. The most important variables defining the crater shape and size are the mass of the explosive, *W*, and the depth of the detonation beneath the air/soil interface, *d*. When *d < 0*, the explosive is detonated above the ground surface, when *d = 0*, the detonation occurs at ground and when *d > 0*, the explosive is detonated underground.

Baker et al. (1991) present a dimensional study to model the crater formation phenomenon in the underground explosions. They obtained the following functional relationship between the depth of the explosive charge and the apparent crater radius, after a dimensional analysis and many empirical observations.

$$\frac{R}{d} = f\left(\frac{W^{7/24}}{\sigma^{1/6}K^{1/8}d}\right)$$
Equation (2.18)

Where, R is the apparent crater radius, d is the depth of the explosive charge, W is the explosive mass, and σ and K are two strength parameters to define the soil properties.

Ambrosini et al. (2002) obtained a following relationship between the depth of the crater and its diameter created by explosions on or above ground level as given in Equation 2.19. In there, they have tested 1, 2, 4, 7 and 10 kg of TNT located at ground, 0.5m above ground level and 1m above ground level. Moreover, Ambrosini et al. (2004) stated that the elastic properties of the soil do not significantly affect on the diameter of the crater. However, a variation of ±5% could be obtained in particular cases.

$$\frac{D}{H_2} = 5.78 + 5.05d$$
Equation (2.19)

2.5   FOUNDATION RESPONSE UNDER GROUND SHOCKS

Previous studies have paid less attention on the effects of blast loading on pile foundation. However, some studies on laterally loaded piles can be found in the literature. Poulos (1991) analysed the behaviour of laterally loaded piles using the continuum theory. It was found that the major factors influencing the pile behaviour are the pile flexibility and the length to diameter ratio, for both fixed-head and free-head piles. Budhu and Davies (1987) presented a numerical analysis of single laterally loaded piles embedded in cohesion-less soil which was modelled as an elastic material. Randolph (1981) studied the response of flexible pile to lateral loading using numerical simulation. Author treated the soil as an elastic continuum with a linearly varying soil modulus and developed a formula to determine the maximum bending moment induced in a free-headed pile.

Furthermore, there are some studies on response of underground structures to blast loading. These investigations are applicable to present study on response of pile foundation subjected to blast loading since the pile foundation, although it is a surface buried structure, can be assumed as a buried structure in some aspects.

To this date large number of computer programs have been developed to study the response of underground structures subjected to blast load. These programs use finite element methods, finite difference methods, or some combination of the two with implementation of various constitutive models, integration techniques and soil-structure interaction interface. Nagy et al. (2009) investigated the response of a buried concrete structure to various factors affecting structural performance by carrying out a parametric study using the FE model. Depths of the structure burial and charge depth of burial were considered as the parameters. Blast wave propagation, the structure response and damage analysis for buried concrete structures were investigated in their study. The authors have concluded that with the same conditions, buried explosions result in significant effects on the buried structure than surface explosions.

Yang et al. (2010) discussed blast resistant analysis for Shanghai metro tunnel using explicit dynamic nonlinear finite element software LS-DYNA. The overall analysis evaluated the safety of the tunnel lining based on the failure criterion. Since there have not been any established common standards governing the design of such a structure, a series of parametric studies have been carried out in order to evaluate the significance of several parameters, such as shear modulus and bulk modulus of soil, on the lining thrust.

Kumar et al. (2010) studied the response of semi-buried structure subjected to non-contact blast loading. Finite element analysis was carried out using ABAQUS. Authors have concluded that the soil-structure interaction between surrounding soil and structure plays an important role in blast load analysis. Authors have also concluded that the displacement and von Mises stress in the structure decreases with increase in buried depth.

2.6   SOIL-PILE INTERACTION

Soil-pile interaction is extremely complex when non-linear conditions and dynamic conditions exist simultaneously and also it plays a significant role in the pile response to external loads. In the analysis of soil-pile interaction through modelling, it involves deformation of soil forces such as pressure, displacement, strain stresses, mises, etc

around the pile. Soil-pile interaction analyses under dynamic lateral loads are performed mainly by Winkler approach, Boundary Element Method (BEM) and Finite Element Method (FEM).

The effects of blast loading on dynamic soil-pile interaction are not considered in past studies. A number of studies are available to account for dynamic soil-pile interaction under seismic and lateral loads. Although, they are usually based on the assumption that the soil behaviour is governed by the law of linear elasticity or visco-elasticity and the soil is perfectly bonded to a pile. However in reality, the bond between the soil and the pile is rarely perfect, but often, slipping or even separation occurs in the contact area (Wu and Finn, 1997).

2.6.1 Winkler approach

This model is also known as Beam on Non-linear Winkler Foundation (BNWF) and due to its simplicity, this model is commonly used in professional engineering practices. The displacement at any point of the soil medium is directly proportional to the stress applied at that depth and independent from any other stress applied at other points along the soil pile interface is the basic assumption for this method. In this method, the pile is modelled as a series of beam-column elements resting on a series of springs and dashpots representing the nonlinear dynamic characteristic of the soil. The shear transfer between soil layers is ignored, because of the theory assumes that the response of each soil layer to the pile loading is independent from the response of adjacent soil layer. Thus, to represent the soil-pile stiffness in each layer, springs elements can be used and the spring stiffness can be determined by using empirical p-y curves which are derived from field tests.

The Winkler models for dynamic analysis of soil-pile interaction under lateral loads are developed by many researchers in the past (Nogami and Konagai, 1988; Nogami et al., 1992). However, this method cannot incorporate the radial and three-dimensional components of interaction. The shear stress which is acting along the side of pile is ignored by this method.

2.6.2   Boundary element method

BEM treats the soil as a continuous medium, and the major advantage of the continuum approach is that it automatically includes the radiation of energy to infinity, known as Radiation Damping, through the complex expression of the pile impedance function. Many researchers in the past (Poulos, 1971) , were developed the formulations based on BEM for dynamic analysis of pile foundations and however, this method is only applicable to visco-elastic materials.

2.6.3   Finite element method

The finite element method is a useful tool in the analysis of soil-pile interaction problems. In certain situations FEM provides a relatively simpler tool for the analysis. This is an appropriate tool to study the response of the single pile and pile groups in the time domain by considering the nonlinearity of the soil medium and separation at the soil-pile interface.

2.7   CHAPTER SUMMARY

Past incidents illustrate that terrorist bomb attacks are mainly targeted at significant and iconic buildings either by indoor and outdoor explosions using a car or a small truck bomb. Therefore, comprehensive investigations are necessary to assess their vulnerability when subjected to blast loads. From the information is available in open literature, it is evident that previous studies mainly investigated the response of structures under air propagated blast shock waves. Also, researchers have put less attention on the blast response of building foundation, especially pile foundation. However, they have studied the pile response under lateral loads such as seismic loads. Also, investigations on the response of underground structures under blast loads can be found in the literature. Since, there is no comprehensive guidance to assess the response of piles to blast loads, future investigated are needed to recommend methods to evaluate the blast damages on pile foundations. Thus, present study was carried out for this purpose.

Since present study was done by using FEM, a brief description about FEM is provided in next chapter.

Chapter 3: Finite Element Analysis

3.1   INTRODUCTION

Today vast number of Finite element (FE) codes are available that are capable of analysing challenging engineering problems. This study was mainly carried out using the explicit nonlinear FE analysis. FE modelling code LS-DYNA was used for the computational simulation during this study. Pre-processing of the FE models, including mesh generation and application of boundary condition, was performed using MSc Patran. The *.key* file, which is the output of MSc Patran, was modified in LS-DYNA with appropriate parameters. The parameters to be modified in LS-DYNA are material models, equation of states, boundary conditions and controlling parameters such as hourglassing and termination. LS-PREPOST was used to visualize the complied results. This chapter describes the theory behind the numerical methods and material models which were used in this study.

3.2   EXPLICIT METHOD

FE analysis can be carried out using either the implicit or the explicit method. The explicit method solves the state of system at a time $t = t + \Delta t$ from the state of the system at time $t = t$, while the implicit method solves the system at a time $t = t + \Delta t$ by iteratively solving sets of coupled equations involving known quantities of the system at time $t = t$ and unknown quantities of the system at time $t = t + \Delta t$. This means that each time increment is computationally inexpensive for the explicit method for which convergence is not an issue. The explicit scheme is conditionally stable and requires very small time steps. Small time step requirement makes the explicit method suitable for short duration dynamic simulations such as blast loading, impact and crash analysis. On the other hand, the implicit method is very popular with most engineering problems where the response is required over a long period of time.

LS-DYNA uses the explicit central difference scheme to integrate the equations of motion. Explicit central difference method is second order accurate, and its geometric representation is shown in Figure 3.1. The critical time increment, Δt_{cr}, for the central

difference method is determined from the highest natural frequency, ω_{max} and the damping ratio, ζ.

$$\Delta t_{cr} \leq \frac{2}{\omega_{max}} \left(\sqrt{1 - \zeta^2} - \zeta \right)$$
<div align="right">Equation (3.1)</div>

For an undamped system, the critical time increment becomes:

$$\Delta t_{cr} \leq \frac{2}{\omega_{max}} = \frac{L}{c}$$
<div align="right">Equation (3.2)</div>

Where, L is the element length and c is the sound speed in the material. The critical time increment must be small enough that the information does not propagate more than one element length during a single time step. If the critical time increment is exceeded, the numerical process becomes unstable.
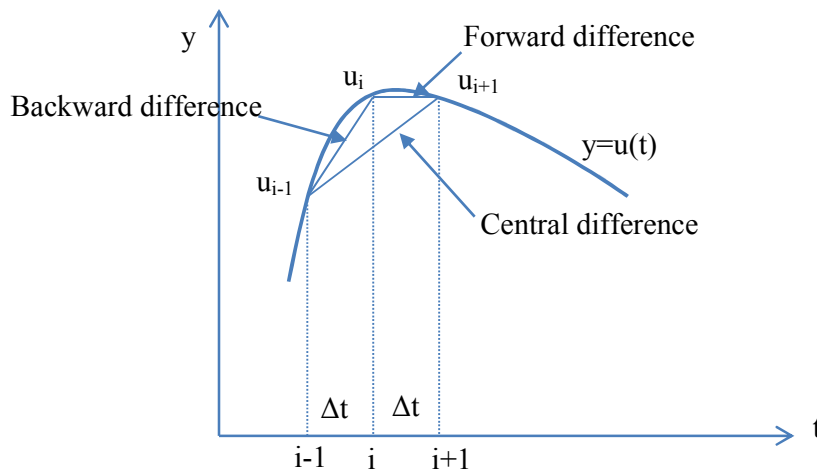
Figure 3.1- Geometric representation of the finite difference formulae

In the explicit FE modelling, two main mesh based formulation can be used to describe the material flow through the elements: Lagrangian and Eulerian formulations. Besides these, a new solver has been developed that combines the Lagrangian and the Eulerian methods: the Arbitrary Lagrangian Eulerian (ALE) solver.

3.3   LAGRANGIAN FORMULATION

In the Lagrangian formulation, the material in an element remains in the element under any deformation. In other words, the numerical mesh moves and deforms with the material, and transportation of materials between the elements does not occur. This behaviour is represented in Figure 3.2. The material interfaces and free surfaces can hence be accurately defined at the cell boundaries in the numerical mesh and the material stress histories can be obtained easily in the Lagrangian domain (Hallquist, 1998). Lagrangian formulation is still dominant for numerical simulation in civil and mechanical engineering. It is well suited for solve problems in solid behaviour.
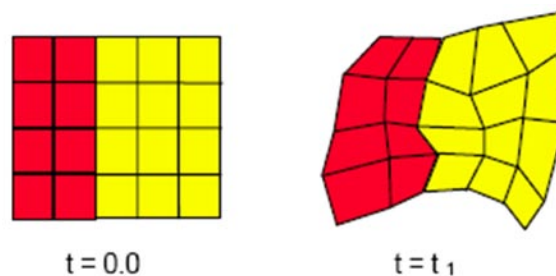
Figure 3.2- Lagrangian representation (Birnbaum et al., 1999)

This Lagrangian formulation is generally suitable for problems without high mesh distortion for large deformation as large distortions of the Lagrangian mesh can give erroneous results or termination of an analysis. However, various methods such as rezoning and erosion can be applied to overcome these problems. Rezoning is normally applied for moderate element distortion cases, and it works by mapping the distorted mesh onto a more regular newly defined mesh. This method will attempt to maintain the global energy balance with old mesh during mapping (Birnbaum et al., 1999). Thus, it may destroy the local energy distribution and gives errors. The erosion criteria also can overcome many problems associated with using a Lagrangian solver for large deformations. When limiting strain or stress is reached within an element, the element is then eroded. When the elements are removed during analysis, their mass and strain energy are also removed from the analysis. Thus, it gives unrealistic results. Generally, Lagrangian formulation is computationally faster than the Eulerian formulation.

3.4   EULERIAN FORMULATION

In Eulerian formulation, the numerical mesh is fixed spatially and material within an element can flow into other elements through stationary mesh as shown in Figure 3.3. Therefore, the time histories of the material properties, material interfaces and free surfaces cannot be accurately tracked as in a Lagrangian solver. The Eulerian formulation is well suited for modelling fluids, gases and large deformation of structural materials. Eulerain solvers are more computationally expensive than the Lagrangian solver. This solver uses a control volume method to solve the governing conservative equations of mass, momentum and energy. In a control volume method, the integral equations are discretised over finite volumes. Each finite volume has a node in the middle. Eulerian solvers use two-step procedure for every calculation time step. The first step is the Lagrangian step where the mesh follows the material flow and distorts. The second step is the advection step where the solution is mapped from the deformed mesh back onto the initial mesh. At the end of each calculation time step of an Eulerain analysis, only the material moves from one location to another while mesh remains stationary.
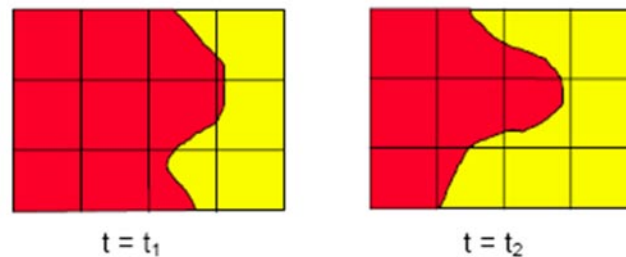
Figure 3.3- Eulerian representation (Birnbaum et al., 1999)

3.5   SIMULATION OF BLAST LOADING IN LS-DYNA

Blast loads are short duration dynamic loads. Their typical duration is about 1000 times shorter than that of earthquakes. Thus, structural response under blast loading could be significantly different than that under much longer duration loading conditions such as an earthquake. Recently different types of numerical methods have been used to investigate the response of underground structures under blast loads. They can be classified as either uncoupled or coupled methods.

The analysis of structures under blast loading can be divided into three phases such as the detonation of explosive charge to form blast shock waves, the propagation of the blast shock waves in the medium (air, water, soil or rock) and the response of structure to the produced blast shock waves. In the uncoupled method, the main physical procedure is divided into several successive stages. The free field stresses are measured first and then these stresses are applied on the structure to evaluate its response. Many numerical investigations were carried out using the uncoupled method (Yang, 1997; Gui and Chien, 2006). In the coupled method all the stages are combined in a single model.

Uncoupled method has been used to analysis of blast loads on structures in different ways in LS-DYNA. First, the time histories of blast pressures are computed empirically with ConWep (Hyde, 1988) and applied directly on the Lagrangian elements of the structures. In addition, LOAD_BLAST and LOAD_BLAST_ENHANCED options available in LS-DYNA can be used to generate blast pressure histories on the structure. Since this method does not model the detonation process of the explosive charge, the computational cost is reduced. However, this method cannot be applied with confidence for near field problems because of the complexity of the flow processes involved in the formation of a blast wave (Luccioni, et al., 2006).

The Multi-Material Arbitrary Lagrangian Eulerian (MM-ALE) method can be used for the full coupled approach including the explosive in LS-DYNA. In this method, two separate meshes, one for the explosive and another for the surrounding medium (soil or air) are required; and they are modelled using multi-material ALE formulation. Multi-material option means that up to three different materials can be modelled within same mesh (Wang, 2001). Thus, using this technique, the explosive product is able to expand into the meshes initially occupied by the soil or air.

Another way to model an explosion source in LS-DYNA requires only a mesh of the surrounding medium (air or soil). The explosive can be defined within the surrounding medium through the INITIAL_VOLUME_FRACTION_GEOMETRY option in LS-DYNA. This option is used in conjunction with the ALE multi-material formulation. The explosive geometry can be specified as a sphere or a cylinder or a cube. This option allows user to model different shapes for the explosive without changing the model mesh. Sherkar (2010) has shown that this method gives the best results for blast wave

pressures in air. Hence this method has used to model the explosive charge in FE models in this study.

In this study, the high explosive burn material model was used to model the explosive charge. It controls the explosive's detonation characteristics. In the high explosive burn model material type, an Equation of State (EOS) is used. EOS is an equation relating the pressure, temperature, and specific volume of a substance. Therefore, Jones-Wilkins-Lee (JWL) EOS is used with this material model to model the explosive. The JWL equation of state defines the pressure as a function of the relative volume, V and initial energy per volume, E, such that (LS-DYNA, 2007)

$$P = A\left(1 - \frac{\omega}{R_1 V}\right) e^{-R_1 V} + B\left(1 - \frac{\omega}{R_2 V}\right) e^{-R_2 V} + \frac{\omega E}{V} \qquad \text{Equation (3.3)}$$

Where, A, B, R_1, R_2 and ω are constants pertaining to the explosive.

In the high explosive burn material model, burn fractions, F, controls the chemical energy release for detonation simulations. The burn fraction is taken as that (LS-DYNA, 2007):

$$F = \max(F_1, F_2) \qquad \text{Equation (3.4)}$$

Where

$$F_1 = \frac{2(t - t_l)D}{3\Delta x} \qquad \text{Equation (3.5)}$$

$$F_2 = \frac{1 - V}{1 - V_{cj}} \qquad \text{Equation (3.6)}$$

In the above equations, D is the detonation velocity, ρ is the density, V_{cj} is the Chapman-Jouget volume, V is the relative volume, t_l is lighting time, t is the current time and Δx is characteristic length of element (LS-DYNA, 2007).

If the burn fraction, F, exceeds unity, it is reset to one and is held constant. The high explosive pressure, P, in an element is scaled by the burn fraction such that:

$$P = F. P_{EOS}$$
<div align="right">Equation (3.7)</div>

In the above equation P_{EOS} is the pressure from an EOS (Equation 3.3).

3.6   MATERIAL MODELS

Wide variety of materials were modelled, including high explosive, air, soil, and the RC pile made of concrete and steel in FE models in this research. One of the most difficult tasks associated with FE modelling is the selection of appropriate material properties to accurately model physical behaviour. Material model which was used to model the explosive is described in the previous section, and material models used for the other materials are briefly described in this section.

3.6.1   Air model

Air was modeled using null material model with a linear polynomial equation of state, which is linear in internal energy per unit initial volume, *E*, and the pressure *P*, as given by (LS-DYNA, 2007)

$$P = C_0 + C_1\mu + C_2\mu^2 + C_3\mu^3 + (C_4 + C_5\mu + C_6\mu^2)\ E$$
<div align="right">Equation (3.8)</div>

In the above equation, C_0, C_1, C_2, C_3, C_4, C_5, and C_6 are constants and $\mu = \dfrac{\rho}{\rho_0} - 1$, where

$\dfrac{\rho}{\rho_0}$ is the ratio of current and initial densities. For gases which the gamma law equation of state applies such as air, the above equation 2.8 reduces to,

$$P = (\gamma - 1)\frac{\rho}{\rho_0}\ E$$
<div align="right">Equation (3.9)</div>

Where, *γ* is the ratio of specific heats.

3.6.2   Soil model

Soil behaviour is significantly affected by void ratio, compaction and moisture content. The void ratio is directly related to the compaction. Compaction reduces the void ratio and it results in increasing the strength and bulk modulus of the soil. The moisture content of the soil can affect the elastic moduli, the shear strength and the softening

behaviour of the soil. However, it effects are complicated and different for different soil types (Lewis, 2004). Test data using Split Hopkinson Pressure Bar (SHPB) (Bragov et al., 2005) showed that the density of soil and the shock velocity are increased with moisture content increasing. Moreover, the strength of the soil is pressure dependent, and it increases at high strain rates (An et al., 2011).

Several material models available in LS-DYNA material library can be used to model the soil behaviour. However, FHWA soil material model was chosen for this study as it includes strain softening, kinematic hardening, strain rate effects, element deletion, and most importantly excess pore water effects. This material model was developed by Brett Lewis (Lewis, 2004) with support from the Federal Highway Administration (FHWA). Due to lack of material property data, the model was developed based on a single set of data available for cohesionless soils. Thus, many of the input parameters of material model are not well defined by the developers or evaluators (Lewis, 2004). Reid et al (2004) suggested values for the input parameters; and to reduce the uncertainties in the definitions of the input parameters, Lee (2006) conducted studies to determine the effects of the major parameters.

FHWA material model assumes that the elastic properties of the soil are isotropic. Bulk and shear moduli are two of the main input parameters. To simulate the effects of voids, the bulk modulus has made to be a function of volumetric strain. As the volumetric strain increases, the bulk modulus increases to simulate the collapse of voids and the stiffening of the material. The effects of moisture content or excess pore pressure are also simulated with changes to the elastic moduli in this material model. The water filled in the voids of the soil causes pore water pressure. As the air voids are reduced during loading, the pore water pressure increases. As pore water pressure increases to excess, the shear strength of the soil is reduced. The pore water pressure, u, is calculated using Equation 3.10 in FHWA material model (Lewis, 2004).

$$u = \frac{K_{sk}}{1 + K_{sk}D_2 n_{cur}} \; \varepsilon_v \hspace{4cm} \text{Equation (3.10)}$$

Where, K_{sk} is the skeleton bulk modulus, n_{cur} is current porosity, D_2 is the material constant controlling the pore water pressure before air voids are collapsed and ε_v is the total volumetric strain.

The effects of excess pore water pressure are simulated as in Equation 3.11 in the material model (Lewis, 2004).

$$K = \frac{K_i}{1 + K_i D_1 n_{cur}}$$

Equation (3.11)

Where, K_i is the nonporous bulk modulus, n_{cur} is current porosity, D_1 is the material constant controlling the stiffness before air voids are collapsed.

Lee (2006) estimated D_1 to be 4.63 per GPa and showed that D_2 has no effect on pore water pressure for fully saturated soil. As strain softening (damage) increases, the effective stiffness of the element can become very small, causing severe element distortion. One solution to this problem is deleting these distorted elements. DAMLEV is the percentage of damage, expressed as a decimal that causes the deletion of an element. EPSMAX is the principle failure strain at which the element is deleted. It is important to note that both DAMLEV and EPSMAX must be exceeded in order for element deletion to occur. Lee (2006) recommended a value of zero (no deletion) as he found that when elements are deleted from a model a detrimental shock wave is produced. Thus element deletion in the soil material model was not considered in the present study as well.

3.6.3 Concrete model

Reinforced concrete is the prime structural material widely used for the construction of protective structures as well as significant buildings. The response of the concrete under the dynamic loading is a complex non-linear and rate-dependent process. According to Bischoff and Perry (1991) the design compressive strength of the concrete can increase by about 25 to 30 precent during dynamic loading of the concrete. However, based on experiments conducted by Ross et al. (1995), the concrete compressive strength enhancement was between 200 to 300 precent at strain rates between 100 to 1000 s^{-1}. Blast pressures normally produce high strain rates in the range of 100 to 10000 s^{-1}.

It is well known that the numerical results are very sensitive to the material properties; thus the ability to define the material model accurately is one of the most important issue in the numerical simulation. The LS-DYNA material library contains several material models that can be used to simulate the behavior of concrete, namely,

material type 5 (soil and foam), material type 14 (soil and foam failure), material type 16 (pseudo tensor), material type 25 (geological cap), material type 72R3 (concrete damage_rel3), material type 84 (Winfrith concrete), material type 96 (brittle damage), material type 111 (Johnson Holmquist concrete) and material type 159 (CSCM concrete). The material model Concrete_Damage_REL3 was used in this investigation for the concrete. It is a plasticity-based model, using three shear failure surfaces and including damage and strain rate effects (Malvar et al., 1997). The literature has shown material concrete_damage_rel3 material model can successfully incorporate non-linear concrete properties (Bao and Li, 2010; Thilkarathna et al., 2010). The advantage of this model is that unconfined compressive strength and density of concrete are the two parameters that are required in the calibration process.

This concrete material model uses three failure surfaces; namely an initial yield surface, a maximum failure surface and a residual surface with consideration of all the three stress invariants (Malvar et al., 1997) as shown in Figure 3.4. Hence it can effectively simulate tri-axial state of stress conditions.

(a)   (b)
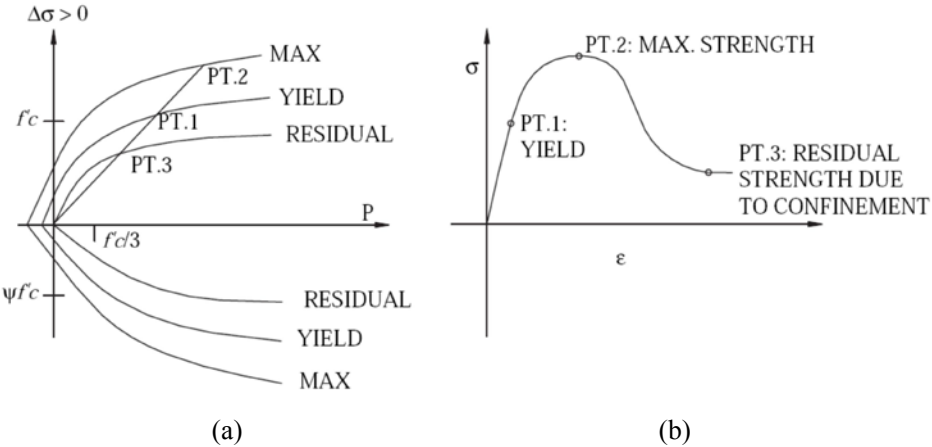
Figure 3.4- (a) Failure surfaces in concrete material model (b) concrete constitutive model (Bao and Li, 2010)

The three failure surfaces are used in the model are defined as follow

Yield surface: $\Delta\sigma_y = a_{0y} + \dfrac{p}{a_{1y} + a_{2y}p}$ 　　　　　　　　Equation (3.12)

Maximum surface: $\Delta\sigma_m = a_{0m} + \dfrac{p}{a_{1m} + a_{2m}p}$ Equation (3.13)

Residual surface: $\Delta\sigma_r = \dfrac{p}{a_{1f} + a_{2f}p}$ Equation (3.14)

Where, p is the pressure and a_{0y}, a_{1y}, a_{2y}, a_{0m}, a_{1m}, a_{2m}, a_{1f}, a_{2f} are constants that must be determined by fitting above equation to the available laboratory test data.

Concrete_damage_rel3 material model uses rate effects to handle shear damage accumulation. A strain rate enhancement factor is used to scale the strength surface when the material subjected to high loading rate. This strength enhancement factor is called the dynamic increased factor (DIF). The dynamic increase factor is the ratio of the strength at a point of interest on the stress strain curve under high strain rate dynamic loading to the strength at the corresponding strain under static loading. The expressions proposed by Malvar et al. (2000) were utilized. The DIF for the concrete compressive strength is given as:

$\text{DIF} = \left(\dfrac{\dot{\varepsilon}}{\dot{\varepsilon}_s}\right)^{1.026\alpha}$ for $\dot{\varepsilon} \leq 30\text{s}^{-1}$ Equation (3.15)

$\text{DIF} = \gamma\left(\dfrac{\dot{\varepsilon}}{\dot{\varepsilon}_s}\right)^{\frac{1}{3}}$ for $\dot{\varepsilon} > 30\text{s}^{-1}$ Equation (3.16)

Where $\dot{\varepsilon}$ is the strain rate in the range of 30 x 10^{-6} to 300 s^{-1}; $\dot{\varepsilon}_s$ is 30 x 10^{-6}s^{-1}; log γ = 6.156α-2; α = 1/(5+9f_c/f_{co}); f_{co} = 10MPa; f_c is the static compressive strength of the concrete. The DIF for concrete in tension is given by:

$\text{DIF} = \left(\dfrac{\dot{\varepsilon}}{\dot{\varepsilon}_s}\right)^{\delta}$ for $\dot{\varepsilon} \leq 1.0\text{s}^{-1}$ Equation (3.17)

$\text{DIF} = \beta\left(\dfrac{\dot{\varepsilon}}{\dot{\varepsilon}_s}\right)^{\frac{1}{3}}$ for $\dot{\varepsilon} > 1.0\text{s}^{-1}$ Equation (3.18)

Where $\dot{\varepsilon}$ is the strain rate in the range of 1 x 10^{-6} to 160 s^{-1}; $\dot{\varepsilon}_s$ is 1 x 10^{-6}s^{-1}; log β = 6δ-2; δ = 1/(1+8f_c/f_{co}); f_{co} = 10MPa; f_c is the static compressive strength of the concrete. Thus, different rate enhancements were included in tension and compression in the concrete material model used in this study.

3.6.4 Reinforcement model

Structures founded on piles are often subjected to lateral loads in addition to the vertical loads. Lateral loads may come from wind, seismic events, explosions and earth pressures. When lateral forces are applied to a pile, bending moments develop in the pile. Where these moments exceed the design bending resistance of the pile, reinforcement is required to resist the bending and tensile stresses.

Both vertical and transverse reinforcements were modelled as elastic perfectly-plastic materials using the plastic kinematic model available in the LS-DYNA for simplicity and applicability. This material model allows a minimum duration of the analysis and can be used with Hughes-Liu beam elements and truss elements (LS-DYNA, 2007). The yield function of the steel is based on the Von-Mises criterion defined as in Equation 3.19.

$$\sigma_y = \beta[\sigma_0 + f_h(\varepsilon_{eff}^p)]$$
Equation (3.19)

Where, σ_0 is the initial yield stress, β represents strain rate effects and $f_h(\varepsilon_{eff}{}^p)$ is the hardening function. Strain rate is incorporated using the Cowper-Symonds model given by (LS-DYNA, 2007)

$$\beta = 1 + \left(\frac{\dot{\varepsilon}}{C}\right)^{1/P}$$
Equation (3.20)

Where, $\dot{\varepsilon}$ is the uni-axial plastic strain rate, C and P are material constants.

3.7 CHAPTER SUMMARY

This chapter presented the theory behind the numerical methods and material models which were used in this research. Numerical simulations were conducted using the FE package LS-DYNA, incorporating the fully coupled simulation technique, different

material models and strain rate effects. Both Eulerian and Lagrangian formulations were used in the models. The soil was modelled using FHWA material model. The concrete_damage_rel3 model was chosen to simulate the concrete with the reinforcement considered as elastic-perfectly plastic material. The explosion process was simulated using the Jones-Wilkens-Lee (JWL) equation of state with high burn material model. Air was modeled using null material model with a linear polynomial equation of state

Chapter 4: Validation of finite element modelling techniques

4.1 INTRODUCTION

Validating the numerical models developed in FE codes verifies the accuracy of the modelling approach and corresponding results. Because small scale or prototype experiments on explosion are very expensive and dangerous, experimental results from the centrifuge model tests by Shim (1996) was used to validate the modelling technique. In addition, validation of concrete material model was carried out by using the experimental investigations (experiment no.2) carried out by Woodson and Baylot (1999). This chapter presents those validations.

4.2 VALIDATION OF THE MODELLING TECHNIQUE

Experimental data from the centrifuge model tests of Shim (1996) were used in the validation process. Shim carried out a series of 70-g centrifuge tests to investigate the blast wave propagation and response of piles embedded in saturated sand. The corresponding prototype model dimensions were used for the numerical simulation.

4.2.1 Experimental set-up

Shim (1996) conducted the centrifuge tests at the 440 g-ton centrifuge facility located at the University of Colorado, Boulder. He carried out a series of 70-g centrifuge tests to investigate the blast wave propagation and response of piles embedded in saturated sand. 14.3cm long Aluminium tubes were used as model piles throughout the tests. Two different boundary conditions at the top of the model piles were employed in the tests. One was the fixed boundary conditions and the other was the free boundary condition with an axial load (Shim, 1996). Cylindrical shape model explosives were placed at the mid-depth of soil in the centrifuge tests. Three different standoff distances from the explosive to the piles were considered in the study. Detailed description of the experiments can be found in Shim (1996).

4.2.2   Development of model and numerical simulation

The numerical models must have the capability to model the detonation of the explosives, blast wave propagation through ground, interaction of the blast wave with the pile and the pile response. The finite element modelling code LS-DYNA was used for the computer simulation to meet these requirements. FE modelling included two parts; first geometry was completed using MSC PATRAN which has been designed based on LS-DYNA solver. In the second part, simulation was completed using LS-DYNA solver. LS-DYNA uses explicit time integration algorithm for solving problems.

The corresponding prototype model dimensions of Shim's centrifuge model were used for the numerical simulation. In a centrifuge model test, a reduced scale model is subjected to centrifugal acceleration so that correct prototype stresses and strains are created in the centrifuge model. This is possible when the model is constructed to 1/N scale and is subjected to an acceleration of Ng (g is the acceleration due to gravity) and mass density of the material in prototype and centrifuge model are the same. When the geotechnical centrifuge is rotating with an angular velocity of ω, the centrifugal acceleration at any radius R is given by

$$\text{Centrifugal acceleration} = R \times \omega^2 \qquad\qquad \text{Equation (4.1)}$$

In a centrifuge test, this centrifugal acceleration is matched to the gravitational acceleration, g, with the same factor which is used to scale down the prototype (i.e. N) as given in Equation 4.2.

$$N \times g = R \times \omega^2 \qquad\qquad \text{Equation (4.2)}$$

Granier et al (2007) have developed required similitude principles and scaling laws to extrapolate model dimensions to prototype dimensions. Table 4.1 presents the scaling laws for common parameters which link the model to an equivalent prototype with respect to a centrifuge acceleration of Ng, where N is the scale factor and g is the acceleration due to gravity. For example a 1kg charge in a model subjected to 70-g's is equal to 343 ton (or 70^3kg) of prototype (full scale) explosives. Figure 4.1 compares the stresses and strains of a prototype and a 1/N scale centrifuge model. It can be seen that the stresses and strains are equal in both prototype and the centrifuge model.

Table 4.5- Scaling laws (Granier et al., 2007)

Parameter	Model at N-g's	Prototype value
Length	$1/N$	1
Area	$1/N^2$	1
Volume	$1/N^3$	1
Mass	$1/N^3$	1
Velocity	1	1
Acceleration	N	1
Force	$1/N^2$	1
Pressure	1	1
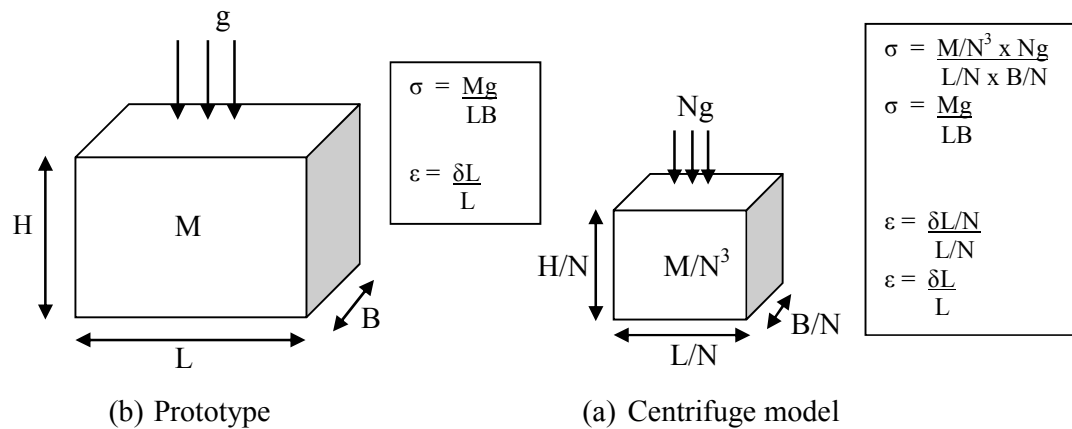
Figure 4.1- Stress similarity in prototype model and centrifuge model (Jayasinghe et al., 2013)

Therefore, FE models are developed for considering an Aluminium pile of 10m length (it corresponds to 14.3cm in centrifuge model dimension) with hollow circular cross section. Table 4.2 shows the pile's dimension and properties. Schematic diagram of the set up with the pile fixed at the top is shown in Figure 4.2. The cylindrical shape blast source is considered at mid depth of the soil (i.e. 5m from top surface) and distance between pile and explosive is equal to 7.5m.

Table 4.2- Dimensions and properties of Aluminium pile (Jayasinghe et al., 2013)

Description	Value
Outer diameter	400 mm
Inner diameter	335 mm
Thickness	65 mm
Alloy and Temper	3003 H-14
Modulus of elasticity	71 Gpa
Ultimate tensile strength	150 Mpa
Yield Strength	145 Mpa
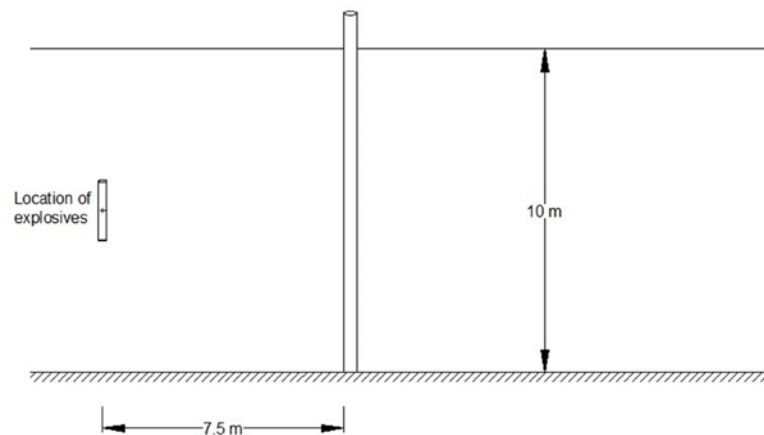
Figure 4.2- Configuration of set-up (Jayasinghe et al., 2013)

The overall the geometric model is divided into different regions representing the soil, air, pile and explosive materials as shown in Figure 4.3. By making use of symmetry, to save computational time, only a quarter of the system was modelled. Eulerian meshes were generated for the explosive, air and for a part of soil that are close to the explosive. This is to eliminate the distortion of the mesh under high deformations. On the other hand Lagrangian meshes were used to model the rest of the system including the pile and the soil region away from the explosive. Eight-node solid elements (brick elements) were used for all parts in the FE model for the 3D explicit analysis. The global uniform

mesh size was set to be 25cm in the model. However, Pile was meshed with 25mm long, 8-node hexagonal brick elements. The 1-point multi material ALE solver (ELFORM=11) was used for the explosive, air and near field soil, while the default constant stress solid formulation (ELFORM=1) was used for the pile and far field soil elements. The materials of the explosive, air and near field soil are specified as multi material using LS-DYNA multi material capabilities (*ALE_MULTI_MATERIAL_GROUP). Thus, using this technique, the meshes are fixed in space and the explosive product is able to expand into the initial soil mesh or air mesh. Similarly the soil can move into the initial air mesh.
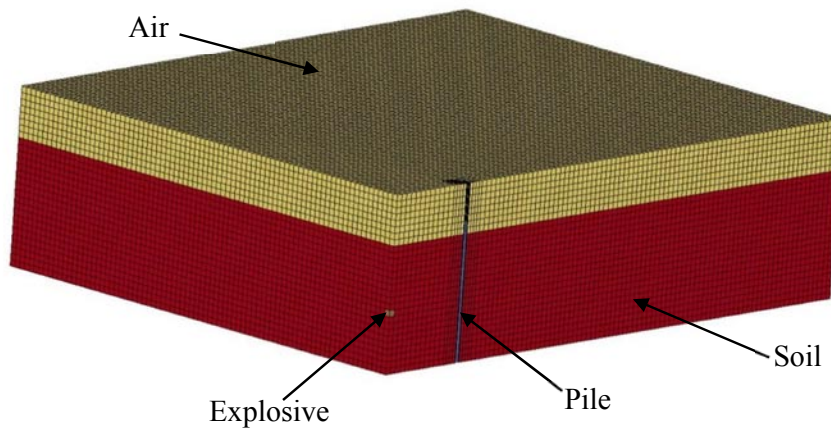
Figure 4.3- Finite element model

LS-DYNA provides different ways to apply the blast load to a model. However, the present study adopts the fully coupled numerical simulation approach. As described in chapter 3, high explosive burn material model was used with the JWL EOS to model the H6 explosive charge. Table 4.3 shows the material constants and EOS parameters used for the H6 explosive (Jones and Northwest, 1995)

Table 4.3- Material model and EOS parameters of the H6 explosive
(Jones and Northwest, 1995)

ρ (kg/m^3)	v_D (m/s)	P_{CJ} (Mpa)	A (GPa)	B (GPa)
1760	7470	24	758.07	8.513
R_1	R_2	ω	V	E_0 (GPa)
4.9	1.1	0.2	1	10.3

The air was modelled using null material model with a linear polynomial EOS. Table 4.4 shows parameters used in the air model.

Table 4.4- Material model and EOS parameters of air

ρ (kg/m^3)	C_0	C_1	C_2	C_3	C_4	C_5	C_6	E_0 (MPa)
1.29	0	0	0	0	0.4	0.4	0	0.25

As seen in section 3.7.2, FHWA material model was used to model the saturated sand. The compressive wave velocity in the selected soil was considered as 1575 m/s. Specific gravity, void of the soil were taken as 2.65 and 0.67, respectively. Degree of saturation of the soil was assumed as 100 percent. The equations in the LS-DYNA theory manual were used to determine the input parameters of the material model.

The pile was modelled using piecewise linear plasticity material model with the material properties of Aluminium alloy 3003 H-14 is given in Table 4.2. Density and Poisson ratio are taken as 2727 kg/m3 and 0.33, respectively for the Aluminium pile.

Furthermore, the bottom of the mesh was constrained in the all the directions to represent the bed rock. To form the symmetry in the FE model, the translational displacements of nodes normal to symmetry planes were constrained. The nodes along the interfaces between the air and soil were merged. Fixed boundary conditions were considered in the top and bottom of pile. The model is subjected to gravity load to provide the hydrostatic pressure and energy on the overburden soil body.

The simulations were conducted in two steps in the model with the pile. The first step was stress initialization to induce steady pre-stress in the model using DYNAMIC_RELAXATION option in LS-DYNA. Due to this dynamic relaxation, stresses in the soil and pile act as initial conditions for the blast analysis. Stress distributions at 600ms show that the model is initialized as shown in Figure 4.4. The convergence and kinetic energy curves for dynamic relaxation are shown in Figure 4.5 and 4.6 respectively. The explosion was initiated as the next phase after the dynamic

relaxation phase. The soil-pile response was analysed in this phase, and the results are discussed in the following sections.
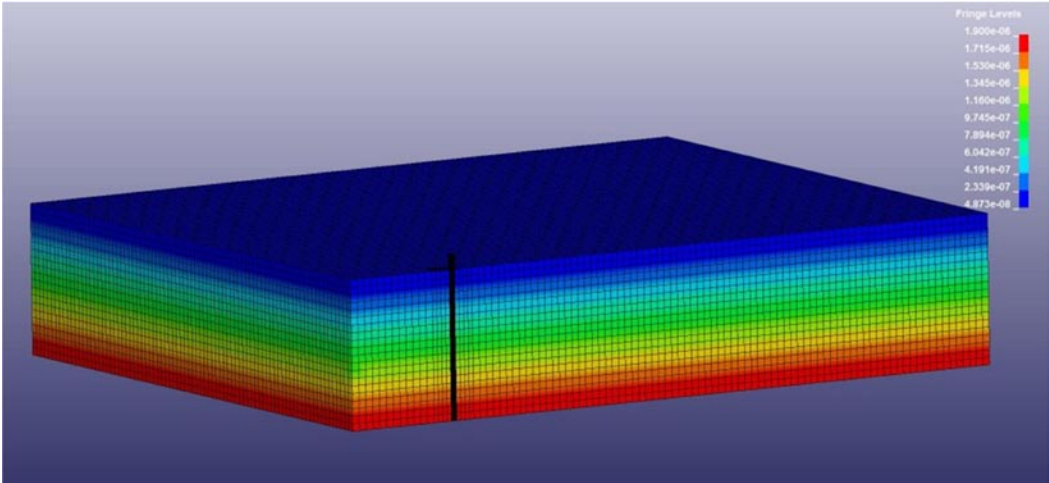
Figure 4.4- Stress initialization at 600ms in the model
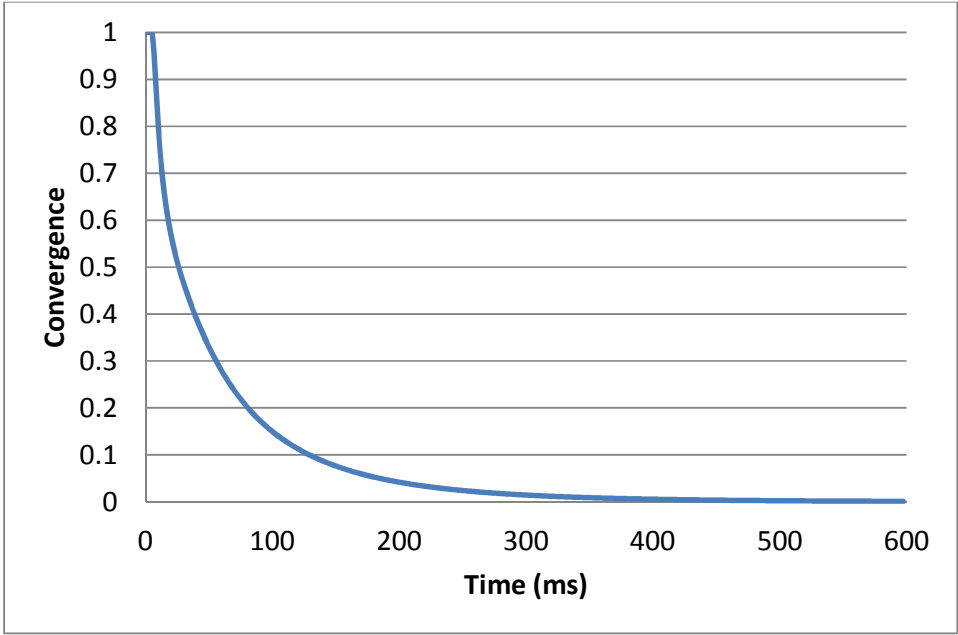
Figure 4.5- Model convergence vs. time
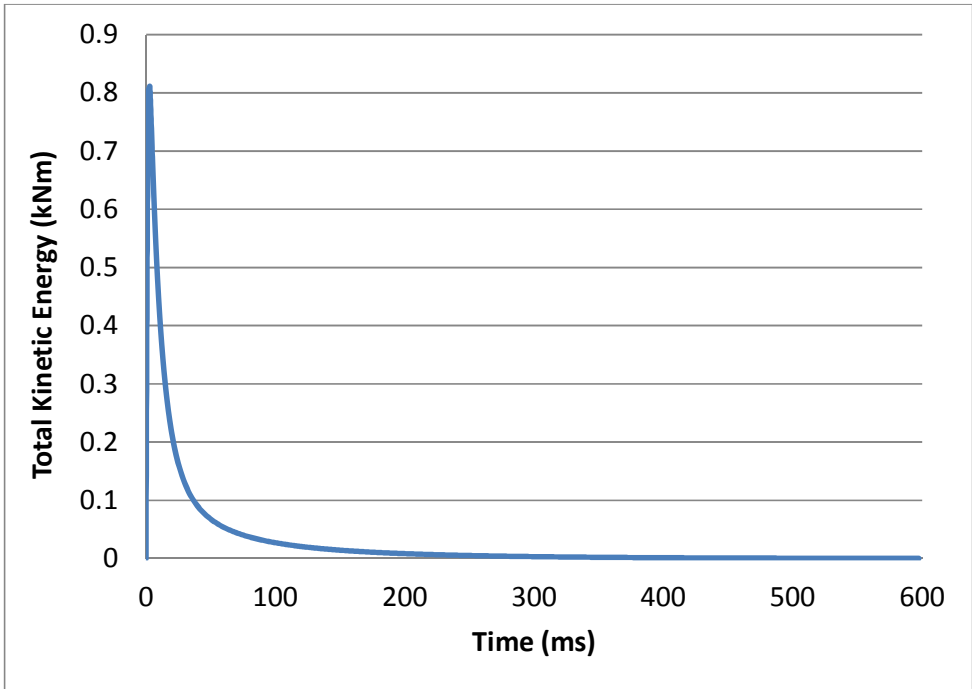
Figure 4.6- Model kinematic energy vs. time

4.2.3 Blast wave propagation through soil

Figure 4.7 shows the progressive wave propagation in the soil at different time incidents. It demonstrates that the pressure waves propagate in the soil in the form of hemispherical waves, with the area of wave front increasing with the wave propagation.

(a)

(b)

(c)

(d)
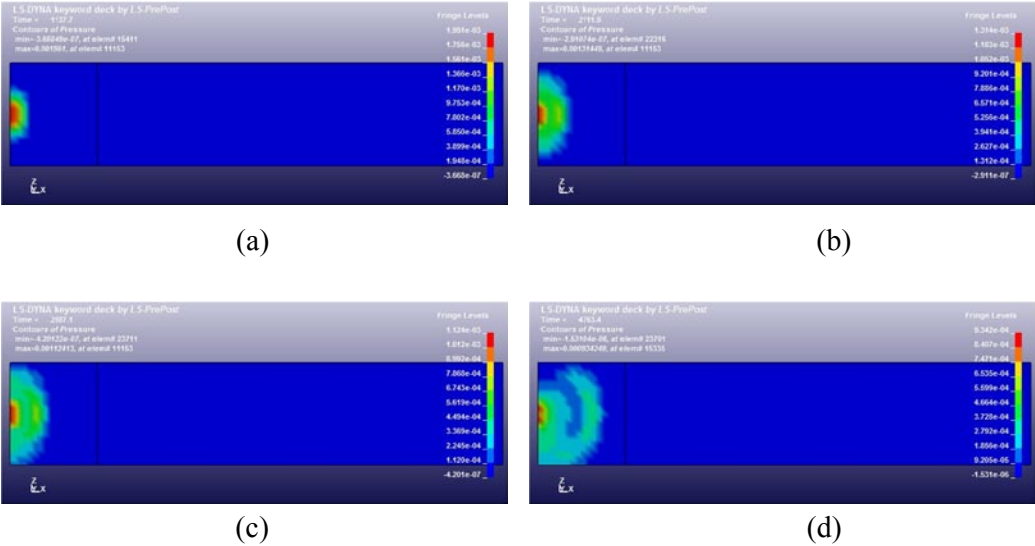
Figure 4.7- Pressure contours in the soil at different times after the detonation

(a) 1.14ms (b) 2.1ms (c) 2.59ms (d) 4.76ms

Stress time histories of the compressive waves at different points in the soil located at 5, 7.5, 10, 12.5, 17, 20 and 25m (measured horizontally) from the charge are presented in Figure 4.8. The propagation and the attenuation of these waves can be clearly seen in this Figure in which the explosive wave pressures are high in the vicinity of the charge and they decrease with the increase of distance.
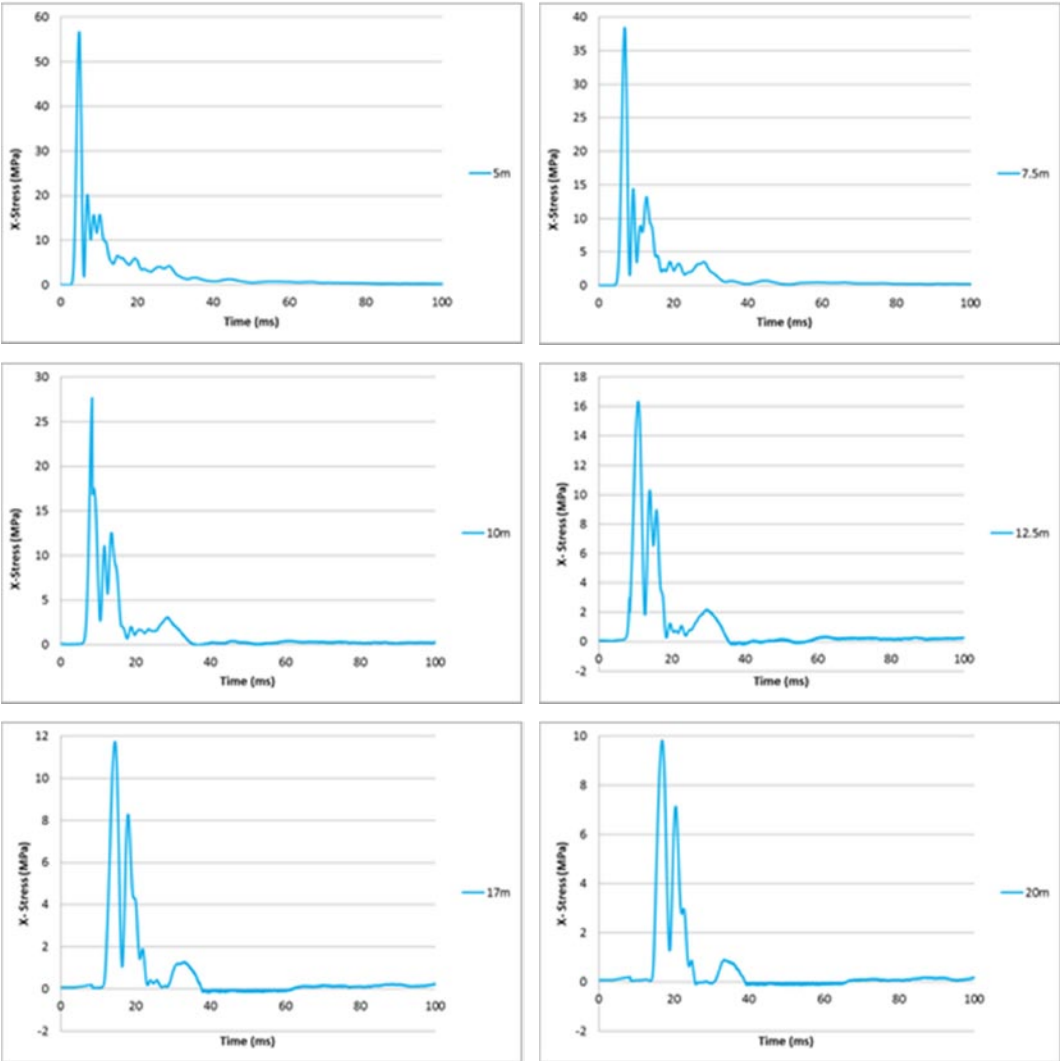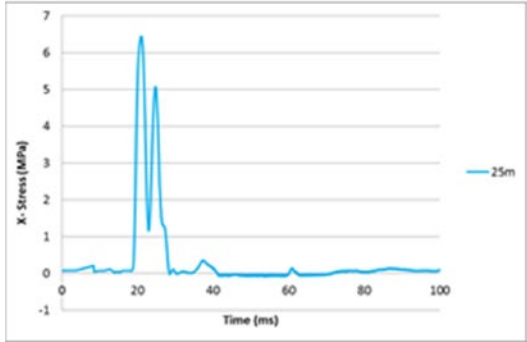
Figure 4.8- Stress time history at different distances in soil from explosive charge

These results for the free field stresses in the soil correspond to the experimental results of Shim (1996) obtained at 7.1, 10.7, 14.3, 17.9, 24.3, 28.6 and 35.7cm respectively. Figure 4.9 shows the peak stress vs. distance plots from the present numerical analysis and those from the Shim's (1996) study. It can be seen that Shim's (1996) experimental results are marginally higher than the present numerical results. This is due to the confinement of charges. The casing of the bomb was not included in the present model, which considered a bare charge in the simulations. Nevertheless, the two sets of results agree reasonably well and provide confidence in the present numerical model.
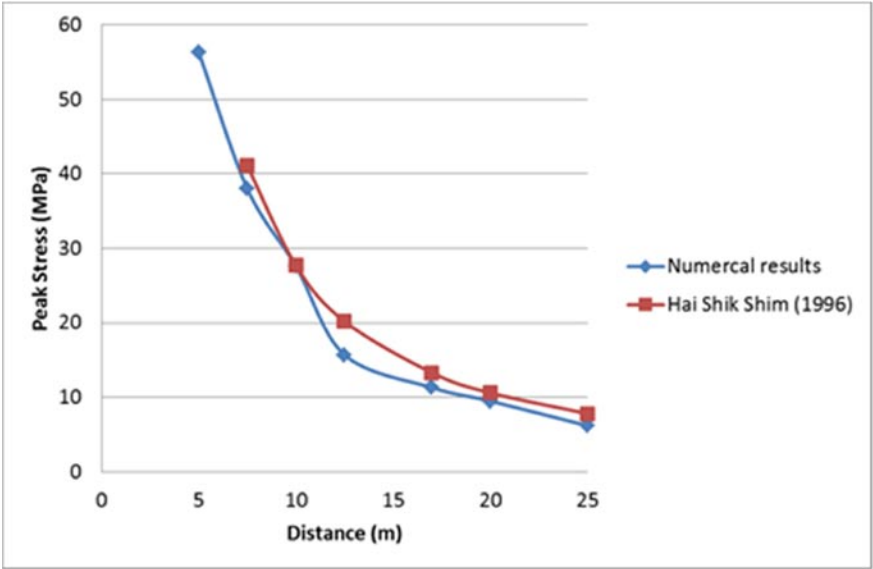
Figure 4.9- Comparison of free field stresses in soil

4.2.4   Response of pile

Considering standoff distances of 7.5m, 12.5m and 17m, pile responses were analysed to compare the results with the corresponding results from centrifuge tests in the reference (Shim, 1996) and hence to validate the model. The horizontal deformation of pile was obtained at 7 monitoring points on the pile as shown in Figure 4.10.
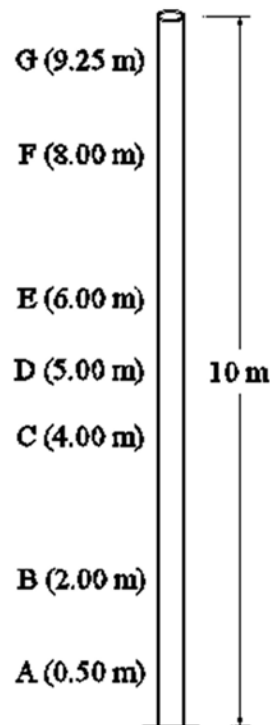
Figure 4.10- Monitoring points on the pile

Figure 4.11 shows the time histories of the horizontal deformation of the pile at the 7 monitoring points for a stand-off distance of 7.5m. It demonstrates that the pile has suffered permanent deformation under the buried blast and the maximum residual deformation of 254mm, occurs at the monitoring point E located 6m above from the pile tip (Figure 4.10). These residual deflections show the occurrence of plastic deformation of the pile under the effect of the blast loads.
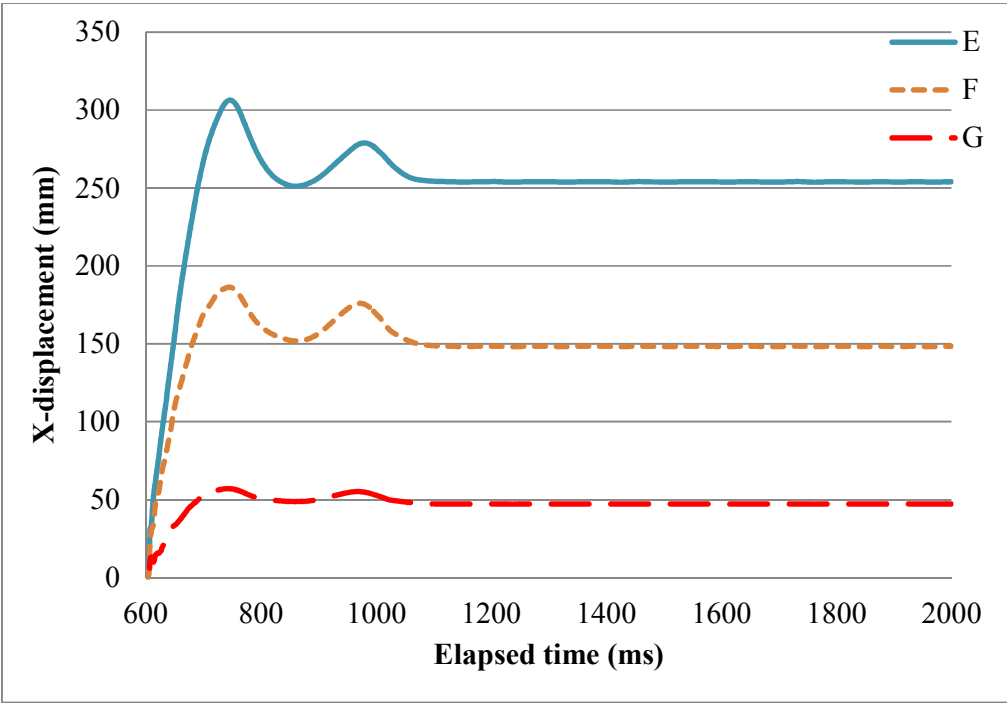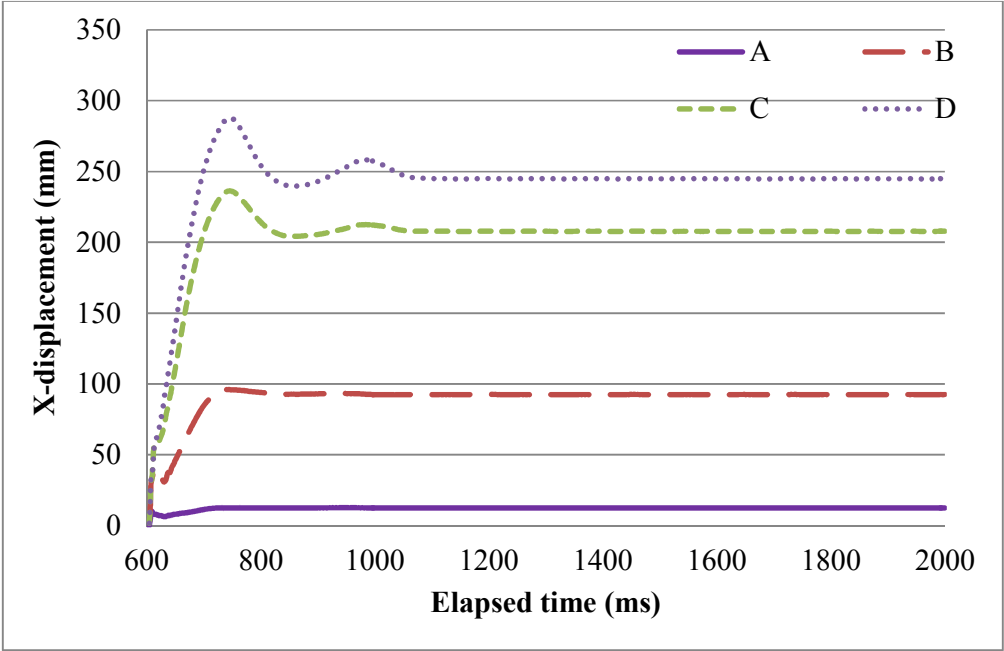
Figure 4.11- Horizontal displacement vs. Elapsed time at seven monitoring points

Figure 4.12 is the comparison of residual horizontal deformations of the pile along its height obtained from the present analysis, for this stand-off distance, and the corresponding prototype values from the experimental results of Shim (1996). The proximity of the two curves indicates a reliable correlation between the present numerical results and the experimental results of the Shim (1996).
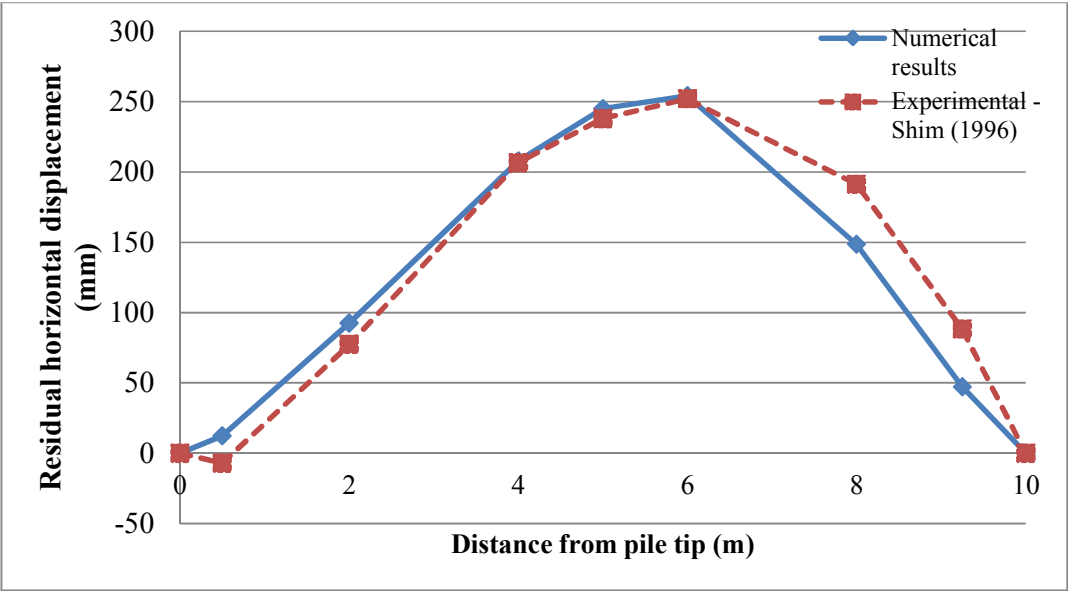
Figure 4.12- Comparison of horizontal deformation of pile

In addition to that, horizontal pile deformation was analysed for the standoff distances 12.5m and 17m cases, also. In Figure 4.13, the horizontal residual deformations of the pile along its height, obtained in the present study for all 3 stand-off distances are compared with those from reference (Shim, 1996). It is evident that the pile response decays dramatically with the stand-off distance or distance from the explosive. It is also clear that results obtained from the present numerical simulations show good agreement with the corresponding prototype values of the experimental results in Shim (1996). Therefore, these results on the pile response provide adequate confidence in the present modelling techniques.
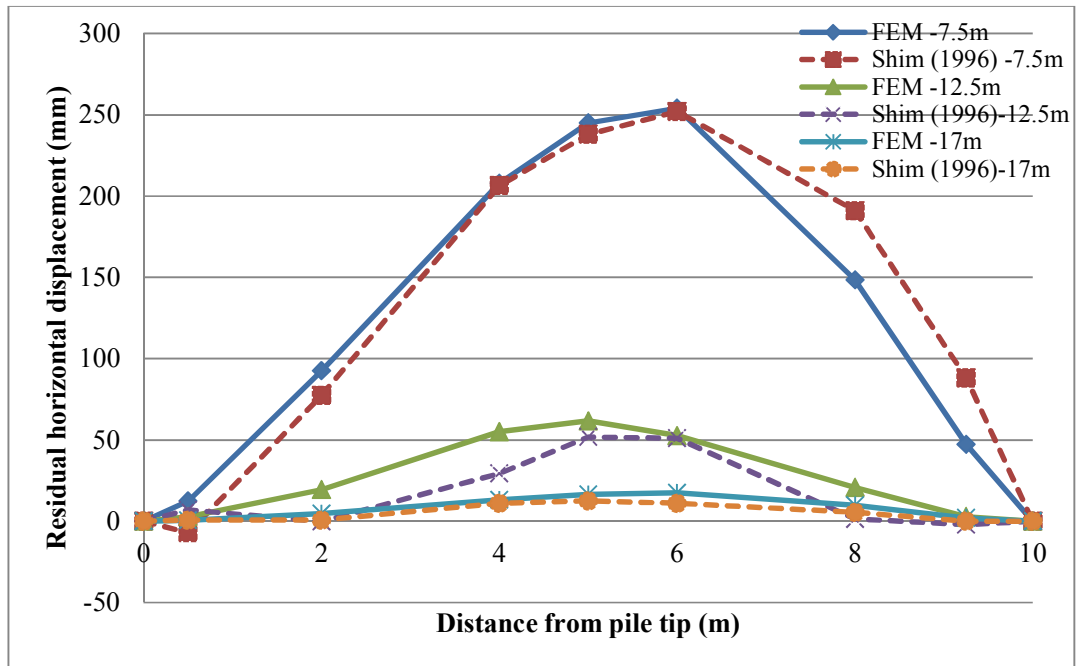
Figure 4.13- Comparison of horizontal deformation of piles

4.3 CONCRETE MATERIAL MODEL FOR BLAST STUDY

The material model Concrete_Damage_REL3 was used in this investigation for the concrete. In this section, the validation of the concrete material model is presented. For that, present study has selected the experimental investigations (experiment no.2) was carried out by Woodson and Baylot (1999).

A series of experiments with five different two-story, quarter-scale RC structures have been conducted by Woodson and Baylot (1999) to investigate the response and damage of the exterior columns when subjected near field blast loads. In each experiment 7.1kg C4 explosive was placed on a plywood table, directly in front of the center column as shown in Figure 4.14. The average unconfined compressive strength of the concrete for these tests was 42MPa.

The first experiment was conducted at a standoff distance of 1.52m. The response of the exterior column was minimal with no measurable permanent displacement. Thus, they carried out experiment No.2 with standoff distance of 1.07m. This experiment has given significant damage on the exterior column. Thus, experiment No.2 was selected to validate the concrete material model used in the present numerical simulation. A

detailed description about the materials and the experiment program can be found in Woodson and Baylot (1999).
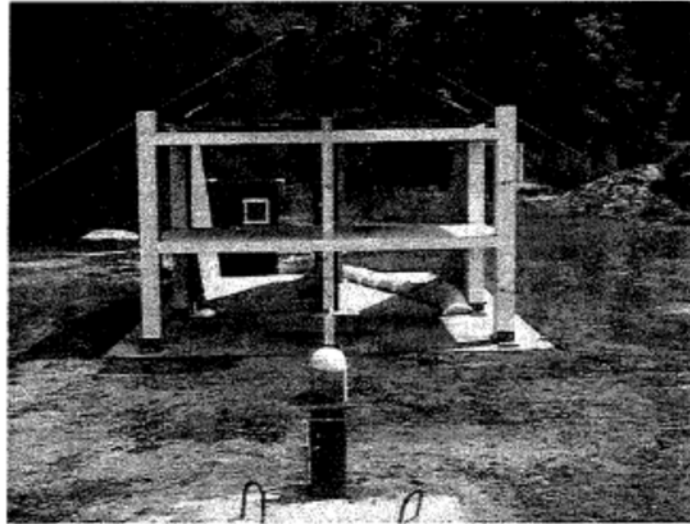
Figure 4.14- Experimental set-up by Woodson and Baylot, 1999

4.3.1   FE model and validation

A 3D FE model for the first floor center column in experiment no. 2 was developed for the validation process as shown in Figure 4.15. Considering the symmetries of the experimental structure, FE model was modelled for the half of critical column (center column) along with the slabs on one side. A part of the slab was modelled and its horizontal movement perpendicular to the blast direction was restricted at the end of the slab panels. Vertical movements were allowed for both first floor and second floor slab panels.

The cross section of the column was 89mm x 89mm square with 8 number deformed wires each having a cross sectional area of 32.2mm^2. Steel wires each having a cross sectional area 3.22mm^2 were provided at 100 mm spacing as cross ties. Weight 7.10 kg of C4 explosive placed 0.2286m above the ground with a standoff distance of 1.07m was considered. A constant pressure of 2.1MPa was applied to the top of the column as a ramp function of time for gravity load initialization before apply the blast load. The load was held constant during the dynamic analysis.

(a)   (b)
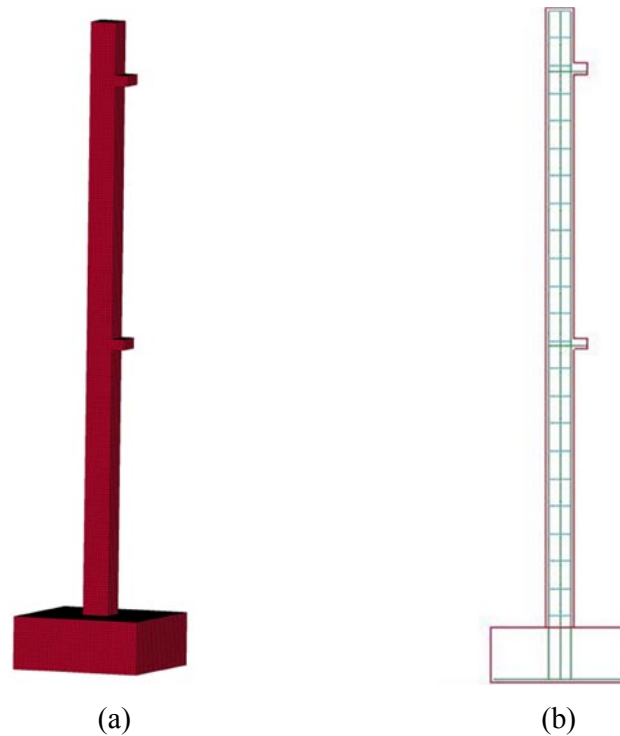
Figure 4.15- Numerical model for validation (a) isometric view (b) 2D view with reinforcement elements

Figure 4.16 illustrates the damage state of the column at different stages of time following the blast by use of an effective plastic strain variation. Effective plastic strain is the damage parameter in concrete_damage_rel3 material model. The colours in the Figure indicate the fringe level which represents the level of damage in the concrete. The blue colour represents the fringe level 0 which indicates elastic state of the concrete, while the red colour represents the fringe level 2 which indicates the residual capacity of the concrete. Other colours which are associated fringe levels 0 to 2 represent the different damage levels of the concrete.

(a)   (b)

(c)   (d)
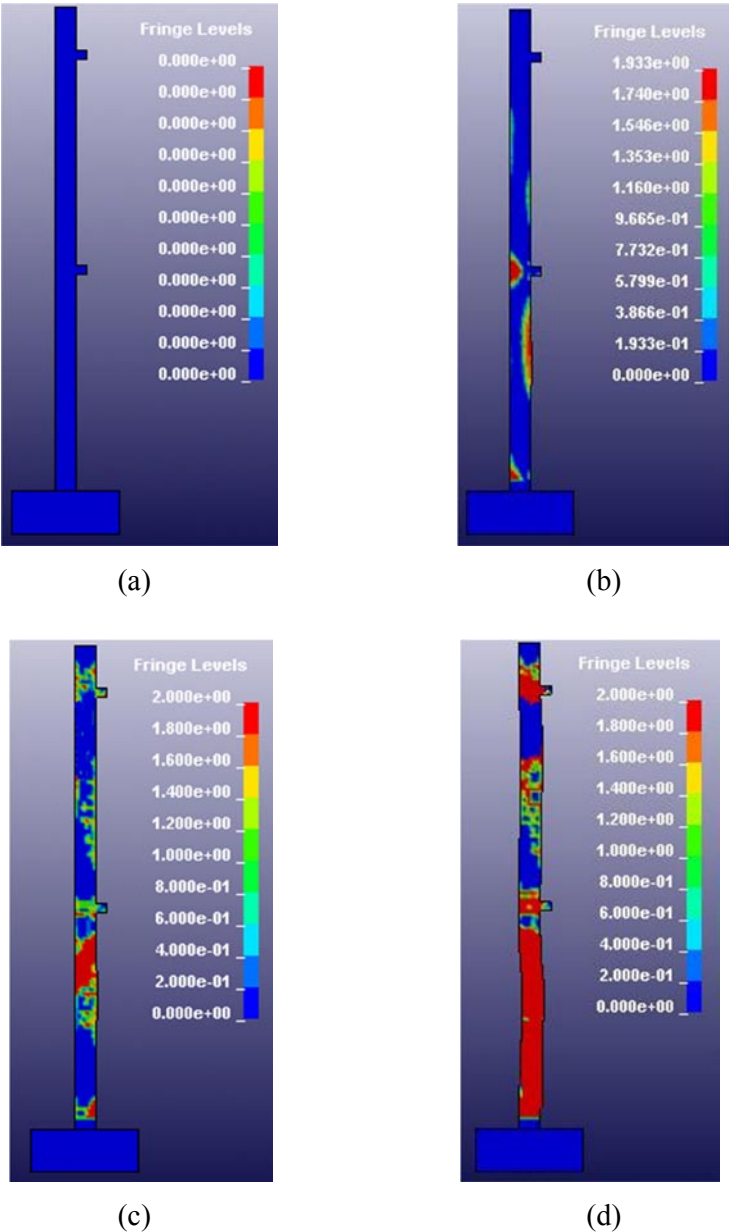
Figure 4.16- Effective plastic strain of concrete at (a) before blast (b) 1ms (c) 4ms (d) 15ms

Figure 4.17 shows the lateral displacement variation with time at the mid-height of the column obtained from the present numerical simulation. Figure 4.18 shows the comparison of the experimental and numerical results for the deflection-time histories at the middle of the column. The present numerical results show good agreement to the experimental results, and better than the numerical results obtained by Woodson and Baylot. This might be due to the better definition of the material models in the present analysis. The peak deflection obtained from the present numerical analysis is a little less

than that in the experimental result. The measured maximum horizontal displacement of the middle height in the experiment was 12.5 mm. It was 12.1 mm in the present numerical simulation. Also, peak deflection of the column occurs at a delayed time instant in the present analysis than the experiment. However, residual deflections are almost same in both present analysis and experimental results. The residual horizontal displacement of the mid-height of the column of 6.3mm was obtained from the experiment. Thus, it shows that the present numerical simulation results agree well with the results from the experimental results in (Woodson and Baylot, 1999) and provide confidence in the choice of parameters and the material models used in this study.
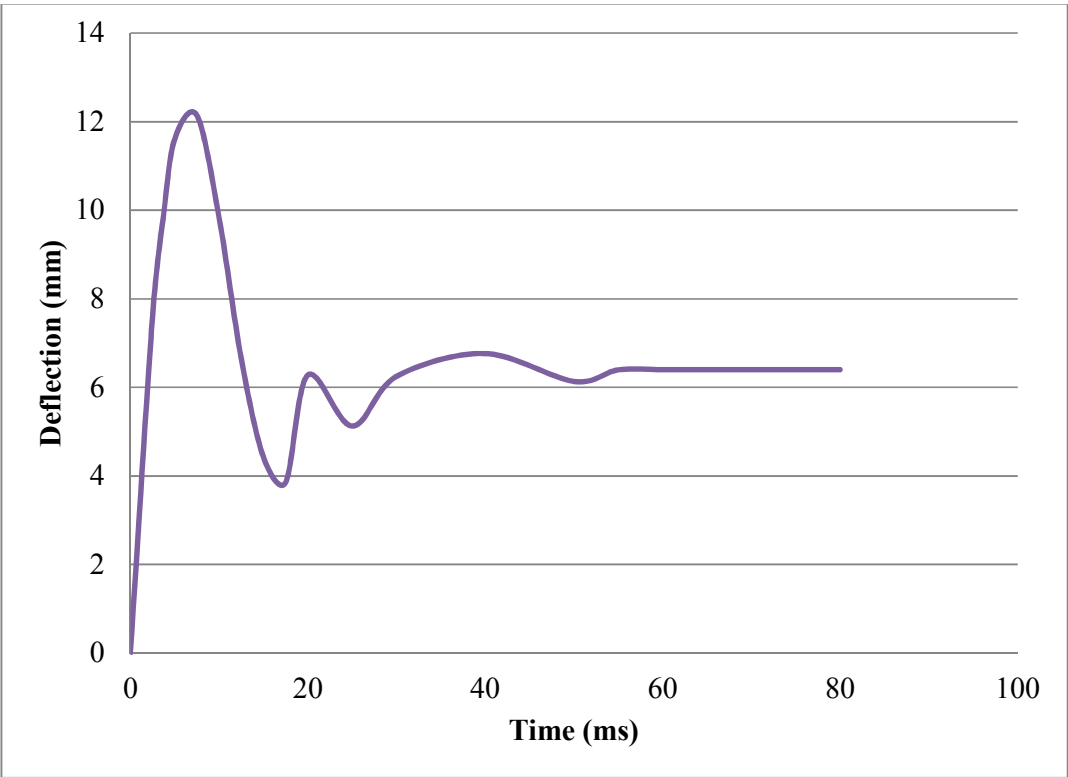
Figure 4.17- mid-height deflection of the column from present study
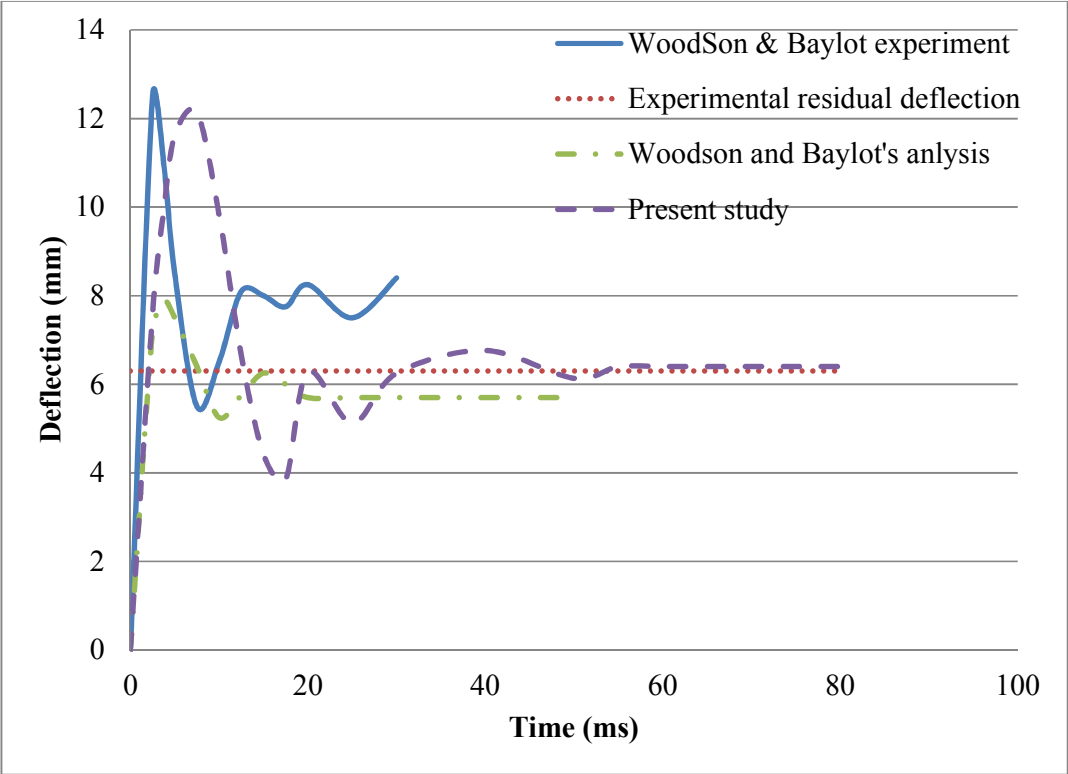
Figure 4.18- Comparison of mid-height deflection

4.4   CHAPTER SUMMARY

In this chapter, numerical method and material models to analyse the RC pile response under blast loads was validated using past experimental data. Experimental results from the centrifuge model tests by Shim (1996) were used to validate the modelling technique. The concrete_damage_rel3 model was chosen to simulate the concrete with the reinforcement considered as elastic-perfectly plastic material. Validation of concrete material model was carried out by using the experimental investigations (experiment no.2) carried out by Woodson and Baylot (1999). The results confirmed the validity of the parameters used in material models, blast load application, boundary conditions, etc., for the detailed investigation of the RC pile under blast loads.

Chapter 5: Effects of blast loads on RC pile embedded in saturated sand

5.1   INTRODUCTION

The previous chapter described the validation of the numerical modelling techniques to investigate the pile response under a buried explosion. For the validation procedure, centrifuge modelling test results by Shim (1996) were used. In there, Aluminium tube embedded in saturated sand was considered in the analysis. The investigation of the response of RC pile foundation subjected to different blast scenarios is however, the focus of the present study. Thus, a single RC pile in saturated sand was simulated by using the same modelling techniques as described in Chapter 4. Various parameters including size and shape of the explosive, depth of burial of the explosive charge and pile reinforcement were considered to study their effects on the dynamic response of RC pile subjected to blast loads. The simulations and the set up are first described and then the results are presented and discussed in this chapter.

5.2   EFFECT OF PILE REINFORCEMENT ON BLAST RESPONSE OF PILE

RC pile in saturated soil subjected to blast loading may fail in several modes such as bending failure, compressive failure of concrete, spalling of concrete, shear failure and excessive settlement. When lateral forces are applied to a pile, bending moments develop in the pile. Where these moments exceed the design bending resistance of the pile, reinforcement is required to resist the bending and tensile stresses. Using the modelling techniques and material models discussed in chapter 2, further numerical simulations were carried out to evaluate the influence of reinforcement on the dynamic response of a 600mm diameter RC pile under blast loading.

The study was carried out for the following cases with different longitudinal and transverse reinforcement ratios. Figure 5.1 and Table 5.1 provide the study cases and the details of the pile reinforcement.

Pile I   Pile II   Pile III

Pile IV   Pile V   Pile VI
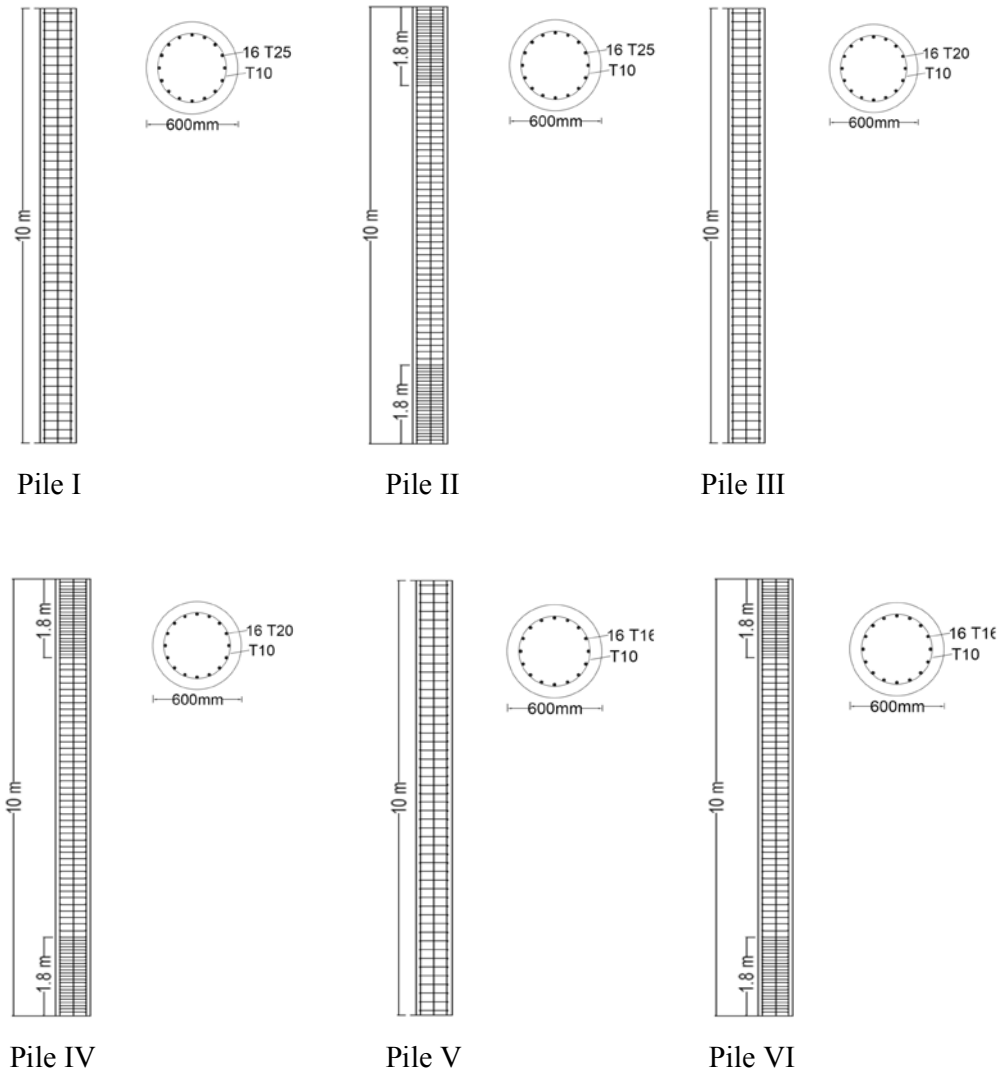
Figure 5.1- Pile geometry and reinforcement details

Table 5.1- Longitudinal and transverse reinforcements of the pile

Pile type	Longitudinal steel	Transverse steel	
		at middle	at ends
I	16T25	T10-200mm $(\rho_v = 0.24\%)$	T10-200mm $(\rho_v = 0.24\%)$
II	16T25	T10-150mm $(\rho_v = 0.30\%)$	T10-65mm $(\rho_v = 0.64\%)$
III	16T20	T10-200mm $(\rho_v = 0.24\%)$	T10-200mm $(\rho_v = 0.24\%)$
IV	16T20	T10-150mm $(\rho_v = 0.30\%)$	T10-65mm $(\rho_v = 0.64\%)$
V	16T16	T10-200mm $(\rho_v = 0.24\%)$	T10-200mm $(\rho_v = 0.24\%)$
VI	16T16	T10-150mm $(\rho_v = 0.30\%)$	T10-65mm $(\rho_v = 0.64\%)$

Longitudinal reinforcement ratio of 2.8%, 1.8% and 1.14% were used to study the effect of the longitudinal reinforcement on the response of pile. Transverse reinforcement ratio ρ_v of 0.24% was used in Piles I, III, V provided at a nominal spacing of 200 mm. For piles II, IV, and VI, spacing of the transverse reinforcement was determined in accordance with the requirement in BS 8004 (1986). This Standard recommends that the minimum lateral reinforcement should be

- 0.2% of the gross volume of the pile in the body of the pile, and
- 0.6% of the gross volume of the pile at each end, distributed across a length of about three times the smaller dimension of the pile cross section.

Thus for piles II, IV and VI, lateral reinforcement of 10 mm diameter bars were spaced at 150 mm ($\rho_v = 0.30\%$) in the body of the pile and at 65 mm ($\rho_v = 0.64\%$) at each end of the pile.

The blast responses of the piles for 500 kg of spherical TNT situated at the mid depth of the soil were determined. Standoff distance was considered as 7.5m for all the cases. The material constants and EOS parameters for the TNT explosive available in Lee et al. (1973) were used in the present study, and they can be found in Table 5.2.

Table 5.2- Material model and EOS parameters of the TNT explosive (Lee et al., 1973)

ρ (kg/m^3)	v_D (m/s)	P_{CJ} (Mpa)	A (GPa)	B (GPa)
1630	6930	21	373.8	3.747
R_1	R_2	ω	V	E_0 (GPa)
4.15	0.9	0.35	1	6

As seen in the section 4.2.2, the FE model involved a quarter of the air domain, soil domain and explosive, and half of the pile, with appropriate boundary conditions at the symmetry edges. However, RC pile was replaced instead of Aluminium pile in the present model. Except for the reinforcing cage, eight noded hexagonal solid elements were used for all parts of the model as in the FE model described in the previous chapter. Figure 5.2 shows the mesh discretization for the concrete elements and reinforcing cage used in this study. Beam elements of 25mm length with 2x2 Gauss integration were used for both the vertical reinforcements and ties. The vertical

reinforcements were defined as Hughes-Liu beam elements with cross integration and ties were defined as truss elements. Vertical reinforcement and ties in reinforced concrete pile were modelled as elastic perfectly-plastic materials using the plastic kinematic model available in LS-DYNA. Material model parameters for steel are listed in Table 5.3.

Figure 5.2- Concrete elements and Reinforcing beam elements

Table 5.3- Material model parameters for Longitudinal and Transverse reinforcements (Thilakarathna et al., 2010)

|	Density (kg/m^3)	Young's modulus (GPa)	Poisson's ratio	Yield stress (MPa)	Tangent modulus (GPa)	Hardening Parameter (β)	C	P
Vertical R/F	7800	210	0.3	548	2	0	40	5
Ties	7800	210	0.3	350	2	0	40	5

5.2.1 Results and Discussion

Blast loads usually have a short duration and high amplitude. Thus, shear stresses develop quickly to a high value, while the flexural deflection has no time to develop. Therefore, shear damage is likely to occur. However, damage modes depend on the properties of the pile. Shear failure is most likely to occur at the top and/or bottom of

the pile because of the fixity at these locations. The transverse reinforcement increases the shear capacity of the pile, and also provides confinement to the core concrete and lateral restraint against buckling of the vertical reinforcement.

As the longitudinal reinforcement and transverse reinforcement ratio increase, both the ultimate moment capacity and shear capacity of the pile increase. Therefore, pile reinforcement is expected to have a significant influence on the failure mode of the piles under blast loading and would improve the blast resistance of the pile with flexural behaviour.

Figure 5.3 shows the time histories of the horizontal deformation of the piles I, III and V. Pile deformations are presented at three heights from the pile tip: 2.5m (point A), 5m (point B) and 7.5m (point C). This Figure demonstrates that the piles have residual deflection. These residual deflections indicate the occurrence of the plastic deformation of the pile and show that the pile has suffered permanent deformation under the buried blast.
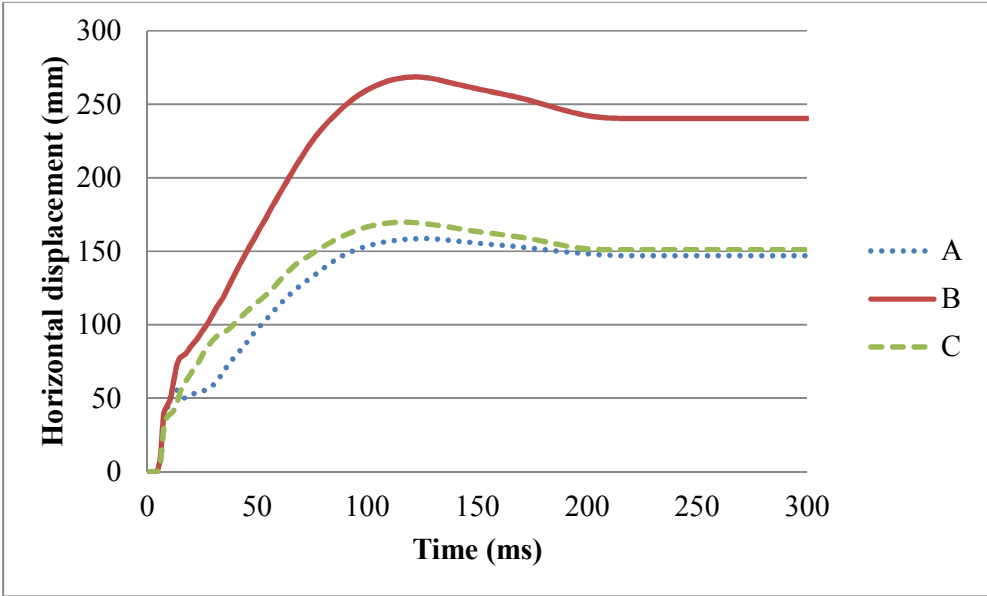
(a)
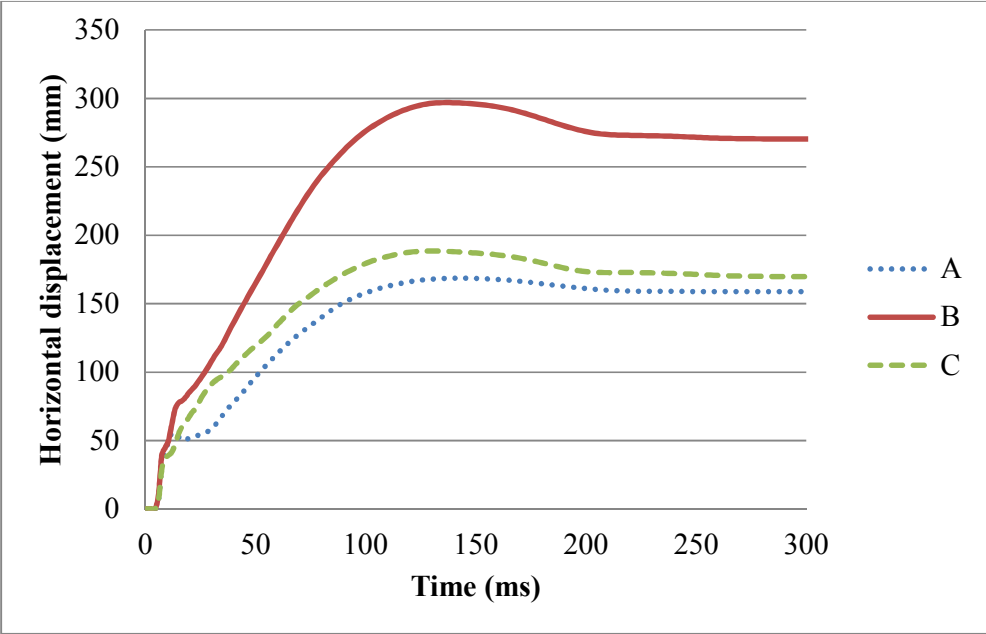
(b)
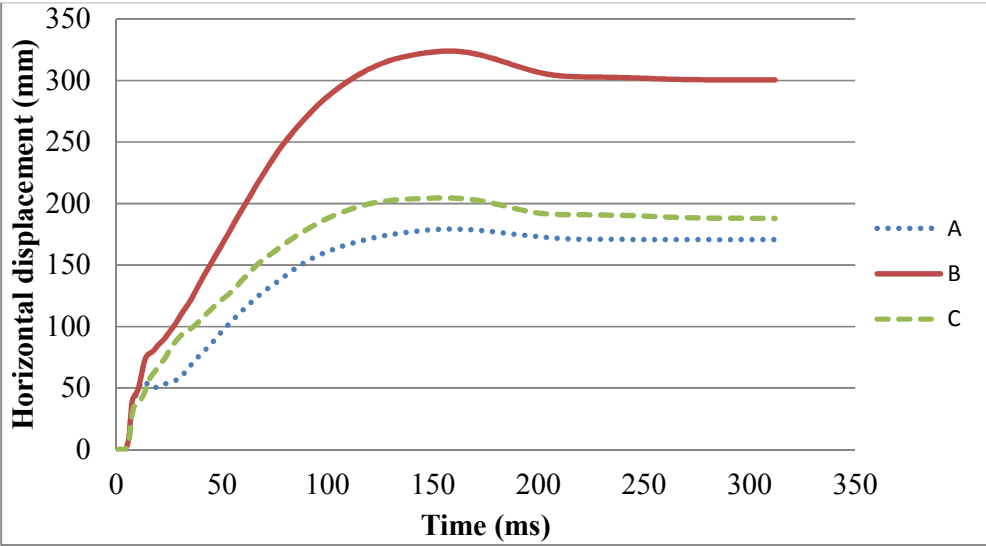
(c)

Figure 5.3- Piles deformation (a) Pile I (b) Pile III (c) Pile V

Figure 5.4 and 5.5 show the effect of the pile reinforcement on the pile deformation. They illustrate the residual horizontal deformations of the RC piles along their heights. Figure 5.4 shows the effect of longitudinal reinforcement ratio on the horizontal displacement response of the piles with the same transverse reinforcement ratio. The maximum residual displacement of 240mm, 271mm and 301mm were obtained for pile

types I, III, and V, respectively. Therefore, it is evident that pile deflections decrease with increase in the longitudinal reinforcement. In Figure 5.5, the results show that the responses of pile types I, III and V (almost) coincide with the responses of pile types II, IV and VI respectively. The pairs of piles with matching residual horizontal deflections have the same longitudinal reinforcement, which has a significant influence. The results in Figure 5.5 also show that the transverse reinforcement of the pile does not have much effect on the pile residual deflections.
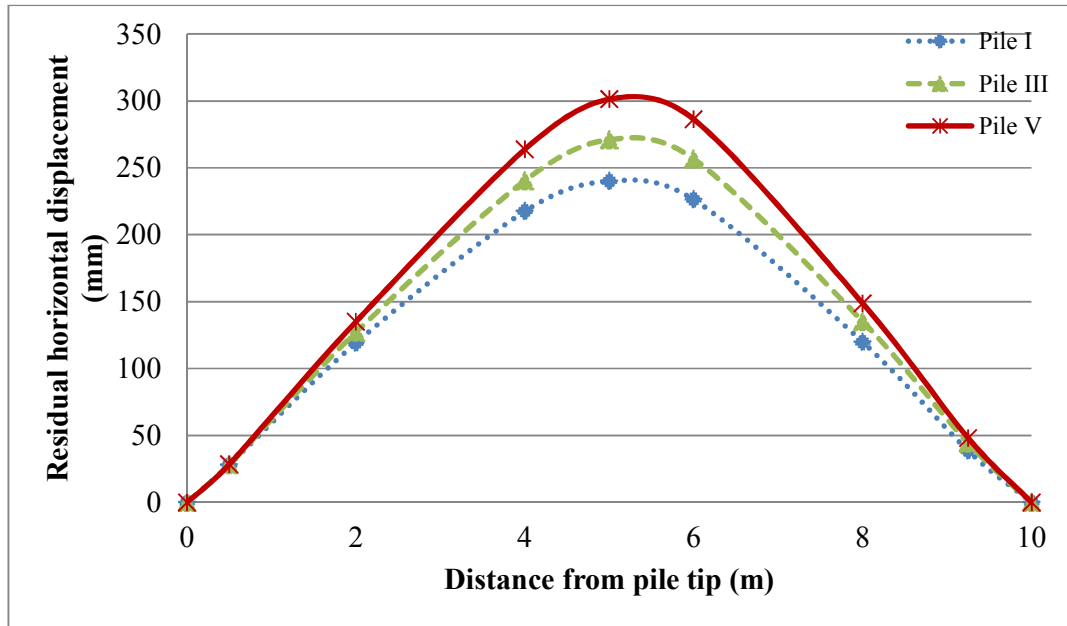

Figure 5.4- Effect of the longitudinal reinforcement on the displacement response of the piles
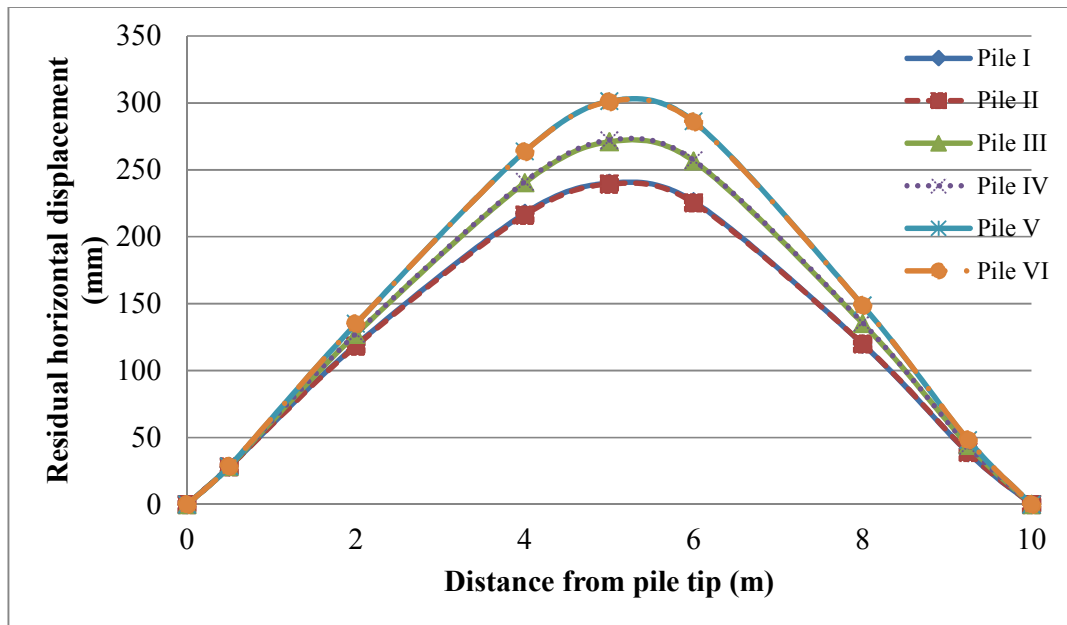

Figure 5.5- Effect of the pile reinforcement on the displacement response of the piles

Blast damage in each pile with the aid of effective plastic strain diagrams and element erosion as obtained from the present numerical simulations, as shown in Figure 5.6. Effective plastic strain is the damage parameter in concrete_damage_rel 3 material model. The colours in the effective plastic strain diagrams denote the fringe level which represents the level of damage in the concrete. The blue colour represents a fringe level 0 which indicates linear elastic state of the concrete while the other colours with associated fringe levels vary from 0 to 2 represent the different damage levels of the concrete. Fringe level 2 indicates maximum plastic yielding of concrete (LS-DYNA, 2007). The element erosion option was implemented to simulate the concrete crushing in the numerical models. The erosion option provides a way of including failure to the material models. This is not a material or physics based property. However, it provides a useful means to imitate concrete spalling phenomena and produce graphical plots which are more realistic representations of the actual events (Elsanadedy et al., 2011). By using this feature, when the material response in an element reaches a certain critical value (strain based, stress based, etc.), the element is immediately eroded and physically separated from the rest of the mesh. In this study, concrete_damage_rel3 material model was used to simulate the concrete behaviour. This material model does not have erosion criteria. However, the erosion algorithm was implemented in FE models by using mat_add_erosion option in LS-DYNA. There may be a variety of criteria governing the material erosion. In this study, the concrete elements in the pile were allowed to erode when the principle tensile strain reached 0.01 (Tai et al., 2011).

It is evident from Figure 5.6 that all the piles were critically damaged. Concrete elements have eroded in the piles ends, which mean that the concrete at the pile ends were totally destroyed in all the cases. Moreover, Reinforcements were found to have severely deformed and concrete elements have eroded at the mid heights of the piles as well. It is therefore evident that the piles have been subjected to a combination of shear and flexural damage. Also, as can be seen in the Figure, under the same blast load, damage in the piles with ties at nominal spacing is slightly greater than that in the piles with ties provided in accordance with BS 8004 (1986).

Based on the above results, it can be concluded that the longitudinal reinforcement in a pile has a significant effect on pile deformations under blast loads. These deformations decrease with increase in the longitudinal reinforcement, as can be expected. Also,

proper detailing of ties in a pile can cause significant reductions in the degree of direct damage under blast loads.

(a) Pile I (b) Pile II (c) Pile III

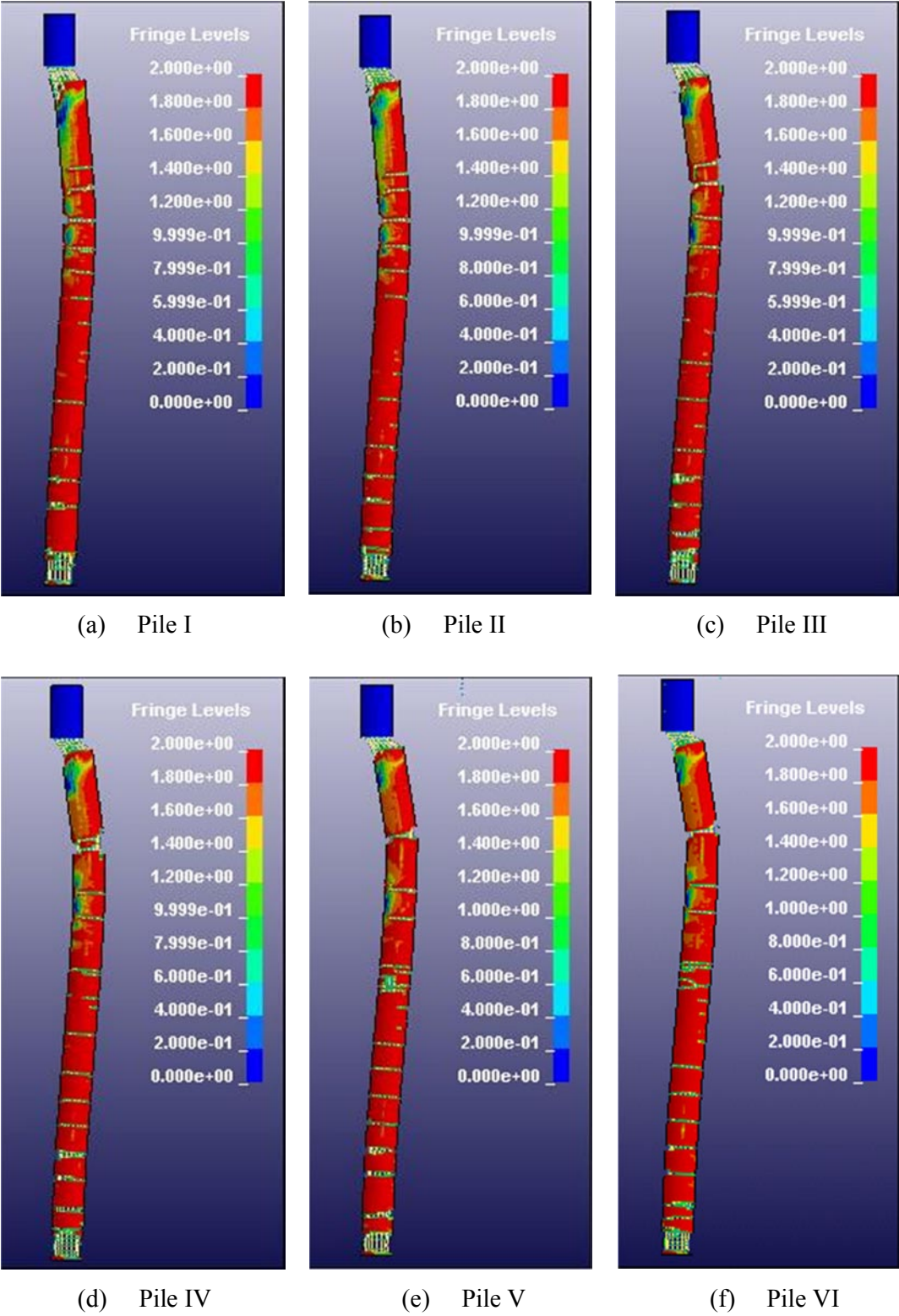(d) Pile IV (e) Pile V (f) Pile VI

Figure 5.6- Damages on piles

Pile III which has longitudinal reinforcement ratio of 1.8% and transverse reinforcement ratio of 0.24% was used for further studies which are described in below sections and chapters.

5.3 EFFECT OF CHARGE WEIGHT & SHAPE ON BLAST RESPONSE OF PILE

In order to study the effect of explosive weight (and hence the intensity of the blast) on the pile response, analyses were carried out using the same finite element model and material parameters. The horizontal deformations of pile for spherical shape of explosive charges varying from 100 to 500 kg TNT situated at the mid depth of the soil were determined. Moreover, in order to study the effect of explosive shape on the pile response, analyses cases of 500 kg cylindrical and cubic shapes of TNT explosives situated at the mid depth of the soil were considered to investigate the pile response. Table 5.4 shows selected blast analysis cases in the current investigation with charge shape, charge weight and calculated scaled distance.

Table 5.4- Analysis cases

Case	Charge shape	Charge weight (kg)	Calculated scale distance (m/kg$^{1/3}$)
1	Spherical	100	1.616
2	Spherical	200	1.282
3	Spherical	300	1.120
4	Spherical	400	1.018
5	Spherical	500	0.945
6	Cubic	500	0.945
7	Cylindrical	500	0.945

5.3.1 Results and Discussion

Figure 5.7 shows the variations of the residual horizontal deformation of the pile along its height for load cases 1 to 5. As expected, the results indicate that pile deformations

increase with charge weight. It can be seen that maximum residual displacement of 271mm was obtained for case 5 and it is approximately 6 times that for case 1.

Figure 5.8 shows the residual horizontal deformations of the pile caused by explosions with different shapes. The pile was found to have a maximum lateral residual deflection of 302mm for the blast loads induced by the cylindrical charge. The corresponding maximum lateral deflection was 260mm for the cubic shape charge occurring at approximately 5m height of the pile. From the above results, it is evident that the shape of the explosive material can influence the response of the pile under same conditions. Cylindrical shape has the maximum effect on the response of the pile. Thus consideration of the shape of the explosive is important in the study of the blast response of pile or any underground structure.
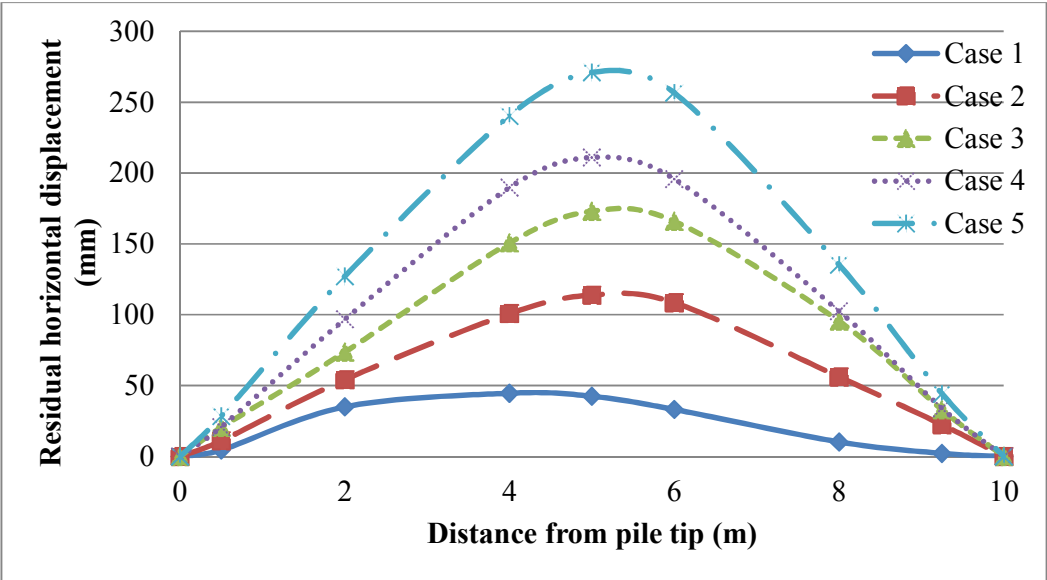

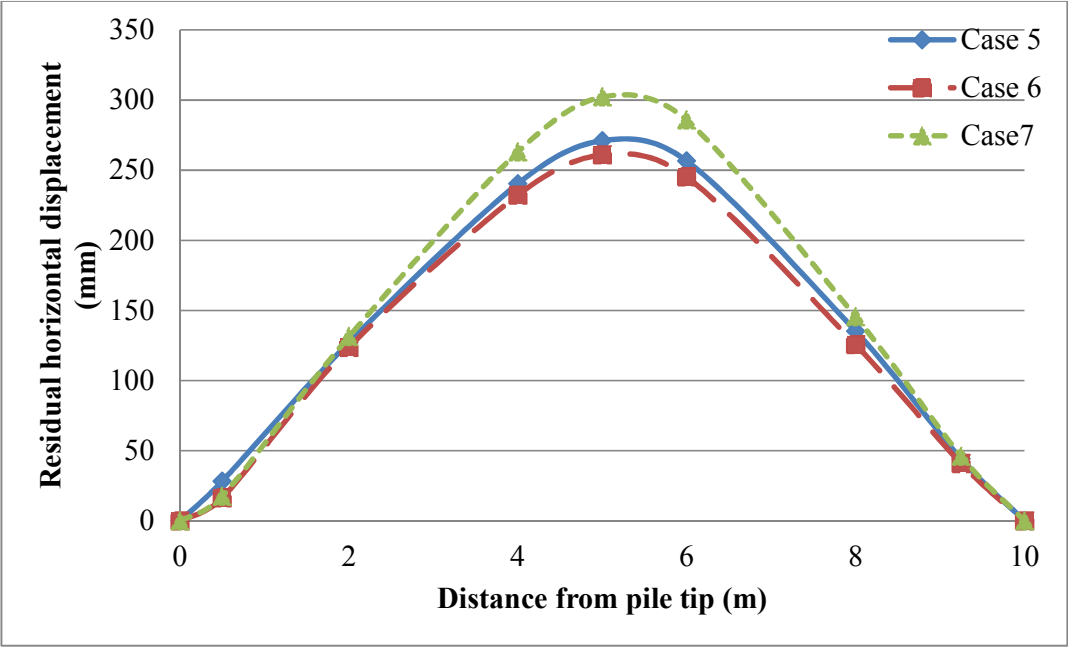Figure 5.7- Comparison of horizontal deformations of pile (cases 1 to 5)

Figure 5.8- Comparison of horizontal deformations of pile (cases 5 to 7)

The damage to the reinforced concrete is also observed from the present numerical simulations. Figure 5.9 depicts the concrete effective plastic strain variations of the piles with the element erosion as observed on the pile for cases 1 and 5 to 7. It illustrates the damage state of the pile after the blast. The colours in the Figure and the legend denote the fringe levels which represents the level of damage in concrete. The blue colour represents the fringe level 0 which indicates elastic state of the concrete, while the other colours with associated fringe levels 0 to 2 represent the different damage levels of the concrete. Fringe level 2 indicates maximum plastic yielding of concrete (LS-DYNA, 2007). As can be seen, it is clear that pile was significantly damaged at it ends due to shear force generated by the blast loading. Concrete spalling was observed in pile ends in all the cases. Reinforcements were found to have severely deformed in case 5 to 7 as can be seen in Figure 5.9 (b) to (d). Since concrete elements have eroded at the middle heights of the pile, it is clear that piles have suffered a combination of shear and flexural damage.
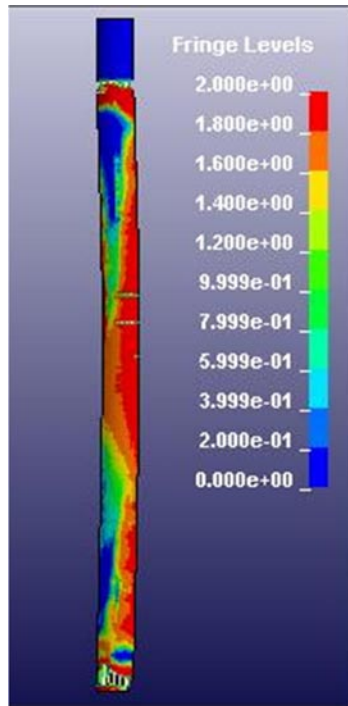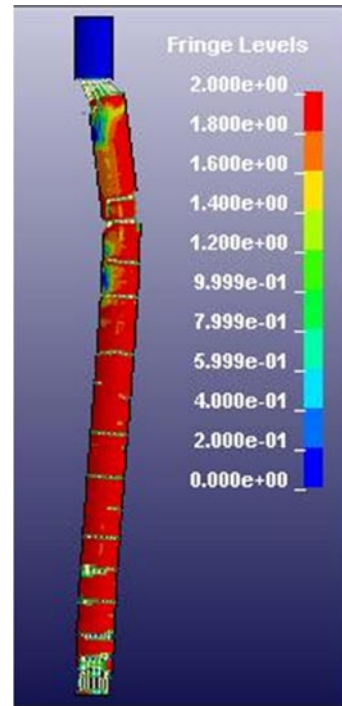
(a)   (b)
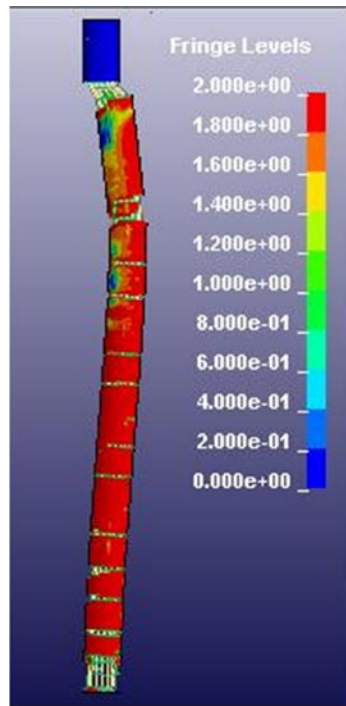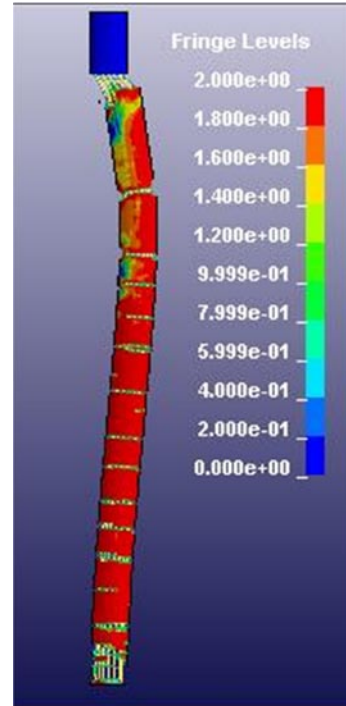
(c)   (d)

Figure 5.9- Blast damages on piles for (a) case 1 (b) case 5 (c) case 6 (d) case 7

5.4 EFFECT OF BURIAL DEPTH OF EXPLOSIVE ON BLAST RESPONSE OF PILE

Further studies were carried out to investigate the effect of burial depth of the explosive charge on the RC pile response using the same finite element model and material parameters described in the above chapters. The burial depth of 500kg sphere of TNT explosive charge was considered to be varied from the ground surface to mid-height of the pile (i.e. 5m) as shown in Figure 5.10. Altogether five study cases were considered as shown in Table 5.5. Standoff distance was considered as 7.5m for all the cases.
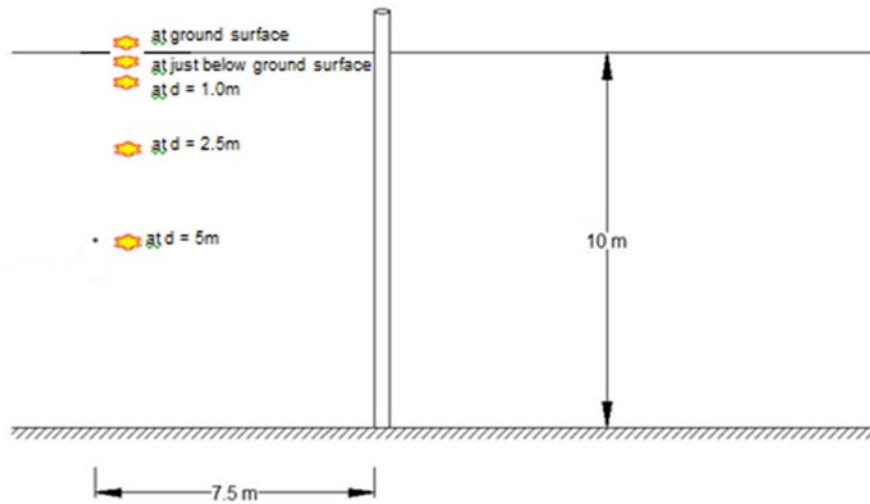
Figure 5.10- Schematic diagram of the study cases

Table 5.5- Study cases

case	Explosive location
1	
2	
3	dob = 1m
4	dob = 2.5m
5	dob = 5m

5.4.1   Results and Discussion

The horizontal deformation of the pile was obtained at different heights on the pile from the pile tip (base). Figure 5.11 shows the horizontal deformations of the pile for study cases 2 to 5. It can be observed that the pile has suffered permanent deformation under the blast loads and the maximum residual deformation of 271 mm occurs at the mid-height of the pile in case 5 which in which the buried blast is at the mid-height of the pile. It is evident that the pile has suffered permanent deformation and its response decreases significantly with a reduction in the burial depth of the explosive.
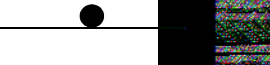
Figure 5.12 presents the results of horizontal pile deformation for study cases 1 and 2. It can be seen that the behavior of the pile has the same trend but with significance difference in maximum residual horizontal displacement. It can be noticed that the maximum residual horizontal displacement of the pile in the case of surface explosion (case 1) is 8.6 mm while in the case of buried explosion (case 2) it is 21.4 mm. Thus the residual horizontal displacement increased in the buried case by 60% as the buried explosion causes more blast energy on the pile foundation. In the case of the surface explosion, some of the blast wave energy is released through the free surface to the air domain causing less energy to be directed to the pile foundation. These residual deflections indicate the occurrence of plastic deformation of the pile under the both surface and underground explosions.
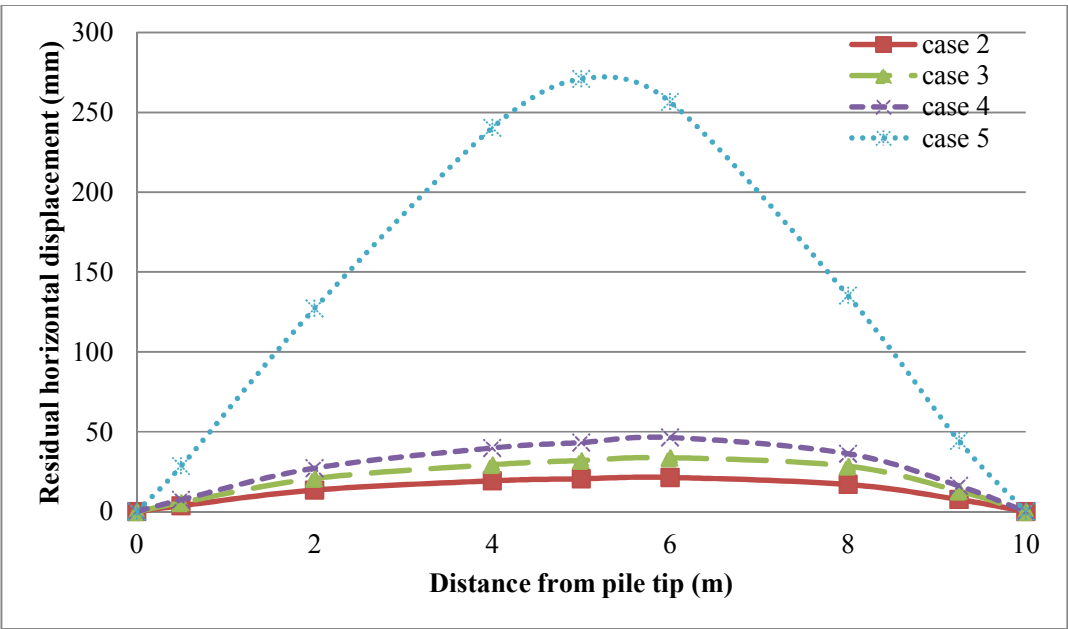
Figure 5.11- Horizontal deformation of the piles for study cases 2 to 5
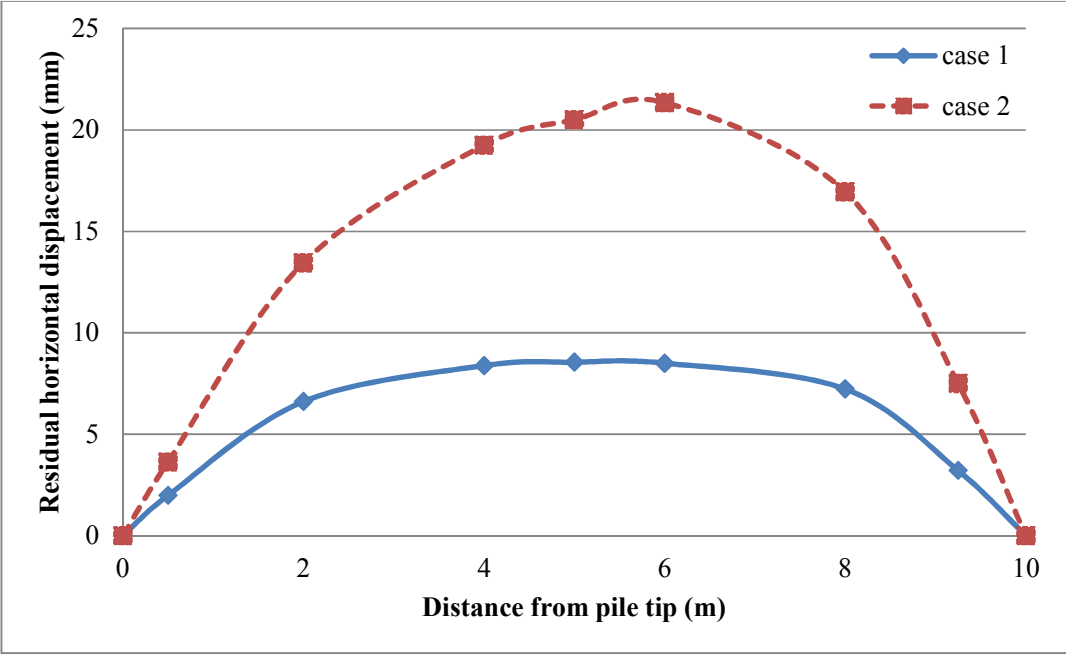
Figure 5.12- Horizontal deformation of the piles for study cases 1 and 2

5.5 CHAPTER SUMMARY

In this chapter, the investigations on the response of RC pile foundation subjected to different blast scenarios were presented. A fully coupled numerical model for a single RC pile founded in saturated sandy soil was developed by using the same modelling techniques described in Chapter 4. Various parameters including size and shape of the explosive, depth of burial of the explosive charge and pile reinforcement were considered in order to study their effects on the dynamic response of RC pile subjected to blast loads. Horizontal pile deformation and damages on the pile were obtained from the numerical simulations. First, the effect of pile reinforcement on the blast response of RC pile was studied. Based on the results, the following main conclusions can be drawn. (1) Longitudinal reinforcement in a pile has a significant effect on pile deformations under blast loads. These deformations decrease with increase in the longitudinal reinforcement. (2) Proper detailing of ties in a pile can cause significant reductions in the degree of direct damage under blast loads.

Then, effect of weight and shape of the explosive charge on the pile response was next studied. It was found that pile deformations increase with the charge weight, as expected. It was also found that shape of the explosive charge can influence on the blast

response of pile and the cylindrical shape explosive has the maximum effect on the pile behaviour.

Different charge weights, standoff distances and soil types have been considered in this study. This means that the blast pressures (or energy) on the piles are different in each case. Since fully coupled analyses were carried out, blast pressures (or energy) on the pile are automatically calculated in the model. The results presented in this thesis (indirectly) show the pile response to the different incident energies on the pile.

Finally, further studies were carried out to investigate the effect of burial depth of explosive charge on the blast response of pile. Depths up to the mid height of the pile were considered. From the results, it was evident that the pile response decays significantly with decrease in the burial depth of the explosive from mid-depth of the soil to ground level. Moreover, the results show that a buried explosion has a significant effect on the pile response compared to a surface explosion, under the same conditions.

This study treated the pile foundation response under both surface and underground explosions. As it was based on numerical simulations, validation of the modelling techniques is very important. The only relevant experimental testing available was that of Shim (1996) as described in Chapter 4. The results from Shim's experiments were used for the validation of the modelling techniques. Since he carried out his experiments for explosion occurring at the mid-depth of the pile (or soil), same scenario was continued to study the influence of some important parameters.in Chapters 5 and 6. However, the study was extended to investigate pile response under surface explosion as described in Chapter 7.

Chapter 6: Effects of soil properties on the blast response of pile

6.1   INTRODUCTION

The study of wave propagation in soils can produce information useful to engineers on the resilient characteristics of a particular site, dynamic soil structure interaction and earthquake analysis. Many researchers have studied the soil behaviour under blast loading (Wang and Lu, 2003; Tong and Tuan, 2007; An J et al., 2011). When the explosion occurs in soil, an explosive cavity with high pressure and high temperature gas is formed. The explosive cavity immediately begins to expand against surrounding soil causing high initial radial displacements and stresses in soil that propagate outward from the explosive. In the vicinity of the explosion, stresses in the soil are extremely high and causes the soil to lose its shear resistance. As the explosion cavity expands, stresses in the soil decreases with distance (TM5-855-1, 1986).

The soil is a three-phase mixture which contains solid mineral particles, water and air. Different characteristics of the deformation of each phase and of the soil skeleton of the soil result in the deformation mechanism of soil to be highly dependent on the ratios of the components in the soil and the loading condition. Thus, the deformation mechanisms of unsaturated and saturated soils are different, and such difference can be more significant under dynamic loading. In analysing the deformation of soils, two basic deformation mechanisms exist. These are the deformation of the solid skeleton and deformation of all the soil phases. When the soil is compressed, both mechanisms will take effect simultaneously.

For dry soils, under static or dynamic loading, the first mechanism becomes predominant while the other is negligible because the initial compressibility of the air is so high that it does not impede the deformation of the skeleton. With increasing pressure, the bonds between the soil particles are deformed and displaced and the soil is compacted so that the second mechanism becomes more and more important, while the first mechanism gradually becomes negligible. However, in saturated soils, the bonds between the solid particles are weak, and the water and air have higher resistance than

bonds of the skeleton. With a rapid dynamic loading, the deformation and resistance of the soils are determined by the second mechanism, particularly by the water and air deformation. However, under a slow static loading of the saturated soil, the water and air pressed out of the voids and compressibility is mainly given by the solid skeleton. Figure 6.1 shows the pressure-deformation relationship for dry and wet soils.
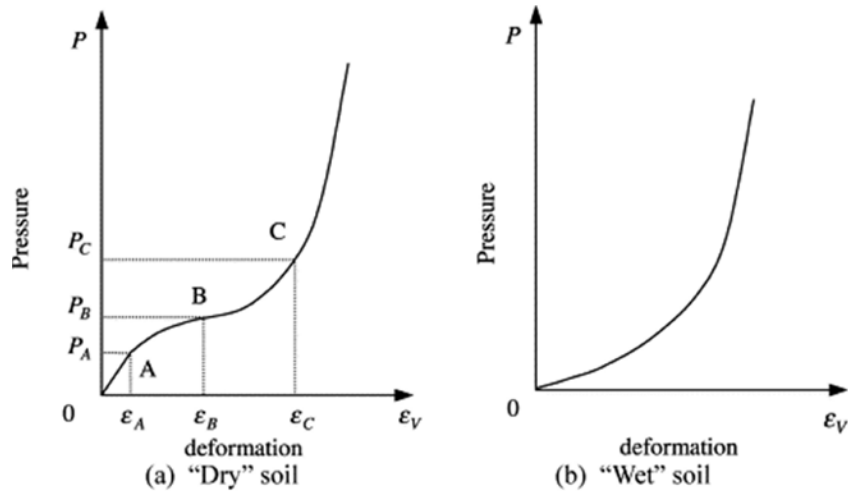
Figure 6.1- Relationship between pressure and deformation (Wang and Lu, 2003)

The study of blast wave propagation in different soils and validation of the soil material model are described in this chapter. A finite element model was developed to validate the free field stresses in soil. It was modelled with the soil 10m high with the explosion occurring at the mid-depth of the soil. The explosive charge used in the tests was 500 kg TNT. The same modelling technique which is described in chapter 4 was adopted. This chapter also presents the evaluation of the effect of soil properties on the pile response under buried explosion.

6.2   SOIL PROPERTIES FOR NUMERICAL SIMULATION

Under blast loading, the physical condition of the soil will change from its initial conditions and such change in turn will affect the soil behaviour. Blast-induced waves in soil are characterized by large stress amplitudes and high stress rates. Modelling such waves is difficult because of the constitutive behaviour of a soil depends on many factors such as stress state, density and the degree of saturation (Wang et al., 2004; Wang et al., 2008, Feldgun et al., 2008).

The present study aims to investigate the blast response of pile embedded in different soil types. The following soil types, saturated soil, partially saturated soil and dry soil as in Table 6.1 were considered.

Table 6.6- Soil properties for numerical simulation

Soil properties	Saturated soil	Partially saturated soil	Dry soil
Composition	Clay	Sand & Clay	Sand
Density	2065 kg/m^3	1960 kg/m^3	1450 kg/m^3
Degree of saturation	100%	85% ($V_a > 4\%$)	0%
Seismic velocity	1575 m/s	500 m/s	175 m/s

6.3   PREDICTION OF FREE-FIELD STRESSES

Ground shock propagation in soil is a complex function of the dynamic constitutive properties of the soil, the explosive products and the geometry of the explosion (Drake and Little, 1983). TM5-855-1 (1986) provides the following equations to predict the peak values of pressure, velocity and acceleration, respectively.

$$P_0 = 160.\,f.\,\rho c. \left(\frac{R}{W^{1/3}}\right)^{-n} \qquad\qquad \text{Equation (6.1)}$$

$$V_0 = 160.\,f. \left(\frac{R}{W^{1/3}}\right)^{-n} \qquad\qquad \text{Equation (6.2)}$$

$$a_0 = \frac{50.\,f.\,c.}{W^{1/3}} \left(\frac{R}{W^{1/3}}\right)^{(-n-1)} \qquad\qquad \text{Equation (6.3)}$$

In these equations, P_0 is the peak pressure in psi, V_0 is the peak particle velocity in ft/sec (fps), a_0 is the peak acceleration in g (acceleration of gravity), f is a coupling factor and is dependent on the scaled depth of the explosion, ρc is acoustic impedance in psi/fps, R

is distance from the explosive source in ft, W is the charge weight in lb, c is the seismic velocity in fps, and n is an attenuation factor and is dependent on the soil type as shown in Table 6.2 (TM5-855-1, 1986).

Table 6.2- Soil properties for calculating ground shock parameters (TM5-855-1, 1986)

Soil types	Unit weight, (pcf)	Seismic velocity, c (fps)	Acoustic impedance, ρc (psi/fps0	Attenuation coefficient, n
Heavy saturated clays and clay shale	120 - 130	> 5000	150 - 180	1.5
Saturated sandy clays and sands with air voids < 1%	110 - 124	5000	130	2.25 - 2.5
Dense sand with high relative density	109	1600	44	2.5
Wey sandy clay with air voids > 4%	120 - 125	1800	48	2.5
Sandy loam, loess, dry sands and backfills	124	1000	22	2.75
Loose, dry sands and gravels with low relative density	90 - 100	600	12	3 - 3.25

6.4   NUMERICAL ANALYSIS AND RESULTS

The LS-DYNA model developed to study the effects of blast loads on pile response in chapter 5 was used to study the influence of the soil properties on blast response of the pile. First, blast wave pressures in the soils obtained from the numerical simulation were compared with the pressures predicted in Equation 6.1. Then, the pile foundation response to the blast loads was investigated under different soil conditions: saturated soil, partially saturated soil and dry soil which are given in Table 6.1.

6.4.1   Comparison of numerical results for free-field stresses with TM5-855-1 predictions

The peak pressures obtained in the wet soil test, the partially saturated test and the loose dry soil are compared with the predicted pressures using the TM5-855-1 in this section. To monitor the blast wave propagation in the soil mass, a group of target points was

selected along the horizontal line to the explosive charge. The target points are located within the range 5 to 25m from the detonation point. Figure 6.2 shows the pressure time histories of the compressive waves at those target points in the wet soil test.
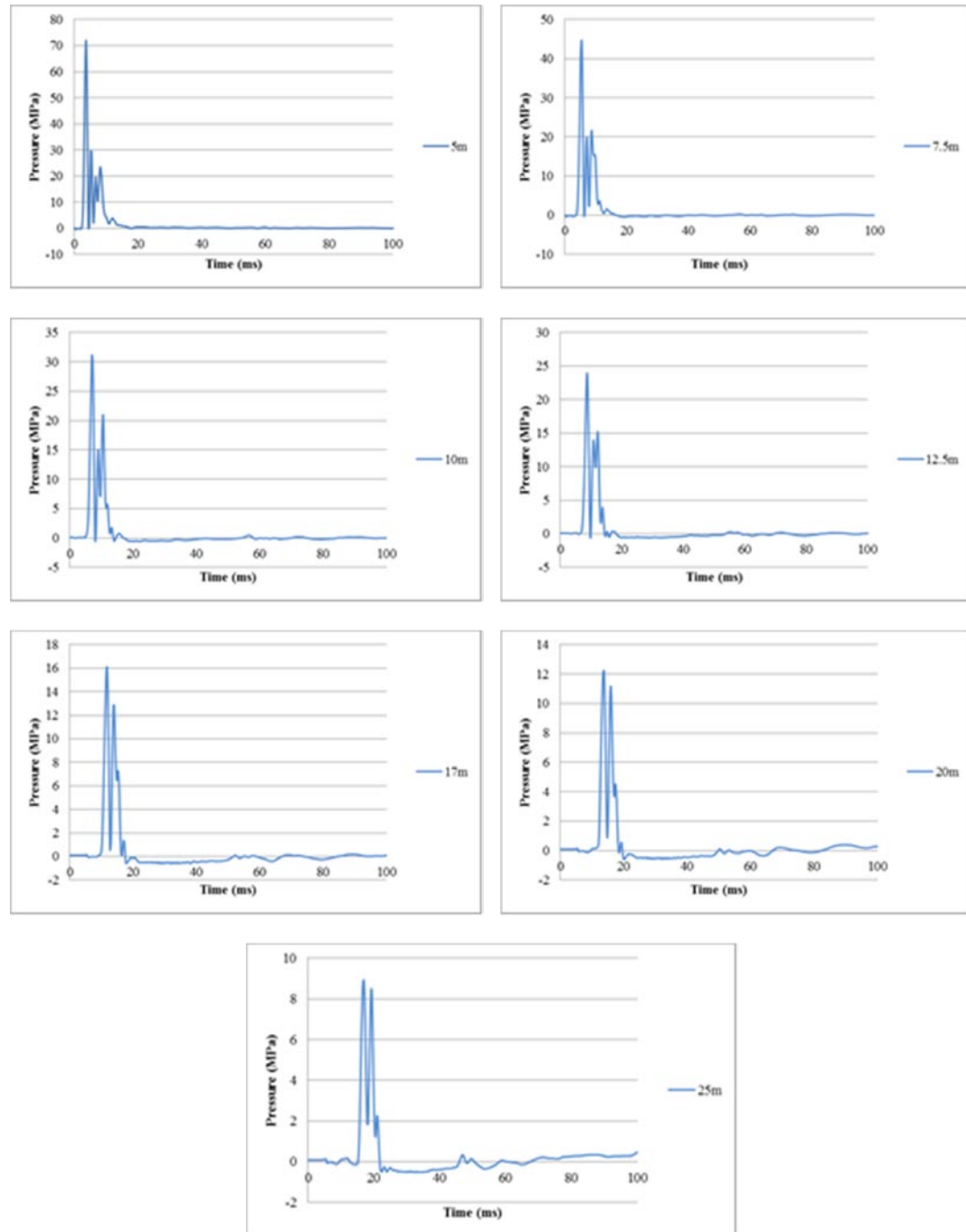

Figure 6.2- Pressure time histories at different distances in soil from charge for saturated soil test

The peak pressures obtained in the saturated soil test from the numerical simulation are compared with the peak pressures given by TM5-855-1 as shown in Figure 6.3 which shows the peak pressure attenuation with the scaled distance. Since soil properties in the TM5-855-1 are given in a range for considered soil type, Figure 6.3 shows two straight lines representing the upper empirical limit and the lower empirical limit of the peak pressure in the saturated soil. It can be noted that the numerical results for the peak pressure are almost in between the upper and lower limits of the predicted peak values for this type of soil. Predicted peak pressures close to the explosion are marginally higher than the numerical results.
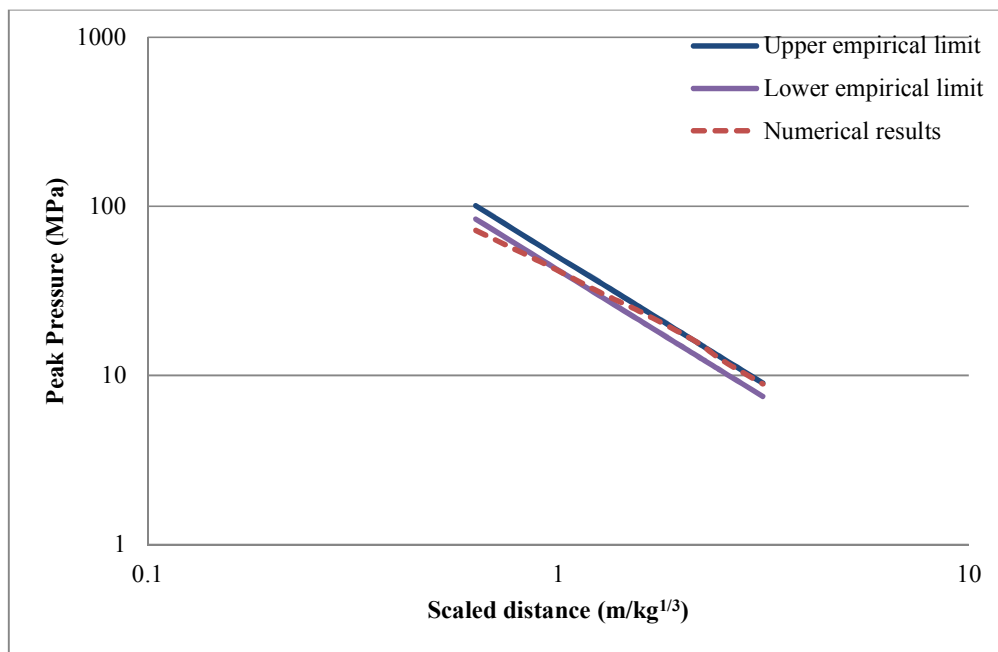
Figure 6.3- Relationship of peak pressures with scaled distance for saturated soil test

Figure 6.4 and 6.5 compare the peak pressures obtained from the numerical simulation with the predicted peak pressures using the TM5-855-1 for the partially saturated soil test and dry soil test, respectively. As shown in those figures, the numerical results of the peak pressure attenuation agree reasonably well with empirical results. Also, results show that attenuation of the peak pressure in the soil occurs with increasing distance from the charge.
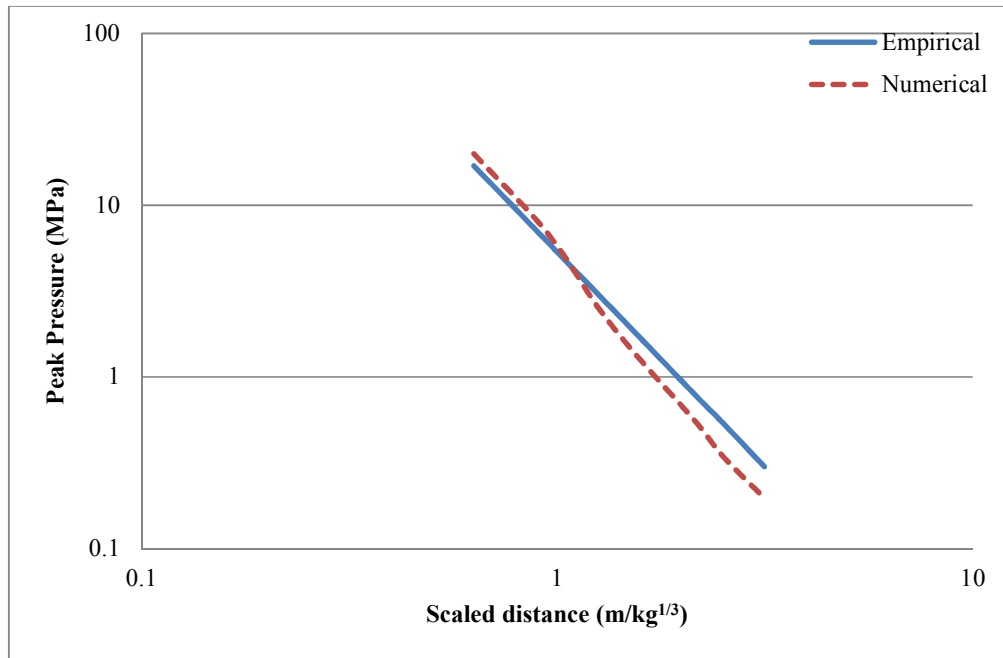
Figure 6.4- Relationship of peak pressures with scaled distance for partially saturated soil test
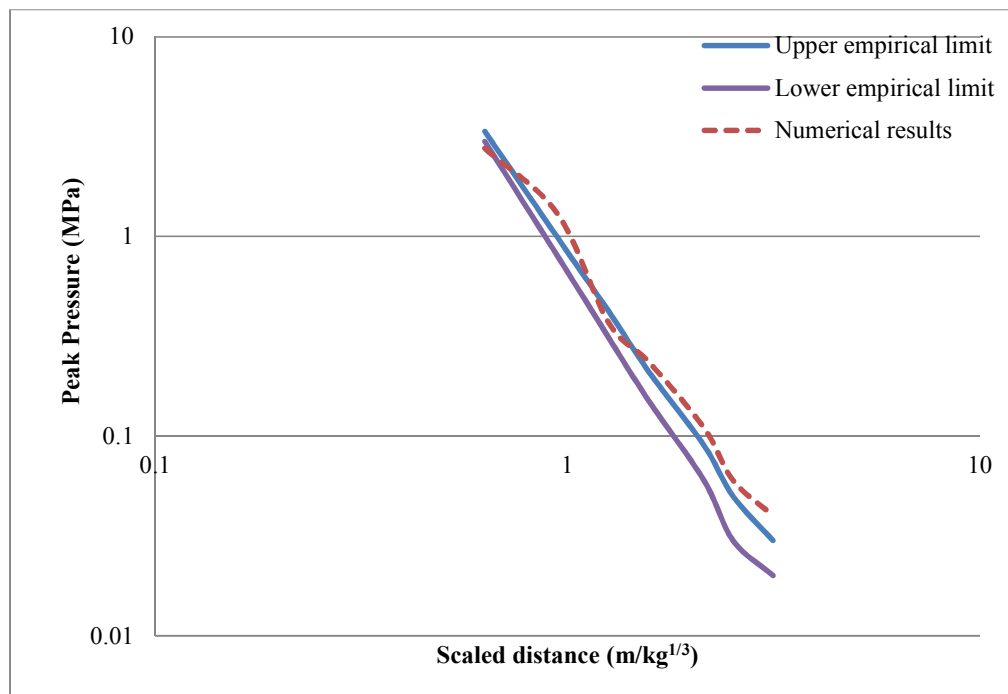

Figure 6.5- Relationship of peak pressures with scaled distance for dry soil test

Figure 6.6 shows a comparison of the numerically obtained results of the peak pressure attenuations plotted against the scaled distance for the wet soil test, the partially

saturated soil and the dry soil test. It can be noted that the peak pressures in dry soil evidently shows smaller values. Saturated soil has highest peak pressures. The small peak pressure in the dry soil results from the slow wave velocity.
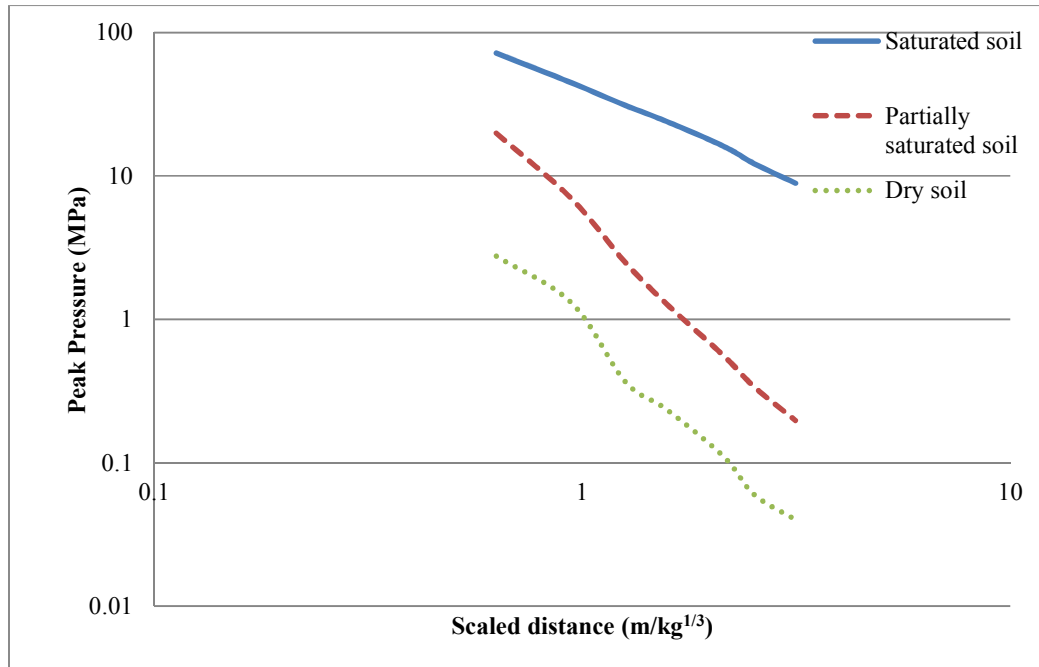

Figure 6.6- Comparison of peak pressure attenuations

6.4.2 Blast response of pile in different soil types

This study investigated the response and damage of the (10m long) RC pile when subjected buried explosion for a standoff distance of 7.5m in different soil types. As shown in Table 6.1, saturated soil, partially saturated soil and dry soil were considered in the analysis. Fixed boundary conditions in all directions were considered at the pile ends, similar to that in the previous studies described in Chapter 5.

Figures 6.7 to 6.9 show the time histories of the horizontal deformation of the pile embedded in different soils. Pile deformations are presented at three heights from the pile tip: 2.5m (point A), 5m (point B) and 7.5m (point C). These Figures demonstrate that the pile has residual deflection in all the cases. These residual deflections show the occurrence of the plastic deformation of the pile and indicate that the pile has suffered permanent deformation under the buried blast. It can be noted that the pile embedded in

the dry soil has highest pile deformation and when it embedded in the partially saturated soil it has the lowest pile deformation. The pile embedded in saturated soil was found to have a maximum horizontal residual deflection of 369 mm, and maximum lateral residual deflection of 247 mm was observed in partially saturated soil. Also, it was found that the pile embedded in dry soil had deflected 400mm.
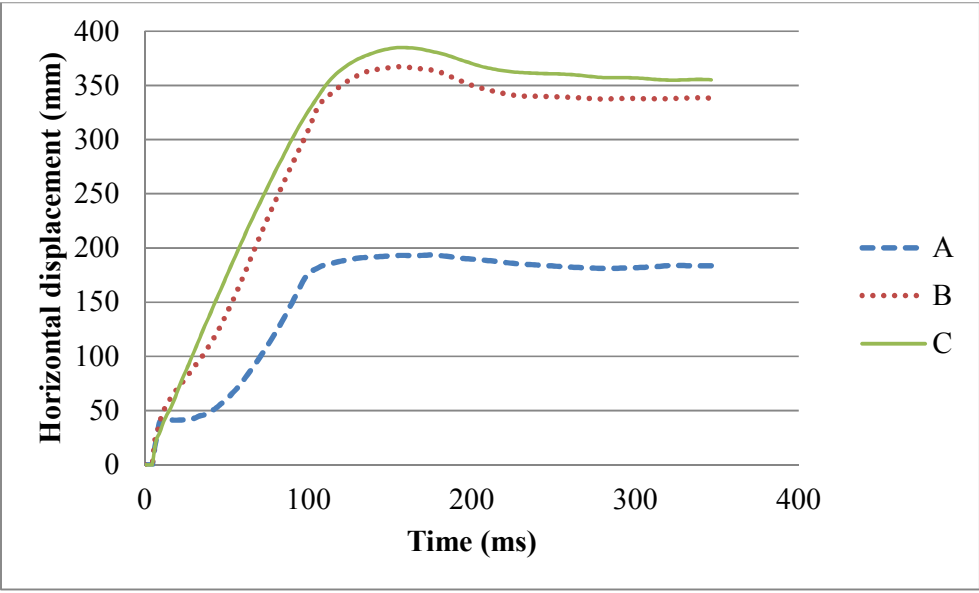

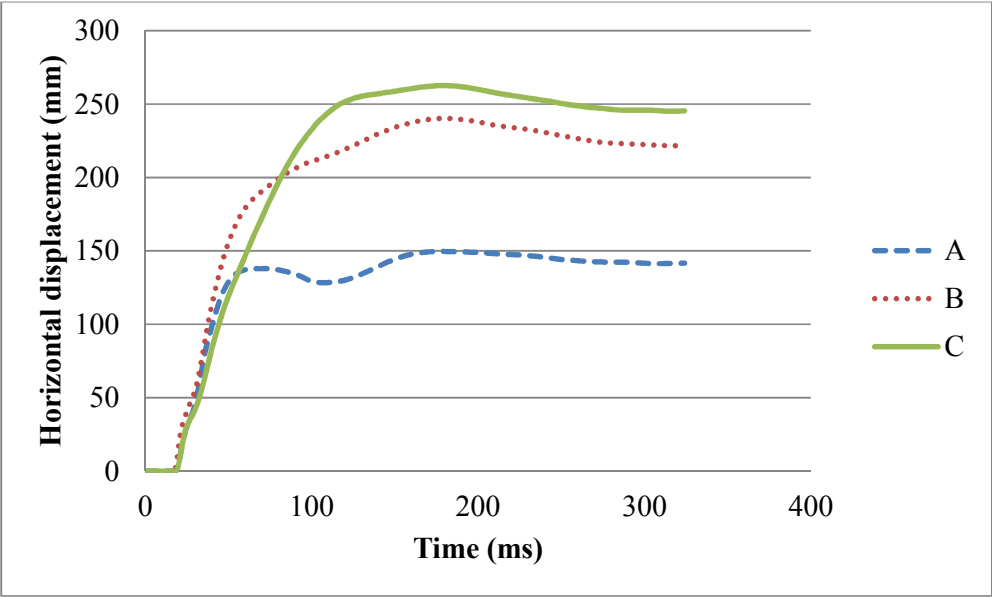Figure 6.7- Pile deformation for standoff distance 7.5m in saturated soil

Figure 6.8- Pile deformation for standoff distance 7.5m in partially saturated soil
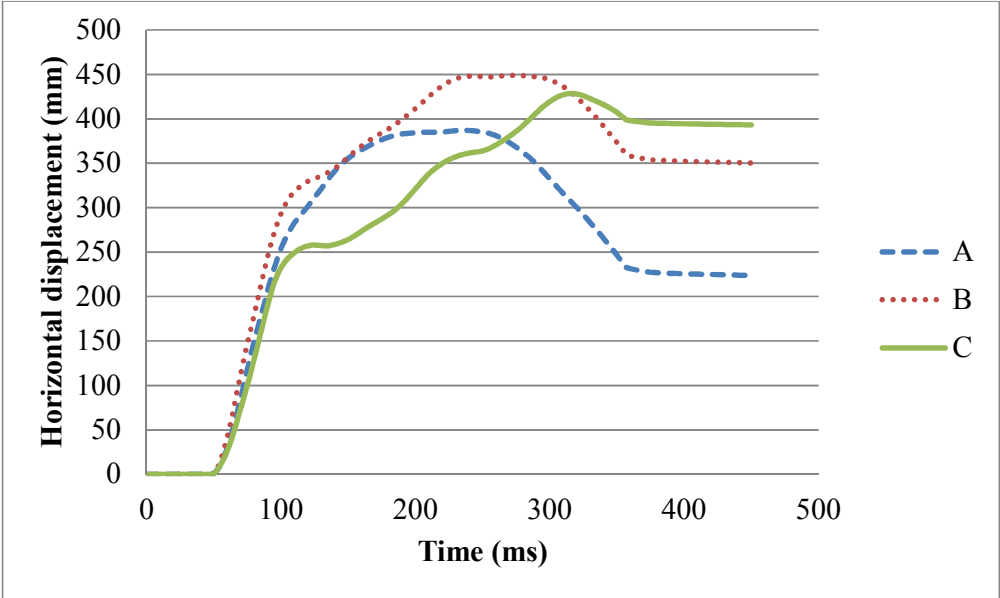
Figure 6.9- Pile deformation for standoff distance 7.5m in dry soil

The damage to the reinforced concrete can be evaluated through the use of effective plastic strain diagrams. Figures 6.10 to 6.12 depict the concrete effective plastic strain variation of the piles with the element erosion that were that observed on the pile for a stand-off distance of 7.5m, for the 3 types of soils. Effective plastic strain is the damage parameter in concrete_damage_rel3 material model which range from 0 to 2. Elastic state of the concrete is represented by 0 with blue colour and the yielding and post yielding in incorporated within the range 0 to 2. The residual capacity of the concrete is indicated by 2. As can be seen, it is clear that pile was critically damaged in all the cases. Concrete elements have eroded in the top end of the pile in all the cases and indicate that the concrete at the top end of the pile was totally destroyed in all the cases. Reinforcements were found to have severely deformed at the top end. Figure 6.10 shows that concrete in the bottom end was also severely damaged in the pile embedded in the saturated soil. It can be noted that the pile embedded in the saturated soil suffered the most damage compared to the other two piles. However concrete in the middle of the pile suffered most damage in the pile embedded in the dry soil as shown in Figure 6.12.
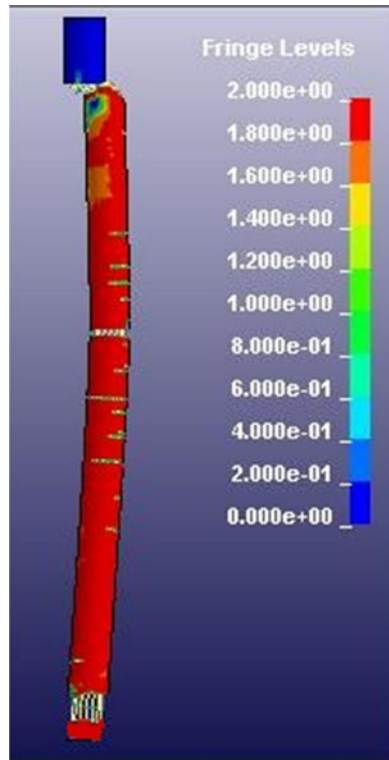
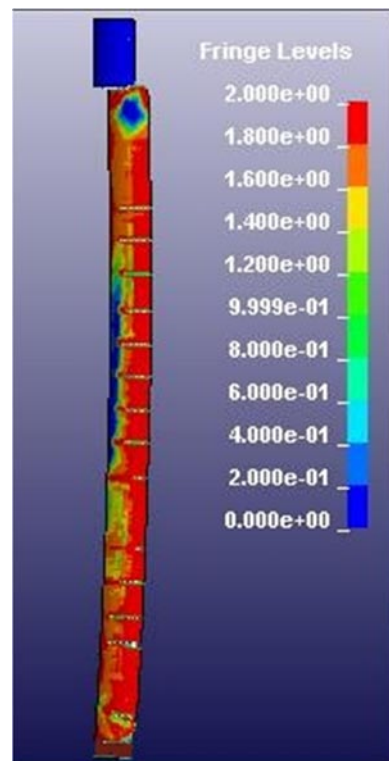Figure 6.10- Pile damage for standoff distance 7.5m in saturated soil

Figure 6.11- Pile damage for standoff distance 7.5m in partially saturated soil

Figure 6.12- Pile damage for standoff distance 7.5m in dry soil

From the above results for pile deformations and pile damage, it can be concluded that under the same buried explosion, piles embedded in saturated soil or loose dry soil suffer more damage than piles embedded in partially saturated soil. As seen in the Figure 6.6, blast wave pressures are high in the saturated soil and this could be the reason for the severe damage in the embedded pile. Even though blast wave pressures are lower in loose dry soil as seen in Figure 5.6, the displacement of the soil could be high due to the poor bond between the soil particles. This could therefore be the reason for the severe deformation of the pile embedded in dry soil under the buried explosion.

6.5   EFFECT OF STANDOFF DISTANCE ON BLAST RESPONSE OF PILE

As described in the section 6.4.1, blast wave pressures in the soil decrease with increase of distance from the charge. Thus, using the proposed numerical method, further studies were carried out to investigate the effect of standoff distance on the blast response of pile embedded in different soil types. In this section, pile deformation and damage are presented for the standoff distances of 10m and 15m from the explosive.

In Figures 6.13 to 6.15, the time histories of the horizontal deformations of the pile at three heights from the pile tip: 2.5m (point A), 5m (point B) and 7.5m (point C) are presented for the standoff distance 10m from the explosion. They also demonstrate that the piles have suffered permanent deformation under the buried blast. It can be noted that the pile embedded in the dry soil has highest pile deformation and when it is embedded in the partially saturated soil it has the lowest pile deformation. The maximum horizontal residual deflections of the piles were 165mm, 157mm and 280mm when embedded in saturated soil, partially saturated soil and dry soil respectively.

Figures 6.16 to 6.18 show the concrete effective plastic strain variation of the pile with the element erosion as observed on the pile for a stand-off distance of 10m. It is clear that piles were critically damaged in all the cases as also observed (in the above section) when the stand-off distance was 7.5m. However, as expected, pile damages and deformations have decreased. In this case also, piles embedded in the saturated soil and in the loose dry soil suffered more damage than pile embedded in the partially saturated soil. However, deformed shape of the pile embedded in the dry soil is different to that in the previous case (stand-off distances of 7.5m) which is described in section 6.4.2.

Figure 6.13- Pile deformation for standoff distance 10m in saturated soil

Figure 6.14- Pile deformation for standoff distance 10m in partially saturated soil

Figure 6.15- Pile deformation for standoff distance 10m in dry soil

Figure 6.16- Pile damage for standoff distance 10m in saturated soil

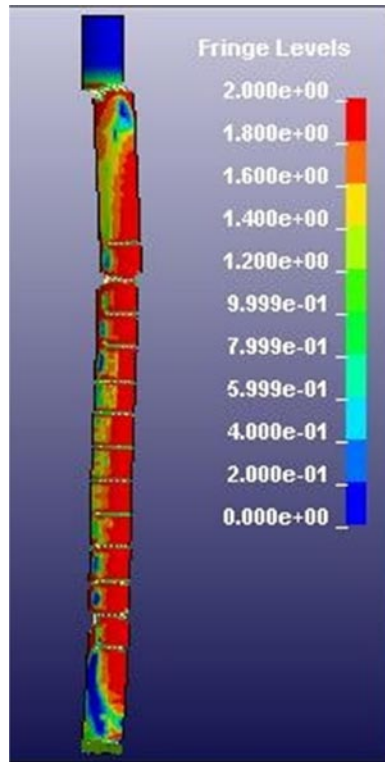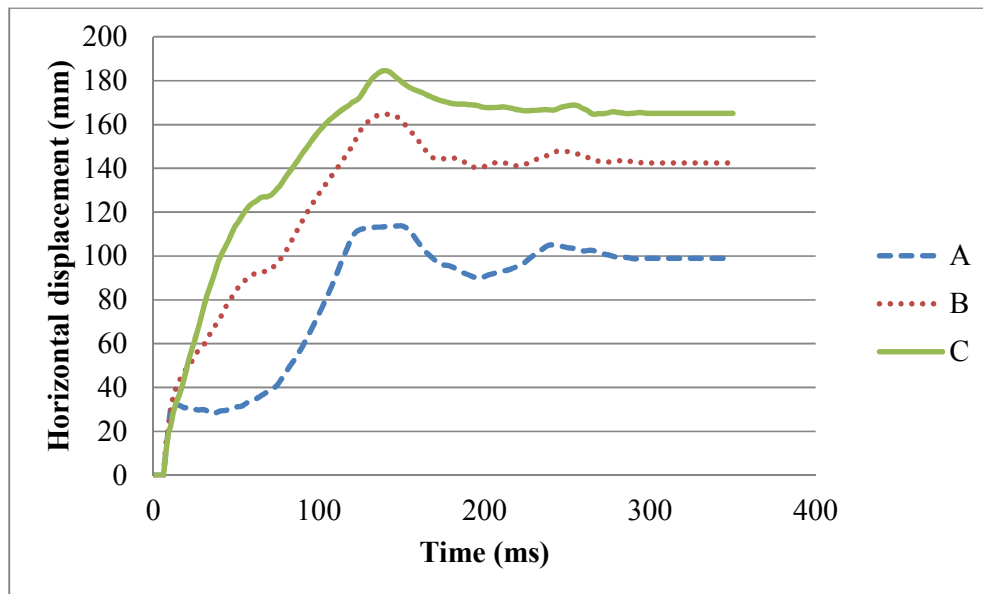Figure 6.17- Pile damage for standoff distance 10m in partially saturated soil

Figure 6.18- Pile damage for standoff distance 10m in dry soil

Figures 6.19 to 6.21 show the concrete effective plastic strain variations in the piles with the element erosion for a stand-off distance of 15m. In this case also, concrete in the top and bottom ends of the pile embedded in the saturated soil were totally destroyed. Maximum horizontal deformation of 85mm was found in the pile. All the horizontal deflections were much smaller than those obtained for stand-off distance of 10m, as expected. Spalling was also observed at the top ends of the piles embedded in the partially saturated soil and in the loose dry soil. The pile embedded in the partially saturated soil was found to have a maximum horizontal residual deflection of 54 mm, and it was found that the pile embedded in dry soil had deflected 80mm. Although the pile embedded in the dry soil had large deformations than other two cases for the standoff distances 7.5m and 10m, the pile embedded in the saturated soil has deformed more for the standoff distance 15m.
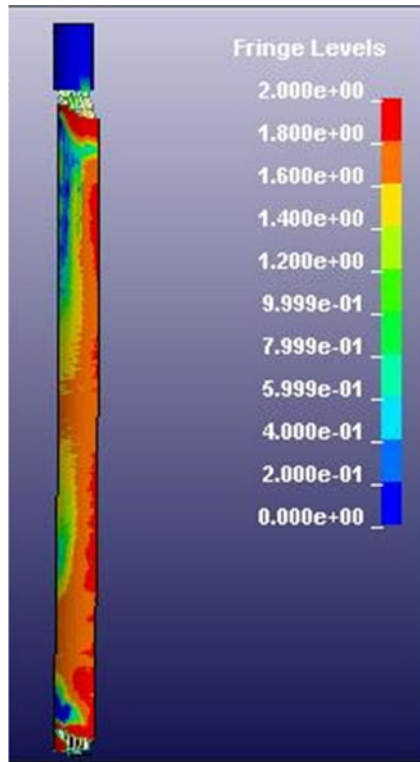
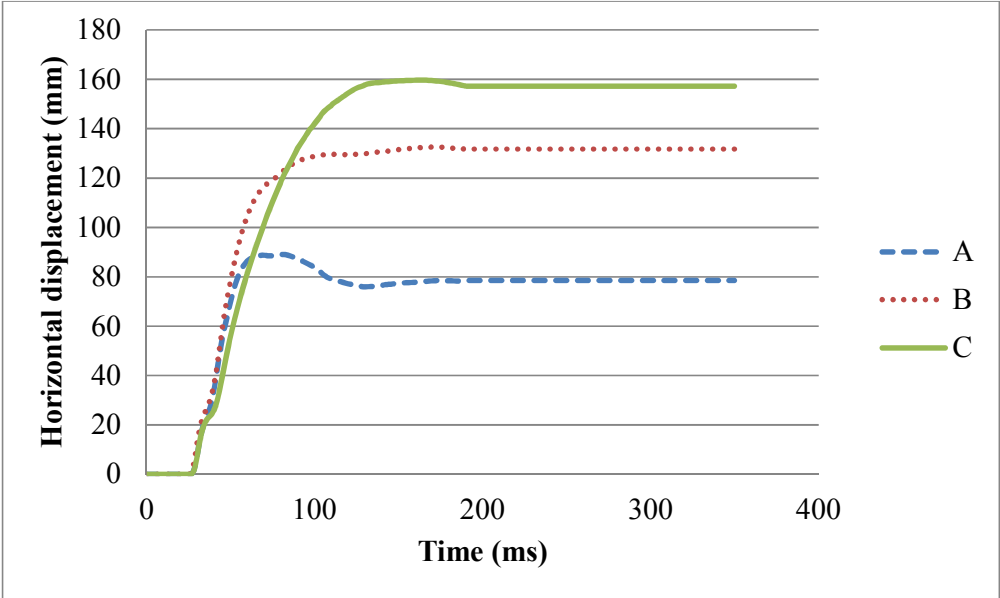Figure 6.19- Pile damage for standoff distance 15m in saturated soil

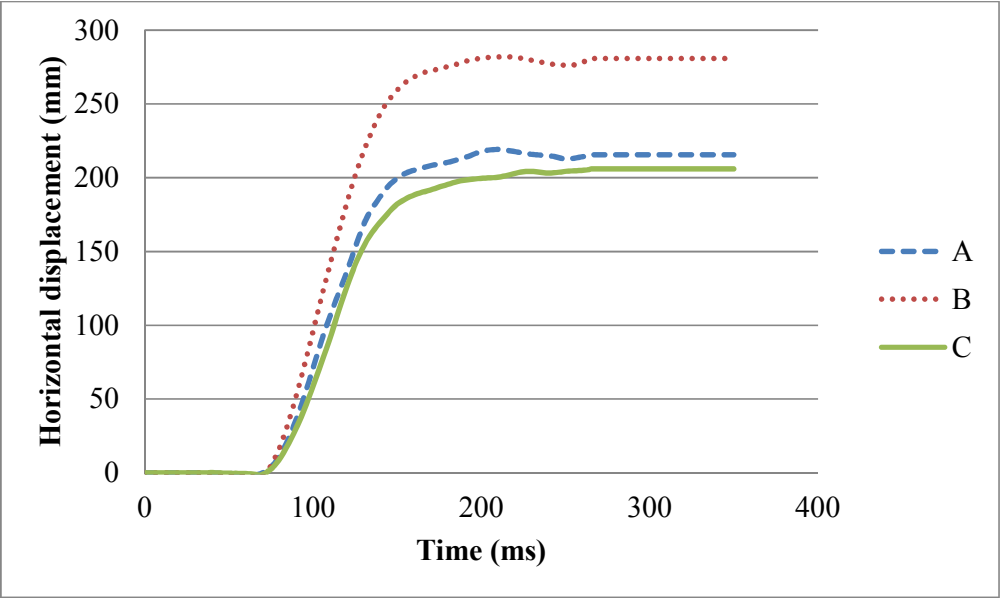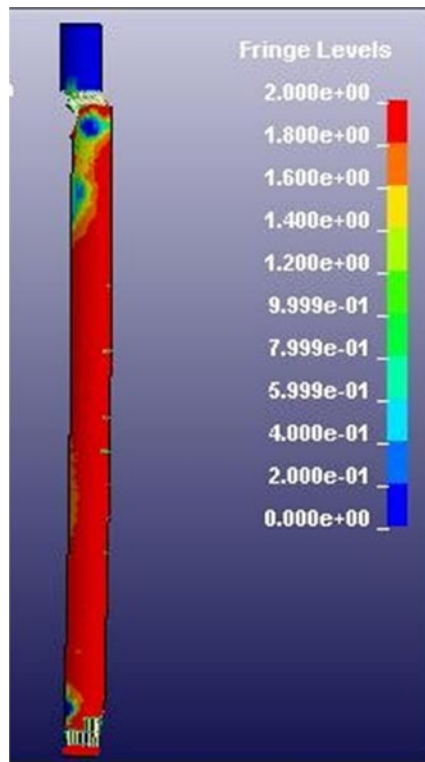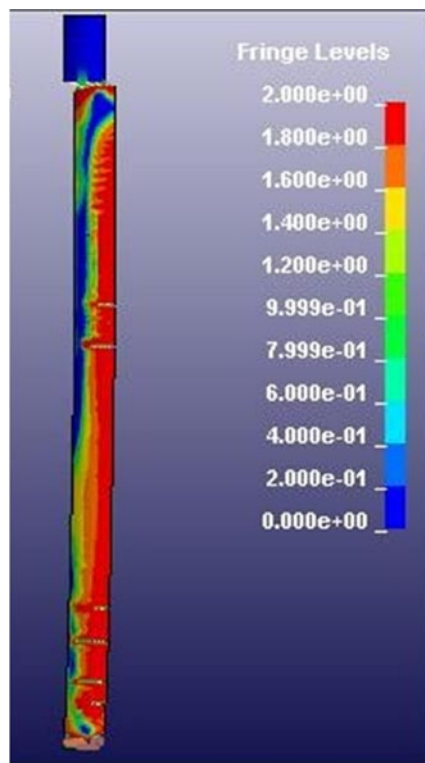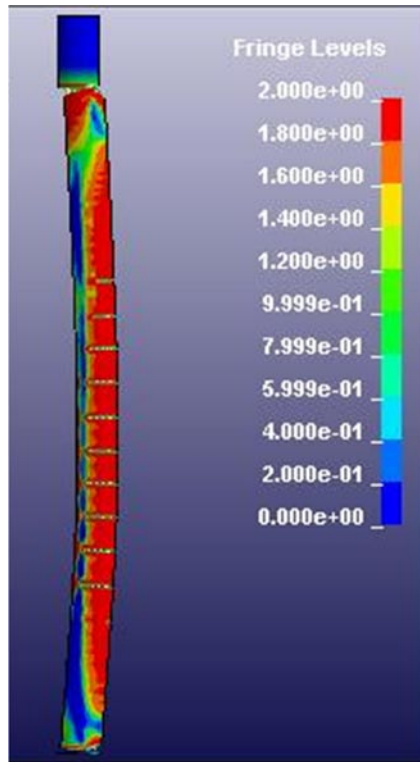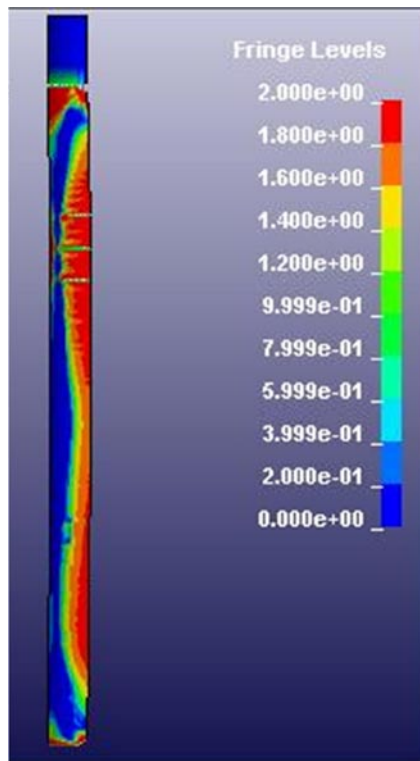Figure 6.20- Pile damage for standoff distance 15m in partially saturated soil
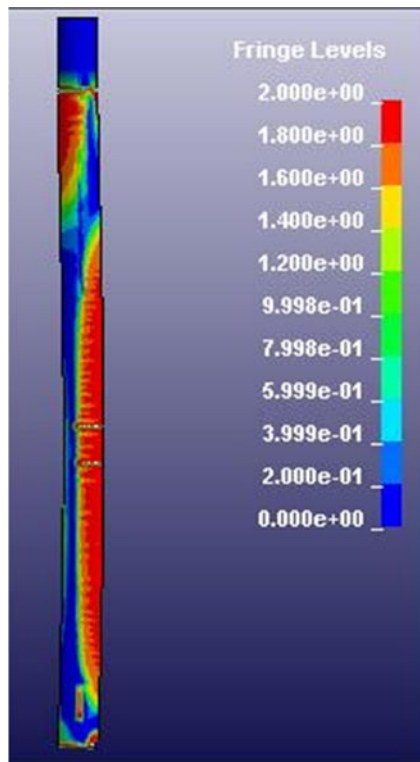
Figure 6.21- Pile damage for standoff distance 15m in dry soil

6.6   CHAPTER SUMMARY

In this chapter, a coupled numerical model which was described in chapter 5 was used to investigate the influence of soil properties on the pile response under buried explosion. Piles embedded in saturated soil, partially saturated soil and dry soil were considered. Moreover, blast wave propagation in soils was studied and results were compared with predicted pressures using the TM5-855-1. Horizontal pile deformation and damages on the pile were obtained from the numerical simulations. Based on the results, the following main conclusions can be drawn.

1. Performance of the piles embedded in saturated soil and loose dry soil are worse than pile embedded in partially saturated soil when subjected to same buried explosion.

2. Since blast wave pressures are high in saturated soil, they cause severe damage in the pile. Even though blast wave pressures are small in loose dry soil, the displacement of the soils might be high due to the poor bond between soil

particles. This might therefore be the reason for the severe deformation of the pile embedded in dry soil under buried explosion

3. Pile damages and deformations decrease with the distance from the explosive, as expected.

4. For scaled distances 1 and 1.3 m/kg$^{1/3}$ (stand-off distances of 7.5m and 10m with a 500kg mass TNT explosive)   the pile embedded in the dry soil has the maximum pile deformation.

5. For scaled distance 1.9 m/kg$^{1/3}$ (stand-off distance of 15m with a 500kg mass TNT explosive), the pile embedded in the saturated soil has the maximum pile deformation.

Chapter 7: Blast response of single pile and pile groups subjected to surface explosion

7.1 INTRODUCTION

This chapter describes the three dimensional FE modelling and analysis to study the response of RC piles (single piles and pile groups) founded in partially saturated soil subjected to blast loads induced by explosion on the ground surface. As in previous chapters, this study also adopts the fully coupled numerical simulation approach employing nonlinear material models to represent the realistic behaviour of the soil-pile system. This chapter is organized as follows. Section 7.2 describes the developed FE model to study the blast wave propagation in soil medium. Two types of boundary conditions at the pile head, fixed head and free head, are considered for the purpose of comparison. Their results are presented and discussed in sections 7.3 and 7.4. Section 7.5 presents some additional results and discussion on the simulated blast response and damage analysis of pile groups. Section 7.6 summarizes the research findings.

7.2 PROPAGATION OF BLAST INDUCED WAVES IN THE SOIL

In the previous chapter, blast wave propagation in soil induced by buried explosion was validated for three different soil types. This chapter is intended to contribute to the understanding of the behaviour of pile foundations embedded in partially saturated soil subjected to blast loads induced by an explosion on the ground surface. Thus, effect of surface explosion on the soil medium is first studied and validated with the chosen soil material model by comparing blast wave pressures in the soil obtained from the present numerical simulation with the predicted pressures using the Equation 6.1.

Past records indicate that the majority of terrorist incidents have occurred using a car or a small truck bomb. For design purposes, vehicle bombs that utilize cars to small trucks typically contain 500 to 4000 pounds (i.e. 230 to 1815kg) of TNT equivalent (NCTC, 2013). Thus, the explosive charge used in the tests was 1000 kg TNT and was assumed to have a spherical shape.

A FE model was developed to study the blast wave propagation in soil. By making use of symmetry, to save computational time, only a quarter of the system was modelled as shown in Figure 7.1. It was modelled with the soil 30m high and the explosion occurring on the soil surface. The soil was considered as partially saturated soil, and Table 6.1 in Chapter 6 presents the properties of partially saturated soil. The same modelling techniques and material models parameters as those described in the previous chapters were adopted in here also.
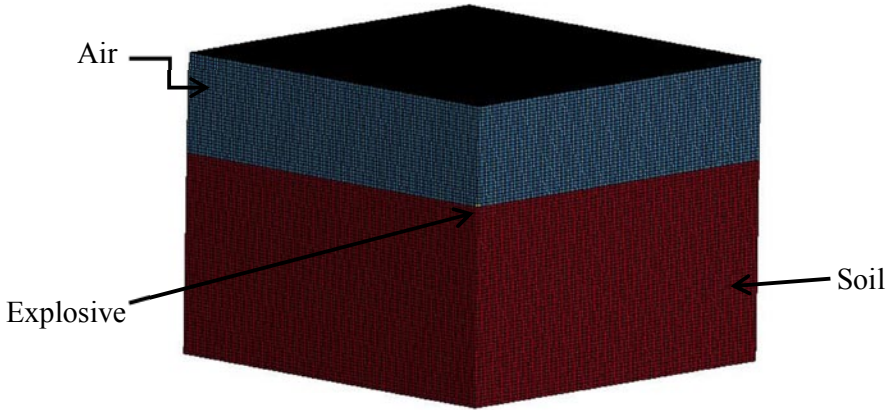
Figure 7.1- FE model for study the blast wave propagation in soil

7.2.1   Results and discussion

Figure 7.2 shows the progressive wave propagation in the soil at different time incidents. It demonstrates that the pressure waves propagate in the soil in the form of hemispherical waves, with the area of wave front increasing with the wave propagation.

t= 1.5ms   t = 10ms

| t = 25ms | t = 45ms |
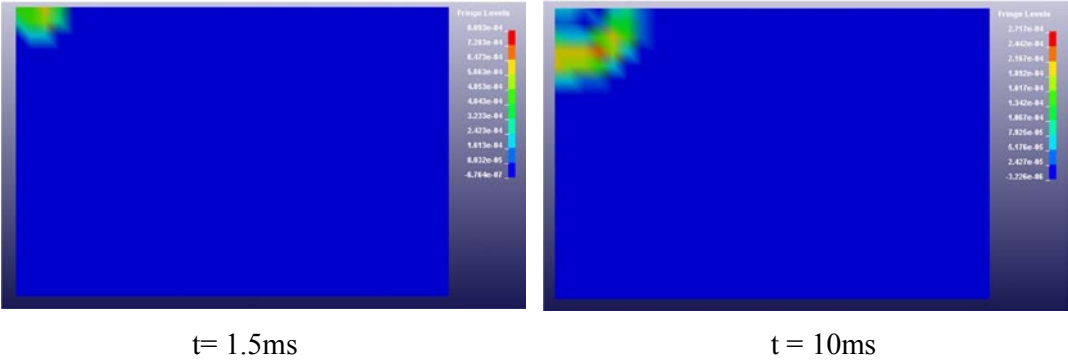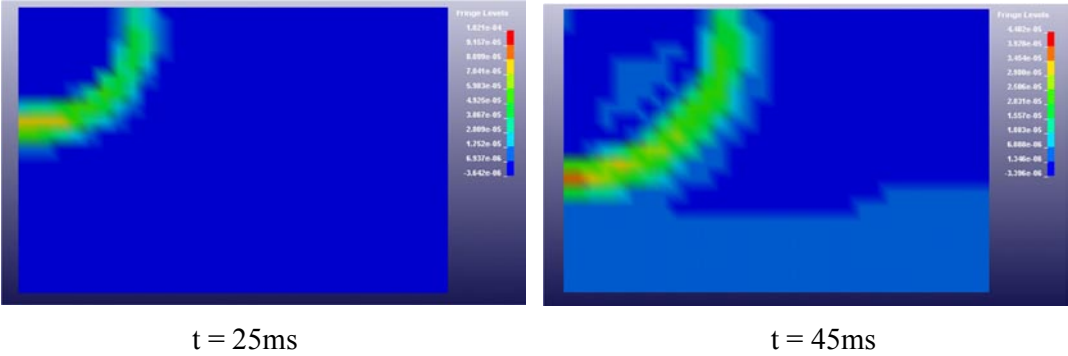
Figure 7.2- Pressure contours in the soil at different times after the detonation

The peak pressures measured in the soil are plotted against the scaled distance in Figure 7.3. The results show that attenuation of the peak pressure in the soil occurs with increasing distance from the charge, as expected.
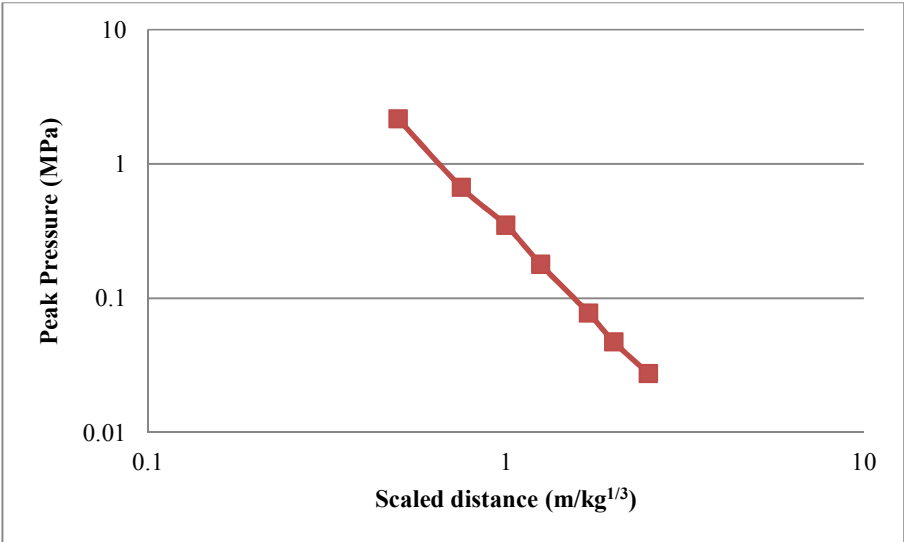
Figure 7.3- Relationship of peak pressures with scaled distance

Equation 6.1 in the previous chapter was used to predict the peak pressures in the soil empirically. In that equation, f is a coupling factor and is different for blasts in air, soil and concrete and depends on the scaled depth of the explosive source. The coupling factor for air is a constant and it is equal to 0.14. This value is also recommended for the surface explosions (TM5-855-1, 1986). Figure 7.4 compares the peak pressures obtained from the numerical simulation with the predicted peak pressures from the manual TM5-855-1 (1986). As shown in the figure, the numerical results for the peak

pressure attenuation agree reasonably well with the empirical results from the manual. The slightly lesser value might be caused by the complicated properties of the soils, which are simplified in the numerical model.
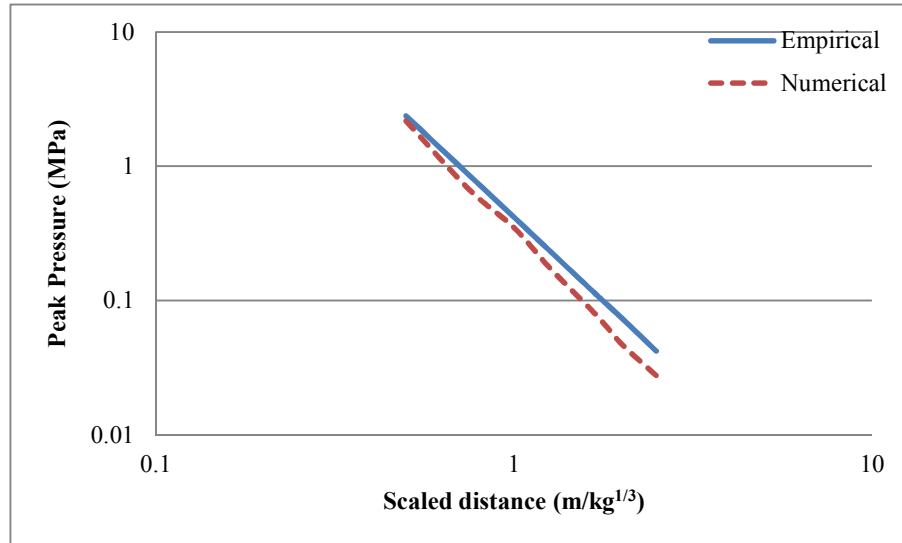
Figure 7.4- Comparison of peak pressures from numerical results and predictions from the manual (TM5-855-1)

7.3   BLAST RESPONSE AND FAILURE ANALYSIS OF FIXED-HEAD RC PILE

The LS-DYNA model developed for a 10m length pile with 600mm diameter circular cross section to study the blast response of a pile subjected to a buried explosion in chapter 5 was used for the study on the blast response of pile foundations subjected to surface explosion. A special consideration incorporated into the analysis of the pile foundation was the pile head restraint. Two types of boundary conditions at the pile head were considered - fixed-head and free-head conditions. In this section, results obtained from the analysis of fixed-head RC pile are presented and discussed.

7.3.1   Numerical results and discussion

This section investigated the response and damage of the fixed-head RC pile when subjected surface explosion for a standoff distance of 7.5m in partially saturated soil. Horizontal pile deformation and pile damage are presented to facilitate failure evaluation of piles.

The horizontal deformation and damage of the pile were obtained at 7 monitoring points on the pile at different heights from the pile tip (bottom): 0.5m (point A), 2m (point B), 4m (point C), 5m (point D), 6m (point E), 8m (point F) and 9.25m (point G).

Figure 7.5 shows the time histories of the horizontal deformations of the pile. The horizontal deformations have a significant influence on pile damage and failure. This Figure demonstrates that the pile has residual deflections along its height. These residual deflections indicate the occurrence of plastic deformation of the pile, which means that the pile has suffered permanent deformation and local failure under the buried blast event. Figure 7.6 presents the residual horizontal deformations of the pile along its height. The maximum residual deformation of 25.3mm occurs at the monitoring point E located 6m above from the pile tip. This could mean that point E is a potential failure region of this pile under the blast loading.
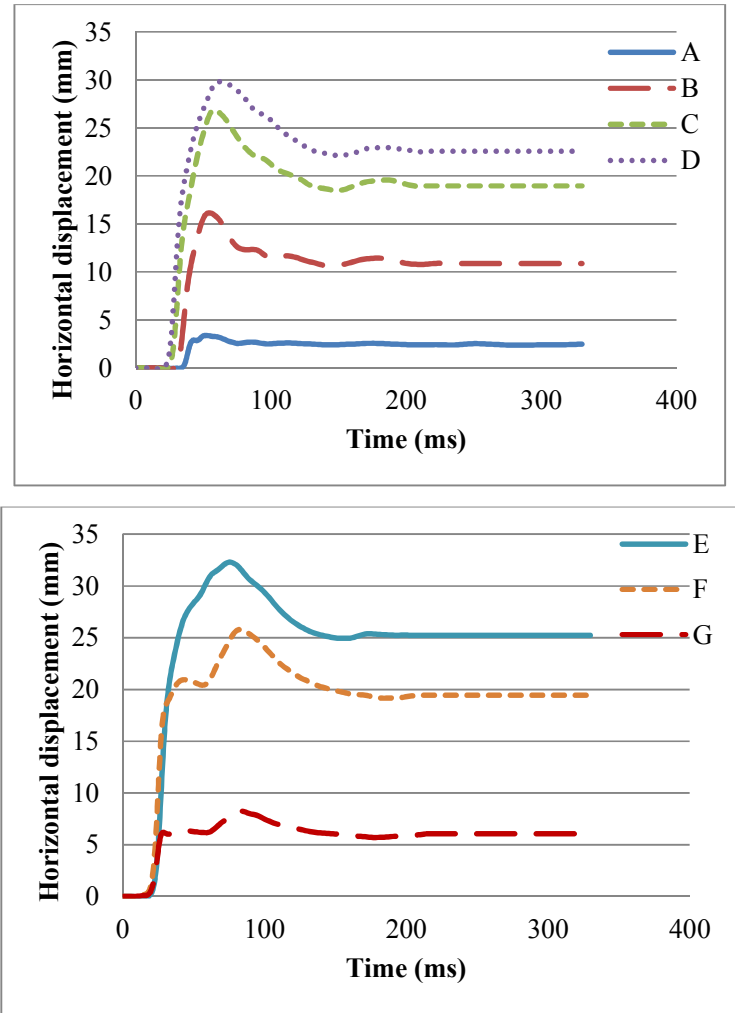
Figure 7.5- Fixed-head pile deformation
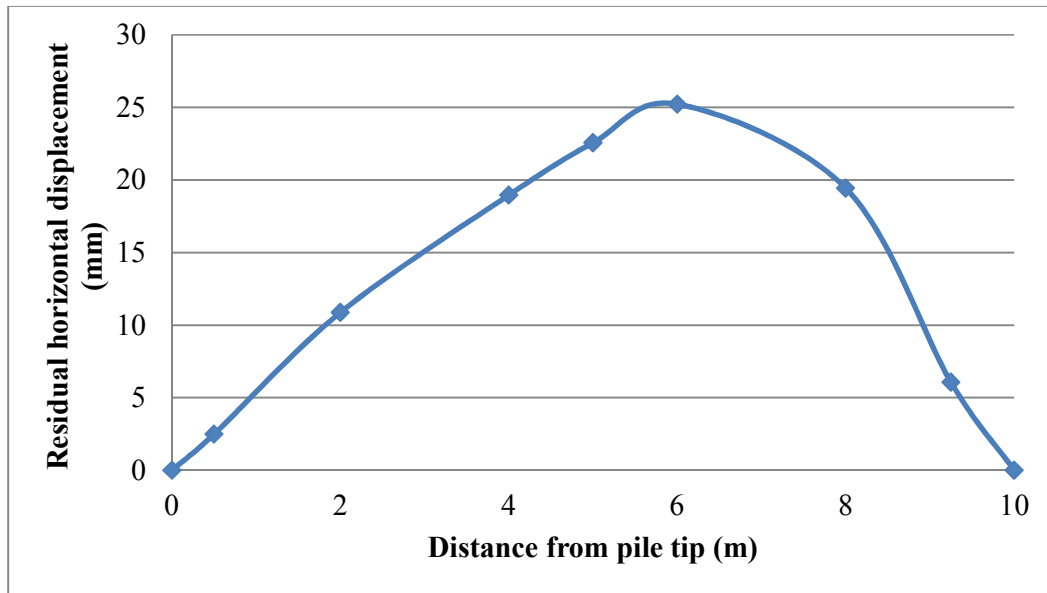
Figure 7.6- Residual horizontal deformations of fixed-head pile along its height

The damage to the reinforced concrete is also observed from the present numerical simulation. Figure 7.7 depicts the concrete effective plastic strain variation of the pile with the element erosions that were observed on the pile. Effective plastic strain is the damage parameter in concrete_damage_rel3 material model which ranges from 0 to 2. The colours in the Figure indicate the fringe level which represents the level of damage in the concrete. The blue colour represents the fringe level 0 which indicates elastic state of the concrete, while the red colour represents the fringe level 2 which indicates the complete yielding of the concrete. The other colours which are associated with fringe levels between 0 and 2 represent the different damage levels of the concrete. Figure 7.8 shows the effective plastic strain diagrams of the concrete cross sections taken at the pile ends and the mid-height. As can be seen, it is evident that the pile was considerably damaged at it ends due to shear force generated by the blast loading. Also, the strain diagram in Figure 7.8(b) indicates that the pile was subjected to damage in about 50% of its section at its mid-height. Potential failure locations of this pile are therefore at the two ends and near mid height where the horizontal deflection was large (as shown in Figure 7.6).
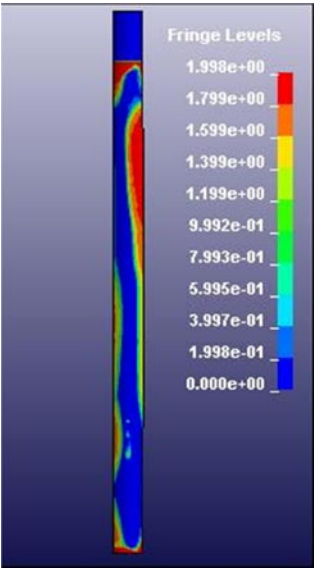
Figure 7.7- Blast damage on fixed-head pile

(a)   (b)

(c)
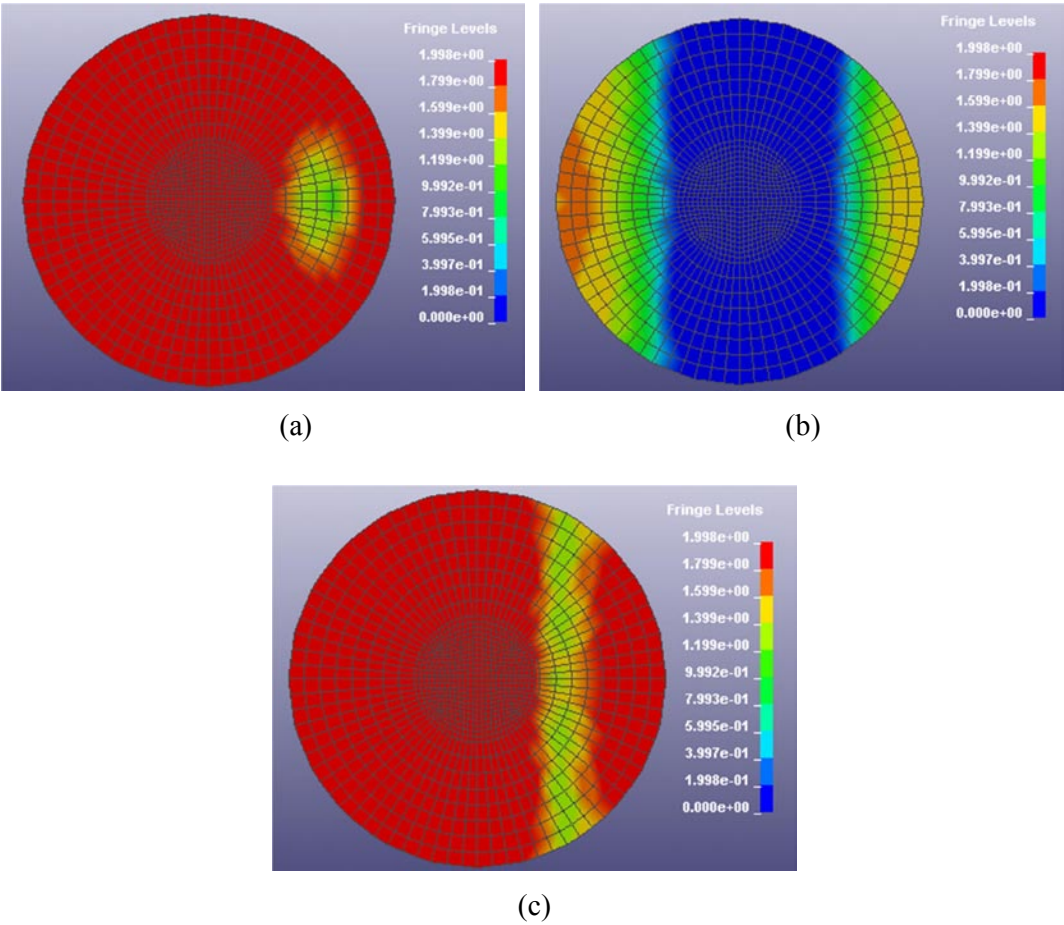
Figure 7.8- Effective plastic strain diagram of concrete cross sections at the (a) pile top end (b) mid-height of the pile (c) pile bottom end

7.4 BLAST RESPONSE AND FAILURE ANALYSIS OF FREE-HEAD RC PILE

Using the FE simulation techniques discussed above, further studies were carried out to evaluate the dynamic response of a free-head RC pile subjected to a surface blast. All translations and rotations were restrained at the bottom end of the pile, as before to depict fixed end conditions. At the top end of the pile both translations and rotations were allowed in all the directions. However, an axial load on the pile was considered in this study. It was added to the pile by placing a 3.75m x 3.75m x 1.875m concrete cube on the top of the pile. The concrete cube simulated an axial load of 600kN on the pile to represent a credible superstructure load on the pile. Figure 7.9 shows an isometric view of the developed model for the free-head pile with the concrete cube at the top of the pile.

Figure 7.9- Numerical model of free-head pile

7.4.1 Numerical results and discussion

In Figure 7.10, the time histories of the horizontal deformations of the pile at different heights from the pile tip: 0.5m (point A), 2m (point B), 4m (point C), 5m (point D), 6m (point E), 8m (point F), 9.25m (point G), and 10m (point H) are presented. It demonstrates that the pile has suffered permanent deformation and possible (local) failure under the blast load induced by surface explosion. Figure 7.11 presents the residual horizontal deformations of the pile along its height. The maximum residual

deformation of 38mm occurs, as expected, at the monitoring point H which is the pile head.
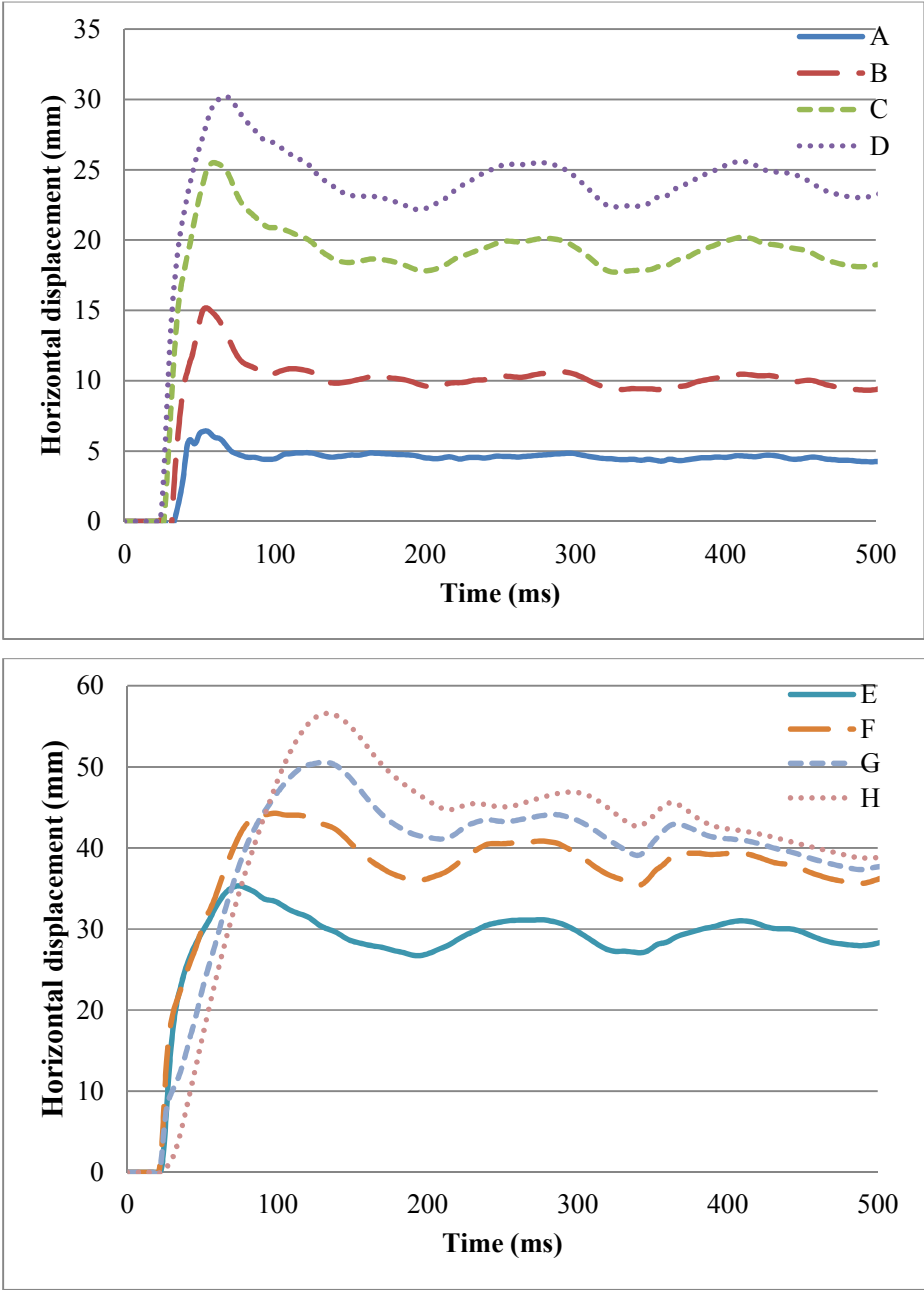
Figure 7.10- Free-head pile deformation
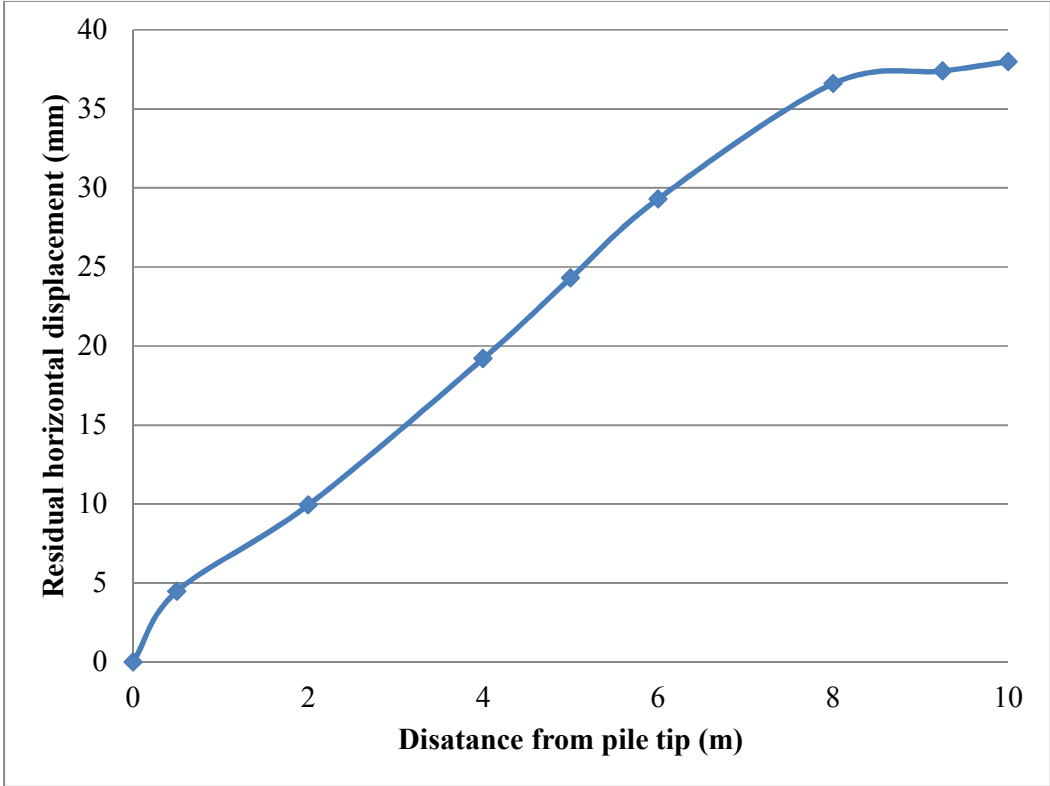
Figure 7.11- Residual horizontal deformations of free-head pile along its height

Figure 7.12 compares the numerical results for the pile deflection obtained in the fixed-head and free-head piles. It is evident that the pile end conditions have significant effect on the pile response under the blast load with respect to the maximum pile deflection and deflected shape of the pile.

Moreover, in order to investigate the effect of axial load on the blast response of pile, further studies were carried out by increasing concrete cube size to 4.45m x 4.45m x 2.225m. It simulated an axial load of 1000kN on the pile. Figure 7.13 illustrates the effect of axial load on the displacement response of the pile under blast loading. As the figure demonstrates, horizontal pile head displacement of the pile with larger axial load is slightly larger. However, further studies are needed to enable firm conclusions to be made on the effect of axial load on the response of piles under different blast scenarios.
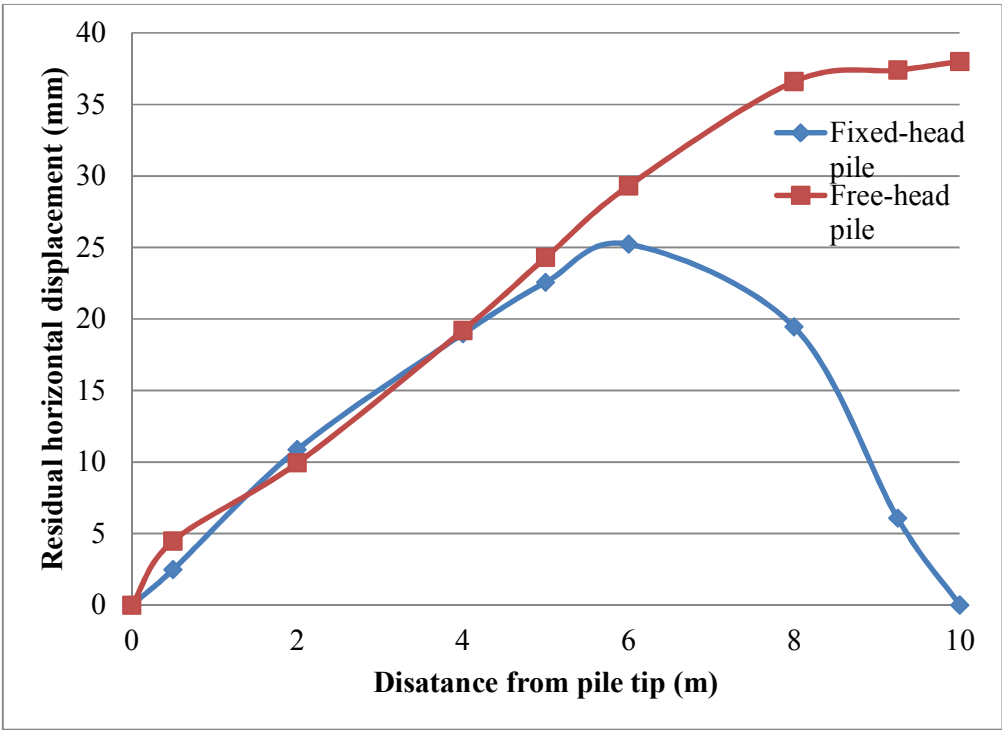
Figure 7.12- Comparison of pile deformation in fixed-head and free-end pile models
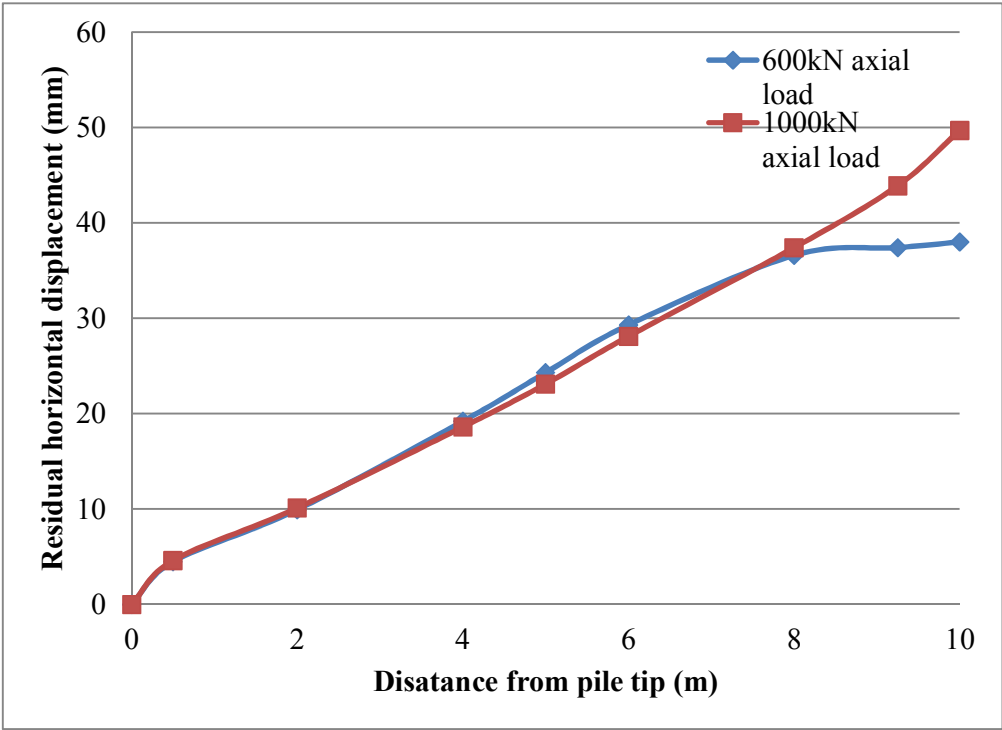
Figure 7.13- Effect of axial load on the displacement response of piles

7.5   BLAST RESPONSE AND FAILURE ANALYSIS OF PILE GROUPS

Piles are usually constructed in groups and tied together by a pile cap at the ground surface. The response of a pile within a group of closely spaced piles could be different from that of a single pile because of the pile-soil-pile interactions that take place in the group. LS-DYNA models were developed to study the blast response of pile groups. Three analysis cases were considered for the purpose of comparison as shown in Table 7.1. Cases 1 and 2 pertain to groups of 2 piles that are closely and widely spaced respectively while case 3 pertains to a group of 4 closely spaced piles. Figure 7.14 (a) and (b) show the FE models developed for the 2-pile (cases 1 and 2) and 4-pile (case 3) groups, respectively. The most important factor is the pile spacing in a pile group. Considering the group of 2 piles, two separate FE models were created with pile spacing of 2.5 times (case 1) and 5 times (case 2) the pile diameter for the blast analysis of the pile groups with closely-spaced and widely-spaced piles respectively. Only half of each model is meshed using symmetry conditions. The rotational restraint at the pile cap connection was considered in all cases.

Table 7.1- Selected analysis cases

Analysis case	No. of pile in group	Spacing between piles/Pile diameter
1	2	2.5
2	2	5
3	4	2.5
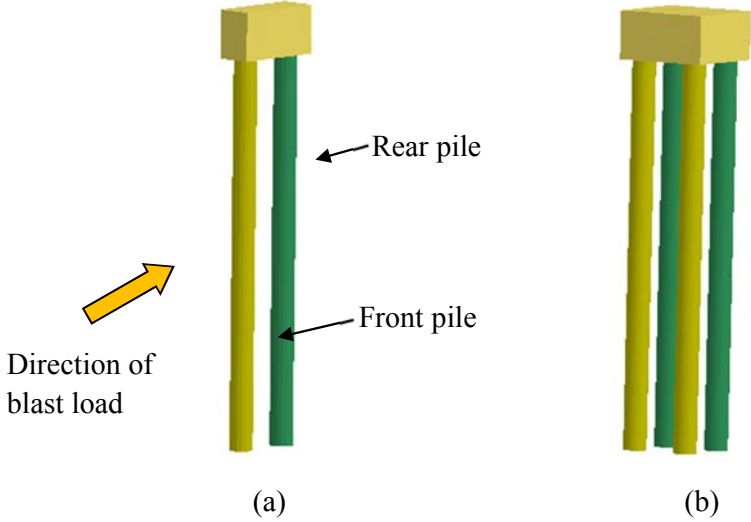
Figure 7.14- FE models for (a) 2-pile group (b) 4-pile group

7.5.1   Numerical results and discussion

In this subsection, results related to the behaviour of pile groups in partially saturated soil under blast loads induced by surface explosion are presented. The residual horizontal displacements along the height of each pile in the 2-pile group in analysis case-1 are plotted in Figure 7.15. As can be seen, it is clear that front pile of the 2-pile group was more deformed than the rear pile. These residual horizontal deformations have a significant influence on pile damage and failure.
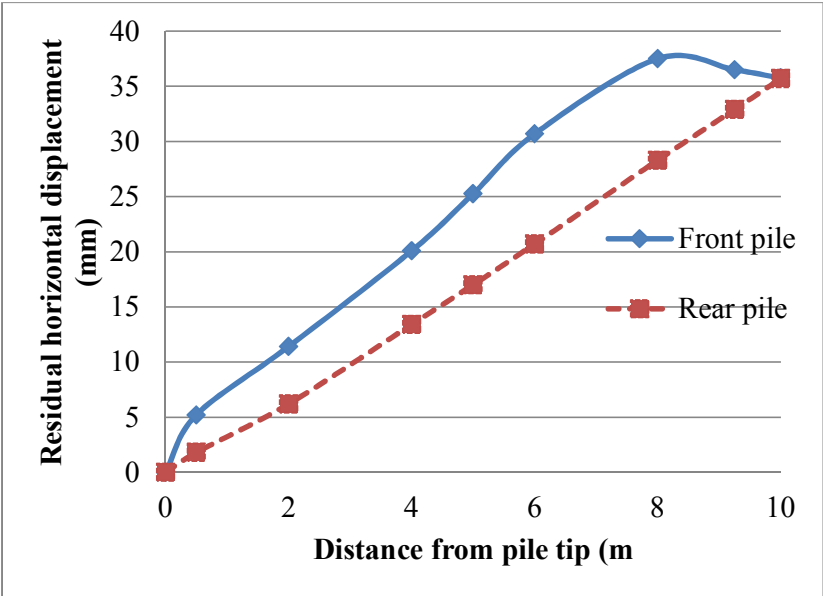
Figure 7.15- Comparison of pile deformation in front and rear piles of case 1 pile group

Figure 7.16 compares the numerical results for the pile deflections obtained in all three cases. Figure 7.16(a) presents the residual horizontal displacements of the front piles in the pile groups. They have maximum lateral residual deflections of 37.5 mm, 40 mm and 37mm in cases, 1, 2 and 3 respectively. Figure 7.16(b) shows that the residual lateral deflections of the rear piles in the pile groups. Maximum lateral residual deflections of approximately 35.7mm, 36 mm and 31.5mm are observed in cases 1, 2 and 3 respectively. Piles in the widely-spaced pile group (case 2) have slightly higher pile head displacements compared to piles in the closely-spaced pile group (case 1). This is due to the lower stiffness and the reduced pile-soil-pile interaction in the widely-spaced pile foundation system. In the closely-spaced 2 pile and 4 pile systems (case 1 and case 3 respectively) the rear piles have maximum pile head displacements of 35.7 mm and 31.5 respectively. Hence, the number of piles in a group and the spacing between piles have an influence on the pile head displacement under surface blasts.
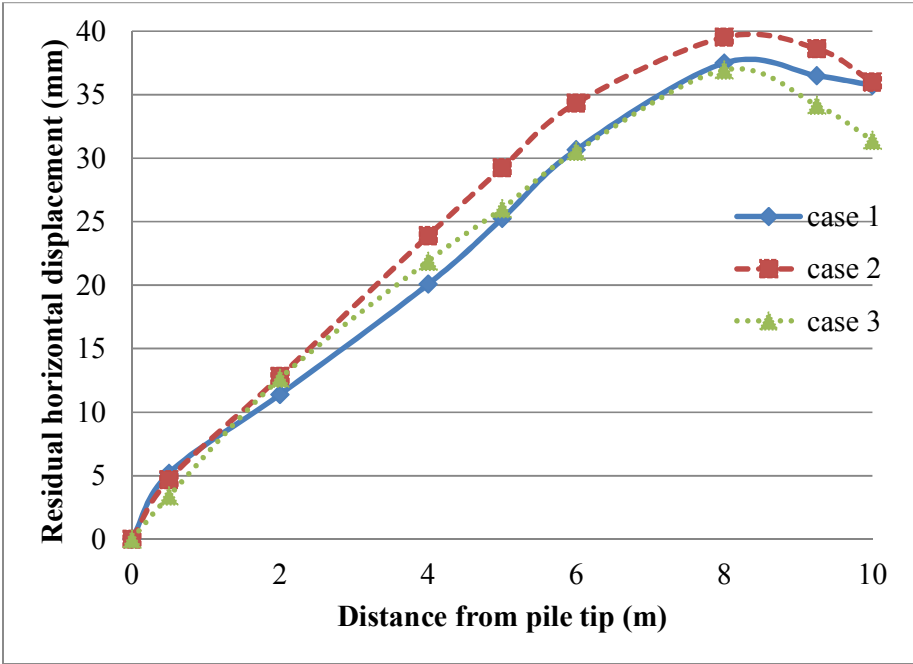
(a)
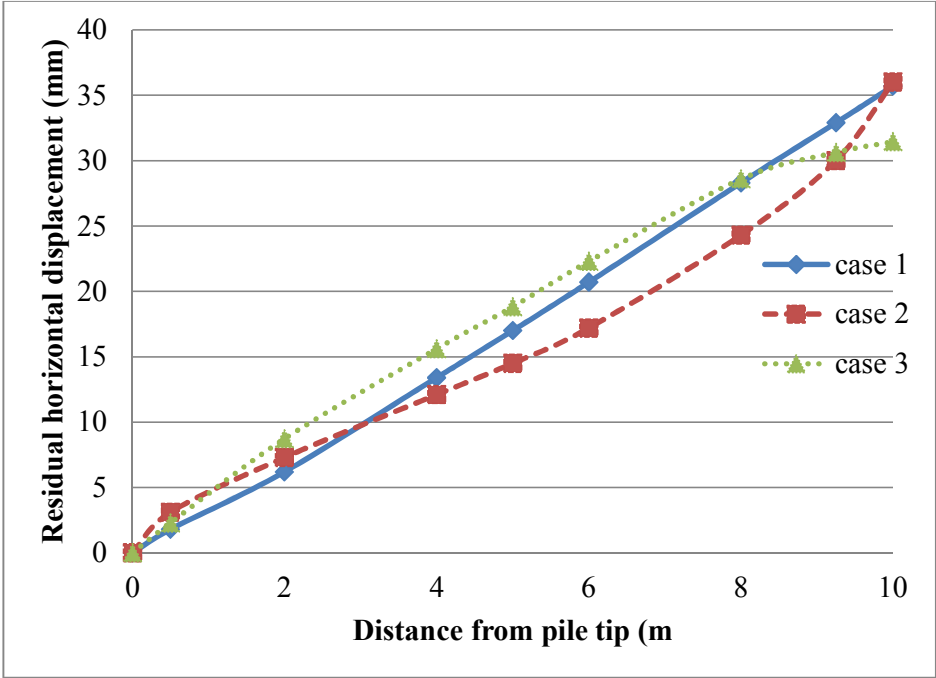
(b)

Figure 7.16- Comparison of pile responses for case 1 to 3 (a) front pile of pile groups (b) rear pile of pile groups

To further study the behaviour of each pile, the effective plastic strain diagrams and blast damage in each pile in the pile groups were examined. Figure 7.17 shows the concrete effective plastic strain variation of each individual pile in the pile groups. As described earlier, the effective plastic strain in Mat72_rel3 concrete material model is the damage parameter which ranges between 0 and 2, with fringe levels 0 and 2 indicating no yielding and maximum yielding of the concrete, respectively. As can be seen in the figure, a significant portion of each pile has suffered damage and local failure, as the effective plastic strains are greater than 0. Piles in the pile group in case-1 suffered more damage than the piles in the other two cases. However, the results show that there were no sign of catastrophic failure in any of the 3 cases considered.
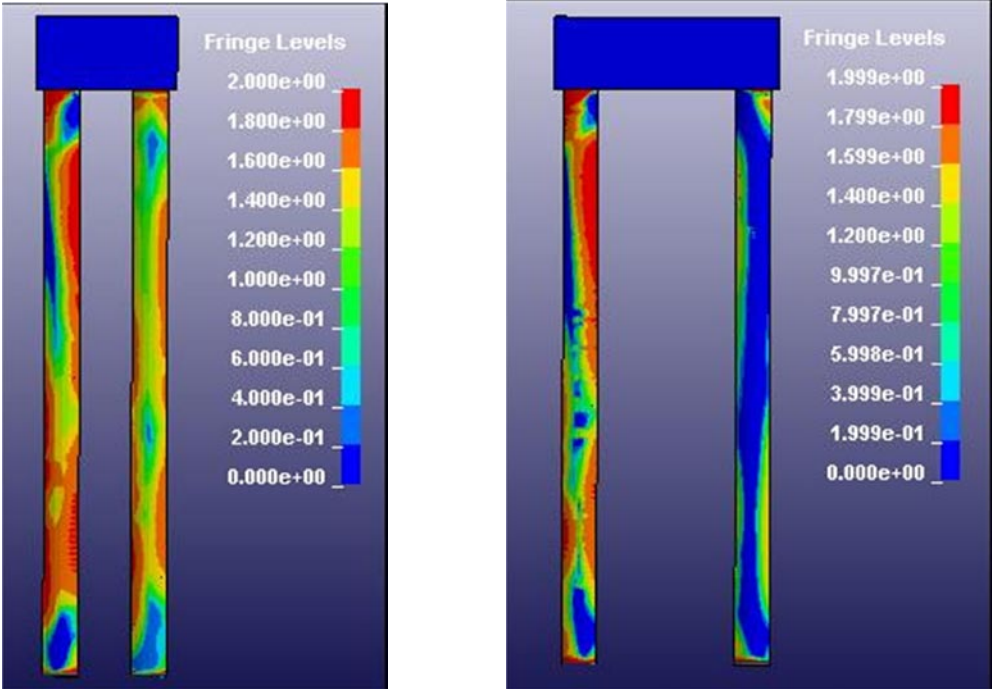
(a)   (b)
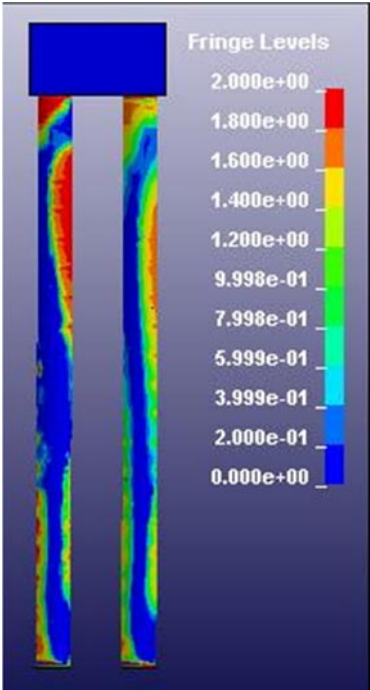
(c)

Figure 7.17- Blast damage on pile groups for analysis (a) case-1 (b) case-2 (c) case-3

7.6 CHAPTER SUMMARY

In this chapter, a coupled numerical model which was described in chapter 4 was used to investigate the dynamic response of RC pile foundations embedded in partially saturated soil under surface explosion. Single piles and pile groups with different pile numbers and spacing were considered. Both free head and fixed head boundary conditions at the pile head were considered in the analysis of single piles. Numerical results show that pile head boundary conditions have significant effects on the pile response under blast loading. Moreover, the effect of axial load on the blast response of pile was also investigated. It was found that horizontal displacement of the pile with the larger axial load is slightly higher for the considered RC pile and blast load condition. In the coupled analysis considered in this study, it is expected that P-Δ effects, if any, will be automatically included. Piles in three different arrangements of pile groups were considered to study the blast response of pile groups. Displacement responses of pile groups indicated that piles in the widely-spaced pile group have slightly larger pile head displacements which are attributed to the lower stiffness and reduced pile-soil-pile interaction of the widely-spaced pile foundation system. It was also evident that the number of piles in a group and the spacing between the piles within a group have an influence on the lateral pile head displacements. Residual lateral deflections and effective plastic strain diagrams of the piles were presented. They can be used to identify local damage in the piles and their potential failure under surface blast loading. The modelling techniques developed and applied in this chapter and its research outcomes can be useful in future studies on the blast response and failure analysis of pile foundations.

Chapter 8: Conclusion

8.1   SUMMARY

This chapter presents the overall conclusion of this research. The research presented in this thesis investigated the blast response and damage analysis of RC pile foundations when subjected to both surface and underground explosions. It used the fully coupled numerical procedure incorporating different material models for accurate evaluation of the dynamic response of reinforced concrete pile foundations to blast loads using the commercial computer program LS-DYNA.

The FE models used in the present research were divided into different regions representing the air, soil, pile and explosive charge. Both Eulerian and Lagrangian formulations were used in the models. Eulerian meshes were generated for the explosive, air and for a part of soil that was close to the explosive to eliminate the distortion of the mesh under high deformations. On the other hand Lagrangian meshes were used to model the rest of the system including the pile and the soil region away from the explosive. Eight-node solid elements (brick elements) were used for all parts except for pile reinforcement. The vertical reinforcements were defined as Hughes-Liu beam elements with cross integration and ties were defined as truss elements. The constrained_lagrange_in_solid option was used to couple concrete solid elements with the reinforcing beam elements.

The modelling techniques used in the present study were validated using previous experimental test results. A parametric study of blast response of RC pile using the developed 3D FE model was performed and the results of this research were discussed. The effects of pile reinforcements, charge weight and shape and burial depth of the explosive charge on the blast response and damage of the pile were investigated. To study the effects of soil properties on the blast response of a single pile, three different soil types were considered: saturated soil, partially saturated soil and loose dry soil. Two types of boundary conditions at the pile head were considered for the purpose of comparison: these include the fixed-head condition and free-head condition. The effect of axial loads on the response of pile was also investigated. The effects of different

arrangement of piles on the blast response and damage of the RC pile group subjected to surface explosion were also treated.

8.2 CONCLUSIONS

Based on the research findings, the following key conclusions of the studies can be drawn.

- This research developed and applied a fully coupled numerical method to investigate the blast response and damage to pile foundations. Comparison and agreement of results from present FE analysis and Shim's (1996) centrifuge study provide confidence in the modelling techniques developed in the present research for predicting the blast response of piles with good accuracy.

- Modelling of the pile reinforcement (in the analysis) and the parametric study on its effect on the blast response of pile provide new information on the benefits of reinforcement in pile design. Longitudinal reinforcement in a pile has a significant effect on blast response of pile. Pile deformations decrease with increase in the longitudinal reinforcement. In addition, proper detailing of ties in a pile can cause significant reductions in the degree of direct damage under blast loads.

- Explosive charge weight and shape influence substantially on blast response of pile foundation. Pile lateral deformations under blast loading increase with the charge weight. The blast pressures generated by a cylindrical charge are significantly greater than those generated by a spherical or a cubic charge. Thus, it was found that cylindrical shape explosive has the maximum effect on the pile behaviour.

- Blast response of pile decays with significantly with the decrease in the burial depth of the explosive. Buried explosions result in significant effects on the blast response and damage of the RC pile than surface explosions, under the same conditions.

- The investigations show that soil properties significantly influence the blast response of pile foundations. Piles in saturated soil and loose dry soil are more vulnerable to blast loads than piles embedded in partially saturated soil when subjected to same buried explosion.

- Pile damage and deformation decrease with the distance of the explosive, as expected.

- Based on the three dimensional nonlinear dynamic analyses of soil-single pile foundation when subjected to surface explosion, boundary conditions at pile head have significant effect on the pile response.

- Axial load on the pile has considerable effect on the RC pile response, and further studies are needed to enable firm conclusions to be made on the effect of axial load on the response of piles under different blast scenarios.

- The pile was damaged due to combined effects of shear and flexural damages in most blast analysis cases.

- Number of piles in a group and the spacing between piles have an influence on the pile head displacement under surface blasts. Largely spaced pile groups have slightly larger pile head responses than closely spaced pile groups. When number of piles in a group increase, the pile head displacement decreases.

8.3   MAIN CONTRIBUTION AND RESEARCH FINDINGS

- A fully coupled computer model has been developed to treat the blast response pile foundations.

- Pile response to both surface explosions as well as underground explosions can be treated.

- Influence of important parameters such as different soil types, pile reinforcement, explosive charge properties, pile head boundary conditions, axial load on the pile and number of piles and spacing between piles in a group have been studied.

- Blast wave propagation in soil also has been studied.

- Pile deformation and pile head displacement due to blast pressure on piles were studied. Blast damages on pile were evaluated using the plastic strain development and material erosion. Therefore, post blast performance capacities can then be evaluated and appropriate engineering decisions can be made for structural safety.

- The present modelling techniques and research findings can serve as a benchmark reference in future developments in this area and in the validation of numerical models.

8.4   FUTURE RESEARCH

Although the numerical studies described in this thesis addressed a wide range of topics, additional study is needed before provide comprehensive design guidance of pile foundations subjected to blast loads. The following topics for future research are recommended.

- Layered soil profiles and uncertainties in soil conditions
  - o The soil is assumed as a homogeneous single layer in the present research. In reality, however, piles are embedded in layered soil profiles with different materials with variable thickness.
- Configuration of pile group foundations
  - o The present research investigated 2-pile and 4-pile group foundations. To further understand the effects of number of piles in a group on pile head response, it is necessary to include more piles in the FE model and compare structural responses from different pile configurations. Based on the results, recommendations can be provided to optimise pile foundation design.
- Axial load on the single pile
  - o The present research considered only two different loads to investigate the axial load effect on the blast response of pile foundation. However, further studies are needed with more variable axial loads to enable firm conclusions to be made on the effect of axial load on the blast response of pile.
- Axial load on the pile groups
  - o The present research did not consider axial load acting on the pile group foundations. Axial load on the pile groups can be influenced on their response under blast loading.
- Boundary conditions at pile ends

- o The present research considered fixed and free boundary conditions at the pile top with fixed boundary condition at pile bottom. In reality, however, pile ends do not have fully fixed or free boundary conditions.
- Modelling of the superstructure
  - o Further research can make the representation of superstructure more realistic to get a more accurate structural dynamic response.
- Damage evaluation of RC pile foundations which have been designed to resist earthquake loads, can form another topic for future investigation.

References

Akhwan, J., The chemistry of explosives, 2nd edition, Springer, New York, 2004.

Ambrosini, R.D., Luccioni, B.M., Danesi, R.F., Reira, J.D. and Rocha, M.M., Size of Craters produced by Explosive Charges on or above the Ground Surface, Shock Waves, Springer Verlag, 2002.

Ambrosini, R.D., Luccioni, B.M. and Danesi, R.F., Influence of the Soil Properties on Craters produced by Explosions on the Soil Surface, Computational mechanics, 23 (2004).

Ambrosini, R.D. and Luccioni, B.M., Craters produced by Explosives above the Soil Surface, Computational mechanics, 26 (2007), pp 2253-2266.

An, J., et al., Simulation of Soil Behavior under Blast Loading, ASCE, 2011.

Anirban De, Numerical simulation of surface explosions over dry, cohesionless soil, Computers and Geotechnics, 43 (2012), pp 72-79.

AS/NZS 1170, Australian/ New Zealand Standard: Structural design actions, Australian and New Zealand standards joint technical committee BD-006, 2002.

AS 3600, Australian Standard: Concrete structures, Standards Australia committee BD-002, 2009.

AS 2159, Australian Standard: Piling – Design and installation, Standards Australia committee CE-018, 2009.

Baker, W.E., Westine, P.S. and Dodge, F.T., Similarity Methods in Engineering Dynamics, Elsevier, Amsterdam, 1991.

Bao, X. and Li, B., Residual Strength of Blast Damaged Reinforced Concrete Columns, International Journal of Impact Engineering, 37(3), 295-308, 2010.

Bragov, A.M., Lomunov, A.K., Sergeichev, I.V., Proud, W., Tsembelis, K. and Church, P., *A* Method for Determining the Main Mechanics Properties of Soft Soils at High Strain Rates and Load Amplitudes up to Several Gigapascals, Tech. Phys. Lett., 31(6), PP 530-531, 2005.

Bischoff, P., and Perry, S., Compressive behavior of concrete at high strain rates, Materials and structures, 24 (6) (1991), pp 425-450.

Birnbaum, N.K., Francis, N.J., and Gerber, B.I., Coupled technique for the simulation of fluid-structure and impact problems, computer assisted mechanics and engineering sciences, 6 (3-4), 1999, 295-311.

Bretz, T.E., Soil liquefaction resulting from blast-induced spherical stress waves, PhD thesis, Department of Civil Engineering, Colorado state university, Fort Collins, CO, 1989.

BS 8004, Code of practice for foundations, Section seven (Pile foundations), 1986.

Budhu, M., and Davies, T.G., Nonlinear analysis of laterally loaded piles in cohesionless soils, Canadian geotechnical journal, 24 (2) (1987), pp 289-296.

Cooper, P., Kurowski, S., Introduction to technology of explosives, Wiley-VCH, 1996.

Drake, J.L., and Little, C.D., Ground shock from penetrating conventional weapons, Proc. 1st Symp. On the interaction of non-nuclear munitions with structures, US Air force academy, CO, 1983, pp 1-6.

Elsanadedy, H.M., Almusallam, T.H., Abbas, H., Al-Salloum, Y.A., and Alsayed, S.H., Effect of blast loading on CFRP-retrofitted RC columns – a numerical study, Latin American journal of solids and structures, 8 (2011), pp 55-81.

EN 1991 Euro code 1, Actions on structures, European committee for standardization, 2006.

Feldgun, V.R., Kochetkov, A.V., Karinski, Y.S., Yankelevsky, D.Z., Internal blast loading in a buried lined tunnel, Int. J.Imapct Eng., 35, 172-183, 2008.

FEMA 426, Reference manual to mitigate potential terrorist attacks against buildings, Risk management series, US Department of Homeland security, Washington USA, 2003.

Graff, K.F., Wave motion in elastic solids, Dover publications, NY, 1975.

Granier, J., Gaudin, C., Springman, S.M., Culligan, P.J., Goodings, D., Kutter, B., Phillips, R., Randolph, M.F., and Thorel, L., Catalogue of scaling laws and similitude questions in centrifuge modelling, International Journal of Physical Modelling in Geotechnics, 7 (3) (2007), pp 1-24.

GTB web site, Global terrorism database, http://www.start.umd.edu/gtd/search/Results.aspx?chart=weapon&search=building, (last accessed 2013)

Gui, M.W., and Chien, M.C., Blast-resistant analysis for a tunnel passing beneath Taipei Shongsan airport- a parametric study, Geotechnical and geological engineering, 24 (2006), pp 227-248.

Hallquist, J.O. LS-DYNA Theoretical Manual - Nonlinear Dynamic Analysis of Structures, Livermore, California: Livermore Software Technology Corporation, Livermore, California, 1998.

Hyde, D., User's guide for microcomputer programs, CONWEP and FUNPRO – Application of TM5-855-1, US army engineer waterways experimental station, Vicksburg, MS, 1988.

Jayasinghe, L.B., Thambiratnam, D.P., Perera, N., and Jayasooriya, J.H.A.R., Computer simulation of underground blast response of pile in saturated soil, Computers and Structures, 120 (2013), pp 86-95.

Jayasooriya, R., Thambiratnam, D. P., Perera, N. J., and Kosse, V., "Blast and residual capacity analysis of reinforced concrete framed building", Engineering structures, 2011.

Jones, D.A., and Northwest, E.D., Effect of case thickness on the performance of underwater mines, DSTO Aeronautical and Martine Research laboratory, Melbourne, 1995.

Kinney, G.F. and Graham, K.J., Explosive shocks in Air, 2nd Edition, Springer Verlag, 1985.

Kumar, M., Matsagar, V.A. and Rao, K.S., Blast Loading on Semi-Buried Structures with Soil-Structure Interaction, Proceeding of the IMPLAST Conference, Rhode Island, USA, 2010.

Lan, S., Crawford, J. E., and Morrill, K. B., "Design of reinforced concrete columns to resist the effects of suitcase bombs", International Proceeding of 6th international conference on shock and impacts loads on structures, Australia, 2005, pp 5-10.

Lee, E., Finer, M., and Collins, W., JWL equations of state coefficients for high explosives, Lawrence Livermore Laboratory, University of California, California, 1973.

Lee, W.Y., Numerical modeling of blast induced liquefaction, DAI, 67, no. 06B, 3305, 2006.

Lewis, B.A., Manual for LS-DYNA soil material model 147, Federal Highway Administration, FHWA-HRT-04-095, McLean, VA, 2004.

LS-DYNA, Livermore software technology cooperation, LS-DYNA user's manual, version 971, 2007.

Luccioni, B., Ambrosini, D., and Danesi, R., Blast load assessment using hydro codes, Engineering Structures, 28 (12) (2006), pp 1736-1744.

Lyakhov, G.M., Shock waves in the ground and dilution of water saturated sand, Zhurnal Prikladnov Mekhaniki I. Teknicheskoi, Fiziki, Moscow, 1 (1961), pp 38-46.

Malvar, L.J., Crawford, and Morrill, K.B., K and C concrete material model, release III – automated generation of material model input, Karagozian and Case structural engineers, Technical report 2000 TR-99-24.3.

Malvar, L.J., Crawford, J.E., Wesevich, J.W., and Simons, D.A., A plasticity concrete material model for DYNA3D, International journal of impact engineering, 19 (9-10) (1997), pp 847-873.

Milklowitz, J., The theory of elastic waves and wave guides, Series in Applied mathematics and mechanics, Volume 22, North-Holland publishing Co., Amsterdam, 1978.

Nagy, N.M., Eltehawy, E.A., Elhanafy, H.M., and Eldesouky, A., Numerical modelling of geometrical analysis for underground structures, 13th international conference on Aerospace science & aviation technology, Egypt, May 2009.

NCTC web site, Counterterrorism 2013 calendar, http://www.nctc.gov/site/technical/bomb_threat.html, (last accessed 2013)

Newmark, N.M., Design of structures for dynamic loads including the effects of vibration and ground shock, In Symposium of scientific problems of productive construction, Swiss federal institute of technology, Zurich, 1963, pp 148-248.

Ngo, T., Mendis, P., Gupta, A., and Ramsay, J., Blast loading and blast effects on structures – an overview, EJSE international special issue: Loading on structures, 2007, pp 76-91.

Nogami, T. and Konagai, K., Time Domain Flexural Response of Dynamically Loaded Single Piles, Journal of Engineering Mechanics, 114 (9) (1988), pp 1512-1525.

Nogami, T., et al., Nonlinear Soil-Pile Interaction Model for Dynamic Lateral Motion, Journal of Geotechnical Engineering, 118 (1) (1992), pp 89-106.

Poulos, H.G., Behaviour of Laterally-Loaded Piles, II: Pile Groups, Journal of Soil Mechanics and Foundation Engineering, ASCE, 97(SM5) (1971), pp 773-751.

Poulos, H.G., Behavior of laterally loaded piles: I – single pile, JSMFE, ASCE, 97 (SM5) (1991), pp 711-731.

Randolph, M.F., The response of flexible piles to lateral loading, Geotechnique, 31 (2) (1981), pp 247-259.

Reid, J.D., Coon, B.A., Lewis B.A., Sutherland, S.H., Murray, Y.D., Evaluation of LS-DYNA soil material model 147, Federal Highway Administration, FHWA-HRT-04-094, McLean, VA, 2004.

Remennikov, A, A review of methods for predicting bomb blast effects on buildings, Journal of Battlefield Technology, 6 (2003), pp. 5-10.

Richart, Jr., F.E., Hall, Jr., J.R., and Woods, R.D., Vibrations of soils and foundations, Prentice-Hall, Englewood Cliffs, NJ, 1970.

Rinehart, J.S., Stress transients in solids, Hyperdynamics, Inc., Santa FE, NM, 1975.

Ross, C.A., Tedesco, J.W., and Kuennen, S.T., Effects of strain rate on concrete strength, ACI material journal, 30 (1995), pp 54-62

Sherker, P., Modeling the effects of detonations of high explosives to inform blast-resistant design, Master thesis, the University at Buffalo, State University of New York, 2010.

Shim, H-S., Response of piles in saturated soil under blast loading, Doctoral thesis, University of Colorado, Boulder, US, 1996.

Tai, Y.S., Chu, T.L., Hu, H.T., and Wu, J.Y., Dynamic response of a reinforced concrete slab subjected to air blast load, Theoretical and applied fracture mechanics, 56 (2011), pp 140-147.

Thilakarathna, H.M.I., Thambiratnam, D.P., Dhanasekar, M. and Perara, N.J., Numerical Simulation of Axially Loaded Concrete Columns under Transverse Impact and Vulnerability Assessment, International Journal of Impact Engineering, 37(11), 1100-1112, 2010.

TM5-1300, Structures to resist the effects of accidental explosions, US Army technical manual, 1990.

TM5-855-1, Fundamental of protective design for conventional weapons, US Army technical manual, 1986.

Tong, X. and Tuan, C.Y., Viscoplastic Cap Model for Soils under High Strain Rate Loading, Journal of Geotechnical and Geo-environment Engineering, 133(2), PP 206-214, 2007.

Michigan Tech web site, UPSeis an educational site for budding seismologists, http://www.geo.mtu.edu/UPSeis/waves.html, (last accessed 2013).

Yang, Y., Xie, X., and Wang, R., Numerical simulation of dynamic response of operating metro tunnel induced by ground explosion, Journal of rock mechanics and geotechnical engineering, 2(4), 2010, pp 373-384.

Yang, Z., Finite element simulation of response of buried shelters to blast loadings, Finite element in analysis and design, 24 (3) (1997), pp 113-132.

Wang, J., "Simulation of landmine Explosion Using LS-DYNA3D Software: Benchmark Work of Simulation of Explosion in Soil and Air, Report DSTO-TR-1168", Aeronautreal and Maritime Research Laboratory, Australia, 2001.

Wang, Z. and Lu, Y., Numerical Analysis on Dynamic Deformation Mechanism of Soils under Blast Loading, Soil Dynamics and Earthquake Engineering, Elsevier, 23, 705-714, 2003.

Wang, Z., Lu, Y., Bai, C., Numerical analysis of blast induced liquefaction of soil, comput.geotech., 35, 196-209, 2008.

Wang, Z., Lu, Y., Hao, H., Numerical investigation of effects of water saturation on blast wave propagation in soil mass, J.Eng.Mech., ASCE, 130(5), 551-561, 2004.

Westine, P.S., and Friensenhahn, G.J., Free-field shock pressure from buried detonations in saturated and unsaturated soils, Proc., 1st Symp., on the interaction of non-nuclear munitions with structures, US air force academy, CO, 1983, pp 12-16.

Woodson, S.C., Baylot, J.T., Structural collapse: quarter-scale model experiments, Technical report SL-99-8, US Army Corps of Engineers – Engineer Research and Development center, 1999.

Wu, C., Lu, Y., and Hao, H., Numerical prediction of blast induced stress wave from large scale underground explosion, International journal for numerical and analytical methods in geomechanics, 28 (2004), pp 93-109.

Wu, C., and Hao, H., Modeling of simultaneous ground shock and airblast pressure on nearby structures from surface explosions, International journal of impact engineering, 31 (6) (2005), pp 699-717.

Wu, G., and Finn, W.D.L., Dynamic Nonlinear Analysis of Pile Foundations using Finite Element Method in the Time Domain, Canadian Geotechnical Journal, 34 (1997), pp 44-52.

Yang Z., Finite element simulation of response of buried shelters to blast loadings, Finite element in analysis and design, 24 (3) (1997), pp 113-132.

Zukas, J., and Waters, W., Explosive effects and applications, Springer, New York, 1998.